Finite Difference Methods, Hermite Interpolation and a Quasi-Uniform Spectral Scheme (QUSS)

by

Burhan A. Sadiq

**A dissertation submitted in partial fulfillment
of the requirements for the degree of
Doctor of Philosophy
(Applied and Interdisciplinary Mathematics)
in the University of Michigan
2013**

Doctoral Committee:

Professor Divakar Viswanath, Chair
Professor John P. Boyd
Professor Robert Krasny
Professor Jeffrey B. Rauch

DEDICATION

To the Sadiq and Mahmood family (including you momo!). I love you guys!

ACKNOWLEDGMENTS

I want to thank my undergraduate teachers at the University of Maryland, College Park who believed in me and made me love mathematics. In particular, I would like to thank Manoussos Grillakis for all of his patience with a young kid who was glued to his office seeking help with this difficult but rewarding subject of mathematics. I would also like to thank Stuart Antman for his amazing lectures that introduced me to the subject of PDEs. I also wish to thank my undergraduate teachers who inspired me: Paulo Bedaque and Steve Anlage for their amazing lectures in Quantum Mechanics, Sylvester James Gates for his amazing insight into the world of Electromagnetism, Frederick Wellstood for introducing me to Classical Mechanics, Philip DeShong for teaching me about Organic Chemistry and all of the other amazing instructors I came across at the University of Maryland, College Park. I wish to express my deepest gratitude to this fine institution for teaching me just about everything I know.

I also wish to thank my educators as a graduate student at the University of Michigan, Ann Arbor: Divakar Viswanath for introducing me to the field of Numerical Analysis, John P. Boyd for introducing me to the world of Spectral Methods, Robert Krasny for teaching me about the equations of Fluid Mechanics and introducing me to the subject of Asymptotic Analysis, Peter Miller for his wonderful lectures in Functional Analysis, Smadar Karni for

her amazing lectures in Complex Analysis and all of the other inspirational instructors whom I have had the pleasure of learning from. I also wish to thank the Regents at the University of Michigan for their financial support through the Regents Fellowship during my first three years here at the University of Michigan, Ann Arbor.

I would also like to thank my thesis advisor Divakar Viswanath, without whose financial, emotional and mathematical support, this thesis would not be possible. I would also like to thank my co-advisor John P. Boyd for all of his patience, guidance and support with me while I went through the phases of life. Thank you Divakar and John!

I would also like to thank the members of my committee: Robert Krasny and Jeffrey Rauch.

Lastly, I want to say thanks to my mom, my wife, my family and my friends for keeping me sane during the roughest times of my life, I LOVE YOU ALL DEEPLY!

TABLE OF CONTENTS

LIST OF FIGURES

CHAPTER I

Introduction

Solving differential equations is relevant to the field of scientific computation. Moreover, numerical methods provide a way in which an approximate solution to a differential equation can be found. In this thesis, we add to two approaches of solving differential equations numerically. One is the method of finite differences and the other is the approach of spectral methods. In Chapters II and III of this thesis we add to the approach of finite differences. Chapter II and its relevant discussion in the introduction of this thesis is from [29] and Chapter III and its relevant discussion in the introduction of this thesis is from [30]. The author notes that both papers were co-authored with Divakar Viswanath. In Chapter IV of this thesis, we add to the approach of spectral methods. In addition, we discuss the problem of interpolation in Chapter I as it is relevant to both spectral and finite difference methods.

1.1 Finite Difference Weights and Increased Order of Accuracy

Finite difference methods involve replacing a derivative of a function with a weighted combination of function values at a given set of grid points. The weights are called finite difference weights. To make our discussion concrete, consider a smooth function of one real variable $f(z)$. Then an example of a finite difference approximation to $f'(\bar{z})$, the first derivative of $f(z)$ at $\bar{z}$, using only the values of f at the real grid points $\bar{z}$ and $\bar{z}+h$ where $h>0$ is the forward difference approximation [25]. The forward difference approximation is given by

$$f'(\bar{z}) \approx \frac{f(\bar{z}+h)-f(\bar{z})}{h}, \tag{1.1.1}$$

where the finite difference weights are given by $\frac{1}{h}$ and $\frac{-1}{h}$ for the grid points $\bar{z}+h$ and $\bar{z}$ respectively. The geometric interpretation of the forward difference approximation is the slope of the secant line connecting the points $(\bar{z}, f(\bar{z}))$ and $(\bar{z}+h, f(\bar{z}+h))$. Alternatively, one could write a finite difference approximation to $f'(\bar{z})$ using only the values of f at the points $\bar{z}-h$ and $\bar{z}$ with the backward difference approximation [25]. The backward difference approximation is given by

$$f'(\bar{z}) \approx \frac{f(\bar{z})-f(\bar{z}-h)}{h}, \tag{1.1.2}$$

where the geometric interpretation is the slope of the secant line connecting $(\bar{z}-h, f(\bar{z}-h))$ and $(\bar{z}, f(\bar{z}))$. Both (1.1.1) and (1.1.2) are one-sided approximations to $f'(\bar{z})$ in the sense that the only information used to approximate the derivative of the function lies entirely either to the right or to the left of $f(\bar{z})$. One could rectify this by taking the average of the above two one-sided approximations. This gives rise to a two-sided approximation, the

centered difference approximation [25], for one derivative

$$f'(\bar{z}) \approx \frac{f(\bar{z}+h) - f(\bar{z}-h)}{2h}, \tag{1.1.3}$$

whose geometric interpretation is the slope of the secant line connecting the points $(\bar{z} - h, f(\bar{z}-h))$ and $(\bar{z}+h, f(\bar{z}+h))$.

The order of accuracy of (1.1.1), (1.1.2) and (1.1.3) is determined by computing the error in the approximation. The error in the approximation can be found by taking a Taylor Series expansion. The relevant Taylor Series are

$$\begin{aligned} f(\bar{z}+h) &= f(\bar{z}) + f'(\bar{z})h + \frac{f''(\bar{z})}{2}h^2 + \frac{f'''(\bar{z})}{3!}h^3 + \frac{f^{(4)}(\bar{z})}{4!}h^4 + O(h^5), \\ f(\bar{z}-h) &= f(\bar{z}) - f'(\bar{z})h + \frac{f''(\bar{z})}{2}h^2 - \frac{f'''(\bar{z})}{3!}h^3 + \frac{f^{(4)}(\bar{z})}{4!}h^4 + O(h^5). \end{aligned} \tag{1.1.4}$$

Then the error in the forward, backward and central difference approximations are given by

$$\begin{aligned} \frac{f(\bar{z}+h) - f(\bar{z})}{h} - f'(z) &= \frac{f''(\bar{z})}{2}h + O(h^2), \\ \frac{f(\bar{z}) - f(\bar{z}-h)}{h} - f'(z) &= \frac{-f''(\bar{z})}{2}h + O(h^2), \\ \frac{f(\bar{z}+h) - f(\bar{z}-h)}{2h} - f'(z) &= \frac{f'''(\bar{z})}{6}h^2 + O(h^3) \end{aligned} \tag{1.1.5}$$

respectively. The order of accuracy of the forward and backward difference approximations are said to be $O(h)$ as the error takes this form. Moreover, the order of accuracy of the central difference approximation is higher by one and is $O(h^2)$.

Finite difference approximations can be used to approximate higher order derivatives. An example of a finite difference approximation to $f''(\bar{z})$, the second derivative of $f(z)$ at $\bar{z}$, using

the values of f at the points $\bar{z}-h$, $\bar{z}$ and $\bar{z}+h$ is the central difference approximation [25] for the second derivative

$$f''(\bar{z}) \approx \frac{f(\bar{z}+h) - 2f(\bar{z}) + f(\bar{z}-h)}{h^2}. \tag{1.1.6}$$

An example of a finite difference approximation to $f''(\bar{z})$ that is uncentered is the forward difference approximation to the second derivative which uses the values of f at the grid points $\bar{z}$, $\bar{z}+h$ and $\bar{z}+2h$. The forward difference approximation to the second derivative is given by

$$f''(\bar{z}) \approx \frac{f(\bar{z}+2h) - 2f(\bar{z}+h) + f(\bar{z})}{h^2}. \tag{1.1.7}$$

Again the error in the finite difference approximations (1.1.6) and (1.1.7) can be computed by Taylor Series expansion. The relevant Taylor Series are shown in (1.1.4) where the Taylor Series for $f(\bar{z}+2h)$ is obtained by plugging in $2h$ for h in the Taylor Series expansion of $f(\bar{z}+h)$.

The errors in (1.1.6) and (1.1.7) are then given by

$$\begin{aligned} \frac{f(\bar{z}+h) - 2f(\bar{z}) + f(\bar{z}-h)}{h^2} - f''(\bar{z}) &= \frac{f^{(4)}(\bar{z})}{12}h^2 + O(h^4), \\ \frac{f(\bar{z}+2h) - 2f(\bar{z}+h) + f(\bar{z})}{h^2} - f''(\bar{z}) &= f'''(\bar{z})h + O(h^2), \end{aligned} \tag{1.1.8}$$

respectively. Thus, the order of accuracy of the central difference approximation to the second derivative is higher by one and is $O(h^2)$.

In general, finite difference approximations can be used to approximate $f^{(m)}(\bar{z})$, the m-th order derivative of $f(z)$ at $z=\bar{z}$ where $m \geq 1$. As we show in the discussion preceding Section 2.1, we may first construct a finite difference approximation to $f^{(m)}(0)$, the m-th

order derivative of $f(z)$ at $z = 0$, and then by merely shifting grid points approximate the m-th derivative of f at any other point. Hence, if given the distinct grid points hz_i, where $1 \leq i \leq N$ and h is the mesh parameter, the basic problem in constructing finite difference approximations is to approximate $f^{(m)}(0)$ using the values of f at these N grid points. The grid points can be taken as $z_1, \ldots, z_N$ by setting the mesh parameter $h = 1$.

In the spirit of formulas (1.1.1), (1.1.2), (1.1.3), (1.1.6) and (1.1.7) the finite difference approximation to $f^{(m)}(0)$ is expressed as

$$f^{(m)}(0) \approx \frac{\sum_{k=1}^{N} w_{k,m} f(hz_k)}{h^m}, \tag{1.1.9}$$

where $\frac{w_{k,m}}{h^m}$ are the finite difference weights. By setting the mesh parameter to 1, the finite difference approximation to $f^{(m)}(0)$ may also be expressed as

$$f^{(m)}(0) \approx \sum_{k=1}^{N} w_{k,m} f(z_k). \tag{1.1.10}$$

If we require (1.1.9) to have an error that is $\mathcal{O}\left(h^{N-m}\right)$ for a smooth function f, the choice of the weights $w_{k,m}$, $1 \leq k \leq N$, is unique (see Section 2.2). However for certain grids, these unique weights imply an error of $\mathcal{O}\left(h^{N-m+1}\right)$, which is one order higher than what is typical for the m-th derivative with N grid points. This is termed as superconvergence or boosted order of accuracy [29].

We have already seen that the centered finite difference approximations for the first and second derivative of a smooth function f at the point $\bar{z}$, equations (1.1.3) and (1.1.6) respectively, exhibit a boosted order of accuracy. There is a false perception that this boosted order of accuracy is related to a symmetric choice of grid points about $\bar{z}$. In fact, there are

unsymmetrical finite difference formulas that too exhibit a boosted order of accuracy. An example of such an unsymmetrical finite difference approximation with a boosted order of accuracy is the finite difference approximation to the second derivative at $z = 0$ using the three grid points where $z_1 = -3$, $z_2 = 1$ and $z_3 = 2$ (see below) [29].

In Chapter II of this thesis we explain when this boosted order of accuracy occurs. We show that if the grid points are fixed, there exists unique weights $w_{k,m}$ such that the order of accuracy of (1.1.9) is $O(h^{N-m})$. And that for real grid points, the order of accuracy can be increased by at most one. The order of accuracy of (1.1.9) is increased by one (i.e. $O(h^{N-m+1})$ which is a boosted order of accuracy) if and only if [29]

$$S_{N-m} = 0, \tag{1.1.11}$$

where S_p is the elementary symmetric function given by

$$S_p := \sum_{1 \le i_1 < \ldots < i_p \le N} z_{i_1} \ldots z_{i_p}. \tag{1.1.12}$$

This algebraic result explains why the example given above of a finite difference approximation to the second derivative at $z = 0$ using the three real grid points where $z_1 = -3$, $z_2 = 1$ and $z_3 = 2$, has a boosted order of accuracy. For the special case $m = 2$ and $N = 3$, equation (1.1.11) requires the grid points to satisfy $z_1 + z_2 + z_3 = 0$ to achieve a boosted order of accuracy. The grid points clearly satisfy this condition.

Moreover we show that if the grid points are allowed to be complex, then the order of accuracy of (1.1.9) can be increased by no more than m, the order of the derivative. The

order of accuracy is increased by b with $1 \leq b \leq m$ if and only if [29]

$$S_{N-m} = S_{N-m+1} = \cdots = S_{N-m+b-1} = 0. \tag{1.1.13}$$

For complex grid points, the maximum boost in the order of accuracy is obtained when the grid points are at the vertices of a regular N sided polygon centered at 0, with 0 being the point at which the derivative is to be approximated.[1]

In Chapter II of this thesis we also discuss an efficient method, the method of partial products, for the computation of the weights $w_{k,m}$. In [16–18] Fornberg describes an algorithm for determining the weights $w_{k,m}$ when the grid points are given by z_k. His derivation begins with the Lagrange interpolant. As is well known (which we shall review), there exists a unique polynomial $\pi(z)$ of degree $N-1$ which satisfies the interpolation conditions $\pi(z_k) = f_k$ for $k = 1 \ldots N$ [11]. The Lagrange form of this interpolating polynomial is given by

$$\pi(z) = \sum_{k=1}^{N} w_k \pi_k(z) f_k \text{ where } \pi_k(z) = \prod_{j \neq k} (z - z_j) \text{ and } w_k = 1/\pi_k(z_k), \tag{1.1.14}$$

where w_k is the Lagrange weight at z_k. The finite difference weight $w_{k,m}$ is equal to the coefficient of z^m in $w_k \pi_k(z)$ times $m!$ (see Section 2.2). The computation of the Lagrange weights w_k takes $2N^2 - 2N$ arithmetic operations [29]. The exact operation count for Fornberg's algorithm is given in Lemma 2 of [29]. The author notes that the method of partial products uses less memory and fewer arithmetic operations than Fornberg's algorithm [29]. The operation count is lower by a factor of $(5m+5)/4$, where m is the order of the derivative, in the limit of large N [29].

[1] We thank Professor Jeffrey Rauch for this observation.

1.2 Barycentric Hermite Weights and Updates

In Chapter III of this thesis, we discuss the problem of Hermite interpolation. Hermite interpolation involves interpolating the value of a function and potentially, *successive* values of the derivative of that function on a set of grid points. An example of a Hermite interpolation problem is to find a polynomial interpolant, $\pi(z)$, that satisfies the conditions

$$\pi(z_1) = f_1,\ \pi'(z_1) = f_1^{'},\ \pi(z_2) = f_2 \text{ and } \pi'(z_2) = f_2^{'}. \tag{1.2.1}$$

where the grid points are $z_1 = -1$ and $z_2 = 1$ [30]. Evidently, the polynomial interpolant that satisfies (1.2.1) must not only pass through the function at z_1 and z_2, but must also pass through the function with the correct slopes at z_1 and z_2. In this example, the number of conditions specified at z_1 and z_2, which we call n_1 and n_2 respectively, are both 2. We let $N := n_1 + n_2$. Davis in [11] shows that there exists a unique polynomial of degree at most $N-1 = 3$, called the Hermite interpolant, that satisfies the conditions (1.2.1). Moreover, the Hermite interpolant may be expressed in either of two forms, the Newton or barycentric form. In this thesis, we consider only the barycentric form due to issues of numerical instability with the Newton form [15,33,34]. The Hermite interpolant $\pi(z)$ in barycentric form, which satisfies (1.2.1), is given by [30]

$$\begin{aligned}\pi(z) &= (z-1)^2(z+1)^2\left(f_1\left(\frac{1}{4(z+1)^2}+\frac{1}{4(z+1)}\right)+\frac{f_1^{'}}{4(z+1)}\right.\\ &\quad \left.+f_2\left(\frac{1}{4(z-1)^2}-\frac{1}{4(z-1)}\right)+\frac{f_2^{'}}{4(z-1)}\right).\end{aligned} \tag{1.2.2}$$

We now provide a thorough explanation of the construction of the above formula. The

Hermite interpolation conditions (1.2.1) are equivalent to the conditions that the Taylor series about $z = z_1$ and $z = z_2$ of $\pi(z)$ is $f_1 + f_1'(z - z_1)$ and $f_2 + f_2'(z - z_2)$ respectively. Moreover, by the uniqueness of $\pi(z)$, $\pi(z)$ is the unique polynomial of degree at most 3 which has these Taylor series about $z = z_1$ and $z = z_2$. Thus, if we can find a polynomial of degree at most 3 that has the "right" Taylor series expansions, then we have the unique Hermite interpolant. With this in mind, we construct $\pi(z)$ with two "fundamental" polynomials of degree 3, p_1 and p_2. The role of p_1 is to ensure that $\pi(z)$ has the right Taylor series about $z = z_1$ while not interfering with the required terms in the Taylor Series of $\pi(z)$ about $z = z_2$. To not interfere with the required terms terms in the Taylor Series about $z = z_2$, p_1 must be $O((z - z_2)^2)$ as $z \to z_2$. Similarly the role of p_2 is to ensure that $\pi(z)$ has the right Taylor series at $z = z_2$ while not interfering with the required terms in the Taylor Series of $\pi(z)$ about $z = z_1$. Hence, p_2 must be $O((z - z_1)^2)$ as $z \to z_1$. These Taylor Series conditions on p_1 and p_2 can be explicitly summarized as

$$\begin{aligned}
p_1(z) &= f_1 + f_1'(z - z_1) + O((z - z_1)^2) \text{ as } z \to z_1, \\
p_1(z) &= O((z - z_2)^2) \text{ as } z \to z_2, \\
p_2(z) &= O((z - z_1)^2) \text{ as } z \to z_1, \\
p_2(z) &= f_2 + f_2'(z - z_2) + O((z - z_2)^2) \text{ as } z \to z_2.
\end{aligned} \tag{1.2.3}$$

The Taylor Series Conditions (1.2.3) are equivalent to the conditions

$$\begin{aligned} p_1(z_1) = f_1, \quad p_1(z_2) = 0 \\ p_1'(z_1) = f_1', \quad p_1'(z_2) = 0 \end{aligned}$$

and

$$\begin{aligned} p_2(z_1) = 0, \quad p_2(z_2) = f_2 \\ p_2'(z_1) = 0, \quad p_2'(z_2) = f_2'. \end{aligned} \tag{1.2.4}$$

If p_1 and p_2 satisfy the above conditions, we can easily see that p_1+p_2 is a degree 3 polynomial that satisfies (1.2.1). Hence, we can construct $\pi(z)$ from p_1 and p_2 in the following manner

$$\pi(z) = p_1 + p_2. \tag{1.2.5}$$

As previously mentioned, it is evident that p_1 must be a degree 3 polynomial that contains the terms $(z-z_2)^2$ and with the right Taylor series expansion of $f_1 + f_1'(z-z_1) + O((z-z_1)^2)$ about $z = z_1$. To construct p_1, we need to have a way to "undo" the effect of multiplication by $(z-z_2)^2$ in the Taylor Series of p_1 about $z = z_1$. To do so, we note that the Taylor Series of $(z-z_2)^{-2}$ about $z = z_1$ is given by

$$(z-z_2)^{-2} = w_{1,0} + w_{1,1}(z-z_1) + O((z-z_1)^2) \tag{1.2.6}$$

where $w_{1,0} = 1/4$ and $w_{1,1} = 1/4$. Let $W_1(z)$ denote the truncated Taylor Series of $(z-z_2)^{-2}$

so that $W_1(z) = (z - z_2)^{-2} + O((z - z_1)^2)$. Hence,

$$W_1(z) := w_{1,0} + w_{1,1}(z - z_1), \tag{1.2.7}$$

and

$$(z - z_2)^2 W_1(z) = 1 + O((z - z_1)^2). \tag{1.2.8}$$

In other words, the polynomial $W_1(z)$ undoes the effect of multiplication by $(z - z_2)^2$ just enough to ensure that $(z - z_2)^2 W_1(z) \times (f_1 + f_1^{'}(z - z_1)) = f_1 + f_1^{'}(z - z_1) + O((z - z_1)^2)$ as $z \to z_1$ and $(z - z_2)^2 W_1(z) \times (f_1 + f_1^{'}(z - z_1)) = O((z - z_2)^2)$ as $z \to z_2$. Thus, $(z - z_2)^2 W_1(z) \times (f_1 + f_1^{'}(z - z_1))$ has the desired Taylor series about $z = z_1$ and $z = z_2$. Unfortunately, $(z - z_2)^2 W_1(z) \times (f_1 + f_1^{'}(z - z_1))$ is a degree 4 polynomial. However, this can be easily fixed, as we will show, by dropping all terms of order $(z - z_1)^2$ and higher in the polynomial $W_1(z) \times (f_1 + f_1^{'}(z - z_1))$ and then multiplying by $(z - z_2)^2$ to obtain the degree 3 polynomial $p_1(z)$.

If we drop all terms of order $(z - z_1)^2$ and higher in the polynomial $W_1(z) \times (f_1 + f_1^{'}(z - z_1))$ we obtain

$$\tilde{W}_1(z) \;:=\; f_1 W_1(z) + f_1^{'}(z - z_1)(W_1(z) - w_{1,1}(z - z_1)). \tag{1.2.9}$$

Multiplying by $(z - z_2)^2$ and observing (1.2.8) yields

$$\begin{aligned} (z - z_2)^2 \tilde{W}_1(z) &= f_1 W_1(z)(z - z_2)^2 + f_1^{'}(z - z_1) W_1(z)(z - z_2)^2 + O(z - z_1)^2, \\ &= f_1 + f_1^{'}(z - z_1) + O((z - z_1)^2). \end{aligned} \tag{1.2.10}$$

This is the desired Taylor Series expansion as $z \to z_1$. Clearly $(z - z_2)^2 \tilde{W}_1(z)$ is $O((z - z_2)^2)$

as $z \to z_2$. Thus, the fundamental polynomial $p_1(z)$ is given by

$$\begin{aligned} p_1(z) &= (z-z_2)^2 \tilde{W}_1(z) \\ &= (z-1)^2(z+1)^2 \left(f_1 \left(\frac{1}{4(z+1)^2} + \frac{1}{4(z+1)} \right) + \frac{f_1'}{4(z+1)} \right) \end{aligned} \tag{1.2.11}$$

where the second line is obtained by factoring out $(z+1)^2$ and plugging in the numerical value for z_2 and the expression for $\tilde{W}_1(z)$ using (1.2.9) and (1.2.7) with the numerical values of $w_{1,0} = 1/4$ and $w_{1,1} = 1/4$.

We can use this same line of reasoning to obtain p_2. Summing the resulting expression for p_2 with p_1 gives the barycentric representation of the Hermite interpolant, $\pi(z)$, in (1.2.2).

We now turn to the general Hermite interpolation problem. Let z_k, where $1 \leq k \leq K$, denote the distinct grid points with the associated data $f^{(0)}(z_k), \ldots, f^{(n_k-1)}(z_k)$ and let $N := \sum_{k=1}^{K} n_k$. The problem of Hermite interpolation is to find the polynomial interpolant of degree $N-1$, $\pi(z)$, that interpolates the value of the function and its first n_k-1 derivatives at each grid point z_k in the list $z_1, \ldots, z_K$. Hence, $\pi(z)$ must pass through all the grid points with the specified slopes. We can express the mathematical conditions that $\pi(z)$ satisfies as

$$\left. \frac{d^r \pi(z)}{dz^r} \right|_{z=z_k} = f_{k,r} \quad \text{for} \quad r = 0, \ldots, n_k - 1, \quad 1 \leq k \leq K, \tag{1.2.12}$$

where $f^{(r)}(z_k)$ is denoted by $f_{k,r}$ [30]. An elegant proof of the uniqueness and existence of the general Hermite interpolant can be found in [11].

The barycentric form of the general Hermite interpolant is given by

$$\pi(z) = \pi^*(z) \sum_{k=1}^{K} \frac{f_{k,n_k-1}}{(n_k-1)!} \left(\frac{w_{k,0}}{(z-z_k)} \right) + \frac{f_{k,n_k-2}}{(n_k-2)!} \left(\frac{w_{k,0}}{(z-z_k)^2} + \frac{w_{k,1}}{(z-z_k)} \right) + \cdots + f_{k,0} \left(\frac{w_{k,0}}{(z-z_k)^{n_k}} + \cdots + \frac{w_{k,n_k-1}}{(z-z_k)} \right), \tag{1.2.13}$$

where $\pi^*(z) := \prod_{k=1}^{K} (z-z_k)^{n_k}$. The general Hermite interpolant, $\pi(z)$, shown in (1.2.13) is clearly a polynomial of degree $N-1$. Moreover, the choice of barycentric weights, $w_{k,r}$, is uniquely determined by the interpolation conditions $\pi(z)$ must satisfy (1.2.12). In Chapter III, we review a derivation to formula (1.2.13) and show why it is the Hermite interpolant.

In this thesis, we are concerned with computing and updating the unique barycentric weights $w_{k,r}$. We provide a more direct derivation of the method of Butcher et al. [24] for computing the barycentric weights. Our approach also lends itself to an efficient method for updating the barycentric weights. If an additional data item is added to a current grid point or at a new grid point, our method uses only $\mathcal{O}(N)$ operations to update all barycentric weights (see Section 3.3).

1.3 The General Finite Interpolation Problem

In this section, we review an elegant approach by Davis [11] to the problem of interpolation that is relevant to Lagrange and Fourier interpolation which are widely used throughout this thesis. This section shamelessly borrows from Chapter 2 of [11]. As is well known, if one has a set of grid points, z_i, where $1 \leq i \leq N$, with the associated data f_i, there exists a unique polynomial interpolant of degree at most $N-1$ that passes through them. Hence, there is a unique polynomial interpolant, $\pi(z)$, whose degree is at most $N-1$ that satisfies

the conditions

$$\pi(z_i) = f_i \quad \text{for} \quad 1 \leq i \leq N. \tag{1.3.1}$$

Davis attempts to generalize the problem of polynomial interpolation via the so called general problem of interpolation by inquiring if one can construct an interpolant (polynomial or other) based instead on any N arbitrary pieces of information.

To state the general problem of interpolation formally, let V denote a vector space of dimension N over a field F and let V^* denote the dual space of V (recall the dimension of V^* is also N [21]). Moreover, let $L_1, \ldots, L_N$ denote N linear functionals in V^*. Hence, L_i, for all $i \in \{1, \ldots, N\}$, is a linear mapping from V to F . The general problem of interpolation then asks if given a list of values f_i, where $1 \leq i \leq N$, does there exist a π in V that satisfies the conditions

$$L_i(\pi) = f_i \quad \text{for} \quad 1 \leq i \leq N? \tag{1.3.2}$$

Davis [11] shows that the answer to this question is: yes, there does exist a solution π in V if and only if $L_1, \ldots, L_N$ form a basis for V^*. Moreover, the solution, π, is unique. We state this result of Davis below. Its proof can be found in [11].

Theorem 1. *Let V and V^* denote a vector space over a field F and its dual respectively with dimension N. Let $L_1, \ldots, L_N$ be N linear functionals in V^*. Then* (1.3.2) *has a solution, π in V, for a list of values f_i where $1 \leq i \leq N$, if and only if $L_1, \ldots, L_N$ form a basis for V^*. Moreover, π is the unique solution.*

To determine if $L_1, \ldots, L_N$ form a basis for V^*, Davis provides a useful result shown below. Its proof can be found in [11].

Theorem 2. *Let V and V^* denote a vector space over a field F and its dual respectively*

with dimension N. Let $\beta = \{P_1, ..., P_N\}$ denote a basis for V and let $L_1, \ldots, L_N$ be N linear functionals in V^*. Then if

$$|L_i(P_j)| \neq 0, \tag{1.3.3}$$

where $|L_i(P_j)|$ represents the determinant of the matrix whose (i,j)-th entry is $L_i(P_j)$, the set of linear functionals $L_1, \ldots, L_N$ form a basis for V^*.

Two applications of the general problem of interpolation are Lagrange and Fourier interpolation. Using the framework of the general problem of interpolation, we review the existence of the Lagrange and Fourier interpolants. We also review an elegant derivation of the Lagrange and Fourier interpolants using a few basic results from Linear Algebra which we now turn to.

1.3.1 Representation of vectors in V and V^* using a basis and its dual

We continue with our notation above and let V represent an N dimensional vector space over a field F and V^* its dual. Let $\beta = \{P_1, ..., P_N\}$ be a basis for V. Then there exists a unique basis, $\beta^* = \{L_1, ..., L_N\}$ for V^* such that $L_i(P_j) = \delta_{ij}$ for $1 \leq i, j \leq N$ [21]. We call β^* the dual basis of β. Moreover for each linear functional L on V, we have [21]

$$L = \sum_{i=1}^{N} L(P_i) L_i \tag{1.3.4}$$

and for each $\pi \in V$ we have the following representation [21]

$$\pi = \sum_{i=1}^{N} L_i(\pi) P_i. \tag{1.3.5}$$

It is readily seen that $L_i(\pi)$ is the i-th coordinate of π expressed in the basis β. We think of (1.3.5) as a way of writing any $\pi \in V$ by merely sampling π. That is by sampling π in accordance to the linear functionals in β^*, we may reconstruct π in terms of the sampled values. Verification of the above statements are shown below [21].

Theorem 3. *Let V and V^* denote a vector space over a field F and its dual respectively with dimension N. Let $\beta = \{P_1, ..., P_N\}$ be a basis for V* and *$\beta^* = \{L_1, ..., L_N\}$ its dual basis. Then any π in V may be expressed as $\pi = \sum_{i=1}^{N} L_i(\pi) P_i$.*

Proof. As the P_i's form a basis for V, we have $\pi = \sum_{i=1}^{N} c_i P_i$. Hence $L_j(\pi) = \sum_{i=1}^{N} c_i L_j(P_i) = c_j$. Thus, $\pi = \sum_{i=1}^{N} L_i(\pi) P_i$. □

Theorem 4. *Let V and V^* denote a vector space over a field F and its dual respectively with dimension N. Let $\beta = \{P_1, ..., P_N\}$ be a basis for V* and *$\beta^* = \{L_1, ..., L_N\}$* its dual basis. *Then any L in V^* may be expressed as $L = \sum_{i=1}^{N} L(P_i) L_i$.*

Proof. As the L_i's form a basis for V^*, we have $L = \sum_{i=1}^{N} a_i L_i$. Hence $L(P_j) = \sum_{i=1}^{N} a_i L_i(P_j) = a_j$. Thus $L = \sum_{i=1}^{N} L(P_i) L_i$. □

1.3.2 Lagrange Interpolation

Let V represent the N dimensional space of polynomials whose degree is at most $N-1$. In the general problem of interpolation, the L_i's specify the type of interpolation. For the case of Lagrange interpolation, we let $L_i(\pi) = \pi(z_i)$ for $1 \leq i \leq N$. The general interpolation

problem applied to the case of Lagrange interpolation is then: given the data f_i at the grid point z_i, $1 \leq i \leq N$, can we find a unique $\pi \in V$ such that

$$L_i(\pi) = f_i \text{ for } 1 \leq i \leq N? \tag{1.3.6}$$

To answer yes, Theorem 1 requires the L_i's to form a basis for V^*. To show that $\beta^* = \{L_1, \ldots, L_N\}$ forms a basis for the N dimensional space V^*, it is sufficient to show that they are linearly independent which we now do.

Lemma. *$L_1, ..., L_N$ are linearly independent functionals on V.*

Proof. Let $L := \sum_{i=1}^{N} c_i L_i$. If $L = 0$ (i.e. $L(p) = 0$ for all $p \in V$), then $L(1) = 0$, $L(z) = 0, ...,$ $L(z^{N-1}) = 0$. As $L_i(\pi) = \pi(z_i)$, we have

$$\begin{pmatrix} 1 & \ldots & 1 \\ z_1 & \ldots & z_n \\ z_1^2 & \ldots & z_n^2 \\ \vdots & \vdots & \vdots \\ z_1^{N-1} & \ldots & z_n^{N-1} \end{pmatrix} \begin{pmatrix} c_1 \\ c_2 \\ c_3 \\ \vdots \\ c_n \end{pmatrix} = 0.$$

As the Vandermonde matrix shown above is non-singular [11], we have $c_i = 0$ for all i. Hence, the linear functionals $L_1, ..., L_N$ are linearly independent. □

To actually construct the Lagrange interpolant, we wish to express π as a linear combination of the data $L_i(\pi) = f_i$. To do so, we merely refer to (1.3.5). Hence, we are now left with finding the basis β for V whose dual is β^*. Equation (1.3.5) then provides the π in V, which we call the Lagrange interpolant, that solves our interpolation problem.

To find the basis $\beta = \{P_1, \ldots, P_N\}$ whose dual is β^*, we need to find polynomials P_j of degree at most $N-1$ that satisfy

$$\begin{aligned} L_i(P_j) &= \delta_{ij} \ 1 \leq i, j \leq N, \\ P_j(z_i) &= \delta_{ij} \ 1 \leq i, j \leq N. \end{aligned} \tag{1.3.7}$$

We observe the following choice of polynomial P_j will satisfy the above condition

$$P_j(z) = \prod_{i \neq j} \left(\frac{z - z_i}{z_j - z_i} \right). \tag{1.3.8}$$

We call the polynomials P_j the *cardinal functions* of polynomial interpolation. By (1.3.5), we have

$$\pi = \sum_{i=1}^{N} L_i(\pi) P_i = \sum_{i=1}^{N} f_i P_i. \tag{1.3.9}$$

Thus, we have constructed the π in V, which solves the Lagrange interpolation problem (1.3.6). Observe $\pi(\bar{z})$, (for some fixed value of $\bar{z}$) can be written in terms of the data values f_i, it simply is: $\pi(\bar{z}) = \sum_{i=1}^{N} f_i P_i(\bar{z})$.

1.3.3 Fourier Interpolation

Let V represent the $2n+1$ dimensional space of trigonometric polynomials where

$$\{v_i\}_{i=0}^{2n} = \{1, \sin(\tau), \cos(\tau), \sin(2\tau), \cos(2\tau), ..., \sin(n\tau), \cos(n\tau)\} \tag{1.3.10}$$

is a basis for V. We consider the following linear functionals $\{L_i\}_{i=0}^{2n} \in V^*$ where

$$\begin{aligned} L_0(\pi) &= \frac{1}{2\pi}\int_{-\pi}^{\pi} p(\tau)dx, \\ L_{2k}(\pi) &= \frac{1}{\pi}\int_{-\pi}^{\pi} p(\tau)\cos(k\tau)d\tau,\ k \in \{1,\dots,n\}, \\ L_{2k-1}(\pi) &= \frac{1}{\pi}\int_{-\pi}^{\pi} p(\tau)\sin(k\tau)d\tau,\ k \in \{1,\dots,n\}. \end{aligned} \tag{1.3.11}$$

We aim to show there is a unique solution, $p(\tau) \in V$, to the interpolation problem

$$\begin{aligned} L_0(p) &= \frac{a_0}{2}, \\ L_{2i}(p) &= a_i \text{ for } 1 \le i \le n, \qquad (1.3.12) \\ L_{2i-1}(p) &= b_i \text{ for } 1 \le i \le n. \qquad (1.3.13) \end{aligned}$$

By Theorem 1 and Theorem 2, it suffices to show $|L_i(v_j)| \neq 0$. Observe by orthogonality, $L_i(v_j) = \delta_{ij}$. Hence, $|L_i(v_j)| \neq 0$ and the interpolation problem, (1.3.13), possesses a unique solution $p(\tau)$.

To construct the Fourier interpolant, we observe that as $L_i(v_j) = \delta_{ij}$ for all $0 \le i, j \le 2n$, $\{L_i\}_{i=0}^{2n}$ is the dual basis of $\{v_i\}_{i=0}^{2n}$. By (1.3.5), we can express the Fourier interpolant as

$$\begin{aligned} p(\tau) &= \sum_{i=0}^{2n} L_i(p)v_i = \frac{a_0}{2} + \sum_{k=1}^{n} a_k\cos(k\tau) + b_k\sin(k\tau), \\ a_k &= \frac{1}{\pi}\int_{-\pi}^{\pi} \pi(\tau)\cos(k\tau)d\tau,\ k \in \{0,\dots,n\}, \\ b_k &= \frac{1}{\pi}\int_{-\pi}^{\pi} \pi(\tau)\sin(k\tau)d\tau,\ k \in \{1,\dots,n\}. \end{aligned} \tag{1.3.14}$$

1.4 Quasi-Uniform Spectral Scheme (QUSS)

What is a QUSS? It is a spectral method that employs a more uniform spatial grid than the Chebyshev grid [5]. Why use a grid more uniform than the Chebyshev grid? Well, a very good reason is that the Chebyshev grid with N points has a grid spacing that's $O\left(\frac{1}{N^2}\right)$ near the endpoints of its interval. Hence, use of a Chebyshev grid for the spatial discretization of a time dependent PDE with an explicit scheme for time marching results in a CFL condition that requires a tiny time step of $O\left(\frac{1}{N^2}\right)$ even for solutions which have no large gradients near the boundary [34]. In Chapter IV of this thesis we explore three different mappings (KT, Elliptic and Theta) that are capable of producing a grid more uniform than the Chebyshev grid. The grids produced by the mappings vary from the Chebyshev grid to the uniform grid as their map parameter, β, varies (see Section 4.6). For reasons explained in Chapter IV of this thesis, we only explore the mappings in the context of a mapped cosine basis (so we don't use a grid more uniform than the Chebyshev grid with a polynomial basis). Hence, when we approximate a function via interpolation with a so called mapped cosine interpolant (see 4.8.2), we move beyond just polynomial interpolation, but rather, to an interpolant that varies from a polynomial to a trigonometric one whose interpolation points vary from Chebyshev to uniform grid points respectively. In our construction of the mapped cosine interpolant to approximate a function $f(x)$, we interpolate the mapped function $F(\tau;\beta) = f(\mathcal{X}(\tau;\beta))$ in the computational coordinate τ with a trigonometric interpolant, $P_{N-1}(\tau;\beta)$, in uniform grid points where $\mathcal{X}(\tau;\beta)$ is one of the three mappings: KT, Elliptic or Theta with map parameter β (see 4.3, 4.4 and 4.5). We obtain our interpolant of $f(x)$, $p_{N-1}(x;\beta)$, by mapping $P_{N-1}(\tau;\beta)$ back to the physical coordinate via $p_{N-1}(x;\beta) = P_{N-1}(\mathcal{T}(x;\beta);\beta)$ where $\mathcal{T}(x;\beta)$ is the inverse of $\mathcal{X}(\tau;\beta)$ (see

4.8.2).

Moving beyond polynomial interpolation is obviously not new and is surveyed elegantly in Chapter 22 of Trefethen's new book [36]. However, our aim in this chapter of the thesis, is to give practical advice of how one should pick the map parameter β (or more, accurately, how not to pick the map parameter, hint: not too close to its uniform limit) and determine if one of the three mappings, KT, Elliptic or Theta is a clear winner in terms of accuracy of interpolating the function

$$f(x; s, \gamma) = \frac{\gamma^2}{\gamma^2 + (x - s)^2} \tag{1.4.1}$$

as γ and N, the number of interpolation points, is varied (see 4.10).

CHAPTER II

Finite Difference Weights and Increased Order of Accuracy

In light of our discussion of Lagrange Interpolation, we would like to generate a finite difference approximation to the m-th order derivative of a function based on only the values of the function at select grid points. Specifically, let $z_1, \ldots, z_N$ be N distinct points with data $f_1, ..., f_N$ as the function values at the grid points respectively (i.e. $f(z_i) = f_i$, $1 \leq i \leq N$). Let V represent the space of polynomials whose degree is at most $N-1$. Then there exists a unique polynomial interpolant $\pi \in V$ such that $\pi(z_j) = f(z_j)$, $1 \leq j \leq N$ [11]. Moreover, as illustrated in Section 1.3, the polynomial interpolant may be expressed as $\pi(z) = \sum_{k=1}^{N} f_k P_k(z)$. Let $\pi_k(z) := \prod_{j \neq k}(z - z_j)$ and $w_k := 1/\pi_k(z_k)$. Then the interpolant is

$$\pi(z) = \sum_{k=1}^{N} w_k f_k \pi_k(z). \tag{2.0.2}$$

By differentiating our interpolant, we can obtain a finite difference approximation for the m-th derivative $f^{(m)}(0)$ (where $1 \leq m \leq M$). That is,

$$\frac{d^m \pi(z)}{dz^m}\Big|_{z=0} = \sum_{k=1}^{N} \frac{d^m P_k(z)}{dz^m}\Big|_{z=0} f_k. \tag{2.0.3}$$

Let

$$c_{k,m} := \frac{d^m \pi_k(z)}{dz^m}\Big|_{z=0}/m! \tag{2.0.4}$$

and

$$w_{k,m} := m! c_{k,m} w_k = \frac{d^m P_k(z)}{dz^m}\Big|_{z=0}, \tag{2.0.5}$$

then we have

$$\frac{d^m \pi(z)}{dz^m}\Big|_{z=0} = m! \sum_{k=1}^{N} c_{k,m} w_k f_k. \tag{2.0.6}$$

Our finite difference formula for the m-th derivative $f^{(m)}(0)$ is then given by

$$\frac{d^m f(z)}{dz^m}\Big|_{z=0} \approx \sum_{k=1}^{N} w_{k,m} f_k. \tag{2.0.7}$$

Moreover, we observe that $c_{k,m}$ and $w_{k,m}/m!$ are the coefficients of z^m in $\pi_k(z)$ and $P_k(z)$ respectively.

In addition, we may by exercise of the chain rule, obtain a finite difference formula using the grid points $hz_1, \ldots, hz_N$. Let $y := hz$. We wish to find a finite difference approximation to $\frac{d^m f(y)}{dy^m}\Big|_{y=0}$. Noting

$$\frac{d^m f(y(z))}{dz^m} = \frac{d^m f(y(z))}{dy^m} h^m, \tag{2.0.8}$$

we have

$$\frac{d^m f(y(z))}{dy^m}\Big|_{y(z)=y(0)} = \frac{d^m f(y(z))}{dz^m}\Big|_{z=0}/h^m. \tag{2.0.9}$$

Hence, the desired finite difference formula is given by

$$\frac{d^m f(y)}{dy^m}\Big|_{y=0} = f^{(m)}(0) \approx \frac{\sum_{k=1}^{N} w_{k,m} f(hz_k)}{h^m}. \tag{2.0.10}$$

Moreover, we may now compute the m-th order derivative of the function at a non-zero point by merely shifting the grid points. That is, to compute our finite difference approximation to $f^{(m)}(\bar{z})$, where $\bar{z}$ is some fixed point, consider the function $g(z) := f(z + \bar{z})$. Then

$$\begin{aligned} g^{(m)}(0) &\approx \frac{\sum_{k=1}^{N} w_{k,m} g(hz_k)}{h^m} \\ &= \frac{\sum_{k=1}^{N} w_{k,m} f(hz_k + \bar{z})}{h^m}. \end{aligned} \tag{2.0.11}$$

Noting $g^{(m)}(0) = f^{(m)}(\bar{z})$, it follows that

$$f^{(m)}(\bar{z}) = \frac{\sum_{k=1}^{N} w_{k,m} f(hz_k + \bar{z})}{h^m}. \tag{2.0.12}$$

2.1 Finite Difference Weights Algorithm Using Partial Products

Let $l_k(z) := \prod_{j=1}^{k}(z - z_j)$ and $r_k(z) := \prod_{j=k}^{N}(z - z_j)$. Observe,

$$\pi_k(z) = l_{k-1}(z) r_{k+1}(z). \tag{2.1.1}$$

Moreover, we denote the coefficients of $1, z, \ldots, z^M$ in $l_k(z)$ and $r_k(z)$ by $L_{k,0}, \ldots, L_{k,M}$ and $R_{k,0}, \ldots, R_{k,M}$, respectively. We compute the coefficients $L_{k,m}$ and $R_{k,m}$ in the order

$k = 1, 2, \ldots, N$ and $k = N, N-1, \ldots, 1$, respectively.

We observe $c_{k,m}$, the coefficient of z^m in $\pi_k(z)$, can be obtained by

$$c_{k,m} = \sum_{s=0}^{m} L_{k-1,m-s} R_{k+1,s}. \tag{2.1.2}$$

The finite difference weight $w_{k,m}$ is obtained by (2.0.5). Computer code may be seen in [29]. The total operation count is fewer than $2N^2 + NM^2 + 8NM - 4M^2 - N + 2M + 2$ [29].

2.2 Increased Order of Accuracy

In this section, we prove a series of theorems regarding the order of accuracy of (2.0.10). We first note the following Lemma.

Lemma 5. *The finite difference formula* (2.0.10) *has an error of* $\mathcal{O}\left(h^{N-m}\right)$ *if and only if*

$$\sum_{k=1}^{N} w_{k,m} z_k^m = m! \quad \textit{and} \quad \sum_{k=1}^{N} w_{k,m} z_k^n = 0 \tag{2.2.1}$$

for $n \in \{0, 1, \ldots, N-1\} / \{m\}$. *The function* f *is assumed to be* N *times continuously differentiable.*

Proof. Suppose $\sum_{k=1}^{N} w_{k,m} z_k^n = 0$ for $n \in \{0, 1, \ldots, N-1\} / \{m\}$ and $\sum_{k=1}^{N} w_{k,m} z_k^m = m!$. Observe by Taylor expansion of $f(y)$ (where $y := hz$) about $y = 0$, we have

$$w_{k,m} f(hz_k) = w_{k,m} \sum_{j=0}^{N-1} (hz_k)^j \frac{f^{(j)}(0)}{j!} + w_{k,m} (hz_k)^N g(hz_k), \quad 1 \le k \le N, \tag{2.2.2}$$

where the last term is the Lagrange Remainder. Hence,

$$\sum_{k=1}^{N} w_{k,m} f(hz_k) = \sum_{j=0}^{N-1} h^j \frac{f^{(j)}(0)}{j!} \sum_{k=1}^{N} w_{k,m} z_k^j + h^N \sum_{k=1}^{N} w_{k,m} z_k^N g(hz_k). \tag{2.2.3}$$

As $\sum_{k=1}^{N} w_{k,m} z_k^n = 0$ for $n \in \{0, 1, \ldots, N-1\} / \{m\}$, we obtain

$$\sum_{k=1}^{N} w_{k,m} f(hz_k) = h^m \frac{f^{(m)}(0)}{m!} \sum_{k=1}^{N} w_{k,m} z_k^m + h^N \sum_{k=1}^{N} w_{k,m} z_k^N g(hz_k). \tag{2.2.4}$$

Moreover, given that $\sum_{k=1}^{N} w_{k,m} z_k^m = m!$, we obtain

$$\sum_{k=1}^{N} w_{k,m} f(hz_k) = h^m f^{(m)}(0) + h^N \sum_{k=1}^{N} w_{k,m} z_k^N g(hz_k). \tag{2.2.5}$$

Thus,

$$\frac{\sum_{k=1}^{N} w_{k,m} f(hz_k)}{h^m} = f^{(m)}(0) + h^{N-m} \sum_{k=1}^{N} w_{k,m} z_k^N g(hz_k). \tag{2.2.6}$$

By continuity of $g(y)$ at $y = 0$, as h approaches zero, the right hand side of the above equation approaches $f^{(m)}(0)$. That is, (2.0.10), has error of $\mathcal{O}\left(h^{N-m}\right)$.

To show the converse, consider $f(z) = z^n$, where $n \in \{0, 1, \ldots, N-1\} /$
$\{m\}$. Then as (2.0.10) has an error of $\mathcal{O}\left(h^{N-m}\right)$,

$$h^{n-m} \sum_{k=1}^{N} w_{k,m} z_k^n = O(h^{N-m}) \text{ as } h \to 0. \tag{2.2.7}$$

As $n < N$, (2.2.7) implies

$$\sum_{k=1}^{N} w_{k,m} z_k^n = 0. \tag{2.2.8}$$

Moreover, to show the last equality, consider $f(z) = z^m$. Then as (2.0.10) has an error of

$\mathcal{O}\left(h^{N-m}\right)$,

$$\sum_{k=1}^{N} w_{k,m} z_k^m - m! = O(h^{N-m}) \text{ as } h \to 0. \tag{2.2.9}$$

Thus,

$$\sum_{k=1}^{N} w_{k,m} z_k^m = m!. \tag{2.2.10}$$

□

Observe the conditions on the weights of the above lemma can be stated as:

$$\begin{pmatrix} 1 & 1 & \cdots & 1 \\ z_1 & z_2 & \cdots & z_N \\ & & \cdots & \\ z_1^{N-1} & z_2^{N-1} & \cdots & z_N^{N-1} \end{pmatrix} \begin{pmatrix} w_{1,m} \\ w_{2,m} \\ \vdots \\ w_{N,m} \end{pmatrix} = m! e_m^N \tag{2.2.11}$$

where e_m^N is the m-th unit vector in R^N. Note the matrix on the LHS of (2.2.11) is the transpose of the Vandermonde matrix, which is non-singular. Hence, if the grid points are fixed, we are guaranteed a unique solution of (2.2.11). We summarize below.

Theorem 6. *There exists a unique choice of weights $w_{k,m}$, $k = 1, \ldots, N$, such that the finite difference formula* (2.0.10) *has error $\mathcal{O}\left(h^{N-m}\right)$.*

Proof. The proof is given in the discussion above. □

Thus, if the grid points are fixed, it is then guaranteed that there exists unique weights $w_{k,m}$ such that (2.0.10) has error $O(h^{N-m})$. However, if we consider the centered difference approximation $\big(f(h) - 2f(0) + f(-h)\big)/h^2$ to $f''(0)$, we observe that its order of accuracy is $O(h^2)$; hence, better than $O(h^{3-2})$. Thus, we are now interested in establishing necessary

and sufficient conditions on the grid points that would ensure that the weights $w_{k,m}$ have this increased order of accuracy. Moreover, we would like to introduce the following terminology. We say that the order of accuracy of (2.0.10) is increased by b if the order of accuracy of (2.0.10) is $O(h^{N-m+b})$.

Lemma 7. *The finite difference formula* (2.0.10) *has increased order of accuracy with an error of* $\mathcal{O}\left(h^{N-m+b}\right)$*, where* b *is a positive integer, if and only if the weights* $w_{k,m}$ *satisfy*

$$w_{1,m}z_1^{N-1+\beta} + \cdots + w_{N,m}z_N^{N-1+\beta} = 0 \tag{2.2.12}$$

for $\beta = 1, \ldots, b$ *in addition to the conditions of Lemma 5. Also the function* f *is assumed to be* $N + b$ *times continuously differentiable.*

Proof. Similar to the proof of Lemma 5. □

We introduce the following notation. By

$$\det\left(z_1, z_2 \ldots, z_N; n_1, n_2, \ldots, n_N\right) \tag{2.2.13}$$

we denote the determinant of the $N \times N$ matrix whose (i, j)-th entry is $z_j^{n_i}$.

Theorem 8. *Let* $w_{k,m}$*,* $k = 1, \ldots, N$*, be the unique solution of* (2.2.11) *so that the finite difference formula* (2.0.10) *has an order of accuracy that is at least* $N - m$*. The order of accuracy is increased by* b*, where* b *is a positive integer, if and only if*

$$\det\left(z_1, \ldots, z_N; [0, 1, \ldots, N-1, N-1+\beta] - m\right) = 0 \tag{2.2.14}$$

for each $\beta = 1, \ldots, b$. *Here* $[0, 1, \ldots, N-1, N-1+\beta] - m$ *denotes the sequence* $0, 1, \ldots N-1, N-1+\beta$ *with* m *deleted.*

Proof. Consider the case where the weights $w_{k,m}$ are real and the grid points z_k are also real. Let

$$\begin{aligned} \gamma_m :&= [w_{1,m}, \ldots, w_{N,m}], \\ v_\beta :&= [z_1^{N-1+\beta}, \ldots, z_N^{N-1+\beta}] \end{aligned} \tag{2.2.15}$$

and W_m be the vector space spanned by γ_m.Then by assumption and Lemma 5 every row of the Gram matrix, excluding the m-th row, is orthogonal to γ_m. As the Gram matrix is non-singular, its row vectors are linearly independent. Since every row of the Gram matrix except the m-th row belongs to $W_m^\perp$(orthogonal complement of W_m) and as $dim(W_m^\perp) = N-1$, we have that the rows of the Gram matrix from a basis for $W_m^\perp$.

By Lemma 7 the order of accuracy of the finite difference method is increased by b if and only if $v_\beta \in W_m^\perp$. Observe this is equivalent to requiring $\det(z_1, \ldots, z_N; [0, 1, \ldots, N-1, N-1+\beta] - m) = 0$ as the rows of the Gram matrix are linearly independent. Moreover, should the weights and the grid points be complex, the above argument can be repeated by swapping γ_m with its complex conjugate $\bar{\gamma_m}$. □

Lemma 9. *If* $z_1, \ldots, z_N$ *are distinct points, then*

$$\det(z_1, \ldots, z_N; [0, \ldots N-1, N] - m) = \prod_{1 \le i < j \le N} (z_j - z_i) \times S_{N-m}, \tag{2.2.16}$$

where

$$S_p := \sum_{1 \le i_1 < \ldots < i_p \le N} z_{i_1} \ldots z_{i_p}. \tag{2.2.17}$$

Proof. Consider the Gram determinant

$$\det\left(z_1, \ldots, z_N, z_{N+1}; 0, \ldots, N-1, N\right). \tag{2.2.18}$$

As is well known, this determinant is equal to

$$\prod_{1 \le i < j \le N} (z_j - z_i) \times \prod_{k=1}^{N} (z_{N+1} - z_k). \tag{2.2.19}$$

Moreover, by expanding (2.2.18) by minors of its last column, we observe that the coefficient of $z_{N+1}^m$is given by

$$(-1)^{N+m} \det(z_1, \ldots, z_N; [0, \ldots N-1, N] - m). \tag{2.2.20}$$

Furthermore, by inspection of (2.2.19), we note that the coefficient of $z_{N+1}^m$is given by

$$\prod_{1 \le i < j \le N} (z_j - z_i) \times (-1)^{N-m} \sum_{1 \le i_1 < \ldots < i_{N-m} \le N} z_{i_1} \ldots z_{i_{N-m}}. \tag{2.2.21}$$

Equating (2.2.20) with (2.2.21) yields the desired result. □

We are now ready to state necessary and sufficient conditions on the grid points that ensure (2.0.10) has an order of accuracy that is increased by one.

Theorem 10. *The finite difference formula,* (2.0.10)*, with distinct grid points* z_k *and weights*

$w_{k,m}$ that satisfy (2.2.11) *has an order of accuracy that is increased by* 1 *if and only if* $S_{N-m} = 0$.

Proof. Observe by theorem 8, the order of accuracy is increased by 1 if and only if $\det(z_1, \ldots, z_N; [0, \ldots N-1, N] - m) = 0$. Then by lemma 9 and the fact that all the grid points are distinct, this determinant will vanish if and only if $S_{N-m} = 0$. □

Corollary 11. *If the grid points $z_1, \ldots, z_N$ are symmetric about* 0 *(in other words z is a grid point if and only if $-z$ is a grid point) and $N - m$ is odd, the order of accuracy is increased by* 1.

Proof. It is sufficient to show

$$S_{N-m} = \sum_{1 \le i_1 < \ldots < i_{N-m} \le N} z_{i_1} \ldots z_{i_{N-m}} \tag{2.2.22}$$

is equal to zero. Consider the non-zero terms in (2.2.22). We denote the symmetric counterpart of the term $z_{i_1} \ldots z_{i_{N-m}}$in (2.2.22) to be the term obtained by swapping each grid point, z_{i_α}, with the grid point $-z_{i_\alpha}$ where $1 \le \alpha \le N - m$. By assumption $-z_{i_\alpha} = z_\beta$ where $\beta \neq i_\alpha$. Moreover, as $N - m$ is odd, the symmetric counterpart of a term in (2.2.22) is itself a *distinct* term in (2.2.22). That is

$$(-1)^{N-m} z_{i_1} \ldots z_{i_{N-m}} = -z_{i_1} \ldots z_{i_{N-m}} = z_{\tilde{i}_1} \ldots z_{\tilde{i}_{N-m}}, \tag{2.2.23}$$

where $z_{\tilde{i}_1} \ldots z_{\tilde{i}_{N-m}} \neq z_{i_1} \ldots z_{i_{N-m}}$. Moreover, note that the symmetric counterpart of $z_{\tilde{i}_1} \ldots z_{\tilde{i}_{N-m}}$ is $z_{i_1} \ldots z_{i_{N-m}}$.

Thus, by pairing each non-zero term in (2.2.22) with its symmetric counterpart, we observe

$S_{N-m} = 0.$ □

Moreover, we now prove the following lemma to attain necessary and sufficient conditions on the grid points that ensure (2.0.10) has an order of accuracy that is increased by two.

Lemma 12. *If $z_1, \ldots, z_N$ are distinct points and $m \geq 1$, then*

$$\det(z_1, \ldots, z_N; [0, \ldots, N-1, N+1] - m) = \prod_{1 \leq i < j \leq N} (z_j - z_i) \times (S_1 S_{N-m} - S_{N-m+1}). \quad (2.2.24)$$

Proof. Consider the determinant

$$\det(z_1, \ldots, z_{N+1}; [0, \ldots, N, N+1] - m). \quad (2.2.25)$$

By Lemma 9, we have

$$\det(z_1, \ldots, z_{N+1}; [0, \ldots, N, N+1] - m) = \prod_{1 \leq i < j \leq N+1} (z_j - z_i) \times \sum_{1 \leq i_1 < \ldots < i_{N-m} \leq N+1} z_{i_1} \ldots z_{i_{N+1-m}}. \quad (2.2.26)$$

Observe as $m \geq 1$,

$$\sum_{1 \leq i_1 < \ldots < i_{N-m} \leq N+1} z_{i_1} \ldots z_{i_{N+1-m}} = \sum_{1 \leq i_1 < \ldots < i_{N-m} \leq N} z_{i_1} \ldots z_{i_{N+1-m}} + z_{N+1} \sum_{1 \leq i_1 < \ldots < i_{N-m} \leq N} z_{i_1} \ldots z_{i_{N-m}}. \quad (2.2.27)$$

Thus,

$$S^{+}_{N-m+1} = S_{N-m+1} + z_{N+1}S_{N-m}, \tag{2.2.28}$$

where

$$S^{+}_{N-m+1} := \sum_{1\le i_1<\ldots<i_{N-m}\le N+1} z_{i_1}\ldots z_{i_{N+1-m}}. \tag{2.2.29}$$

Hence,

$$\det(z_1,\ldots,z_{N+1};[0,\ldots,N,N+1]-m) = \prod_{k=1}^{N}(z_{N+1}-z_k)\prod_{1\le i<j\le N}(z_j-z_i)\times(S_{N-m+1}+z_{N+1}S_{N-m}). \tag{2.2.30}$$

As $\prod_{k=1}^{N}(z_{N+1}-z_k)$ can be expanded as

$$\prod_{k=1}^{N}(z_{N+1}-z_k) = z^N_{N+1} - p_1 z^{N-1}_{N+1} + \ldots + (-1)^N p_N, \tag{2.2.31}$$

where the p_i's are the elementary symmetric polynomials and in particular, $p_1 = S_1$. Thus, the coefficient of z^N_{N+1} in (2.2.25) is given by

$$\prod_{1\le i<j\le N}(z_j-z_i)\times(S_{N-m+1}-S_1S_{N-m}). \tag{2.2.32}$$

Moreover, by expanding (2.2.25) by minors of its last column, we observe the coefficient of $z^N_{N+1}$is given by

$$-\det(z_1,\ldots,z_N;[0,\ldots,N-1,N+1]-m). \tag{2.2.33}$$

Hence,

$$\det(z_1, \ldots, z_N; [0, \ldots, N-1, N+1] - m) = \prod_{1 \le i < j \le N} (z_j - z_i) \times (S_1 S_{N-m} - S_{N-m+1}) \,. \quad (2.2.34)$$

□

Theorem 13. *The order of accuracy of the finite difference formula* (2.0.10) *is increased by* 2 *if and only if* $S_{N-m} = 0$ *and* $S_{N-m+1} = 0$*, where* $m \geq 1$.

Proof. Observe by theorem 8, the order of accuracy is increased by 2 if and only if $\det(z_1, \ldots, z_N; [0, \ldots N-1, N] - m) = 0$ and $\det(z_1, \ldots, z_N; [0, \ldots N-1, N+1] - m) = 0$. As noted in theorem 10, the former condition is equivalent to the condition $S_{N-m} = 0$. Hence by Lemma 12, the conditions $S_{N-m} = 0$ and $\det(z_1, \ldots, z_N; [0, \ldots N-1, N+1] - m) = 0$ are equivalent to the conditions $S_{N-m} = 0$ and $S_{N-m+1} = 0$. □

As noted in the introductory paragraph, if the grid points are real, then the order of accuracy of (2.0.10) can never be increased by more than one. We now prove this result.

Theorem 14. *The order of accuracy of the finite difference formula* (2.0.10) *for the* m*-th derivative can never be increased by more than* 1 *as long as the grid points are real. Here* $m \geq 1$.

Proof. By theorem 13, the grid points $z_1, \ldots, z_N$ must satisfy $S_{N-m} = 0$ and $S_{N-m+1} = 0$ for the order of accuracy of (2.0.10) to be increased by more than one. We aim to show by contradiction that both conditions can not be satisfied. Let $r := N - m$ and recall that $S_0 := 1$. Moreover, observe $1 \leq r \leq N-1$ and $N > 2$.

We first consider the case where zero is not a grid point. Suppose $S_r = 0$ and $S_{r+1} = 0$. As the S_p's are the p-th elementary symmetric functions in $z_1, \ldots, z_N$ (distinct real non-zero points), we have by Newton's Inequality (see page 104 of [19])

$$\begin{aligned} \frac{S_r^2}{\binom{N}{r}^2} &> \frac{S_{r-1}}{\binom{N}{r-1}} \frac{S_{r+1}}{\binom{N}{r+1}} \\ S_r^2 &> \left(\frac{N+1-r}{r} \frac{r+1}{N-r} \right) S_{r-1} S_{r+1}. \end{aligned} \tag{2.2.35}$$

Thus,

$$S_r^2 > S_{r-1} S_{r+1} \text{ for } 1 \leq r \leq N-1. \tag{2.2.36}$$

In particular, (2.2.36) implies $S_r^2 \neq S_{r-1} S_{r+1}$. However, by assumption $S_r = 0$ and $S_{r+1} = 0$; thus, $S_r^2 = S_{r-1} S_{r+1}$. We have an obvious contradiction and this proves the result.

We now consider the case where zero is a grid point (it should be noted that we can have at most one zero grid point as all the grid points are distinct). Denote by z_l, for some $l \in \{1, \ldots, N\}$, the zero grid point. Moreover, denote the elementary symmetric function formed by adding all possible products of r numbers out of $z_1, \ldots, z_N$ excluding z_l by s_r. Observe $S_r = s_r$ for $1 \leq r \leq N-1$. Again let us suppose $S_r = 0$ and $S_{r+1} = 0$. As the s_p's are the p-th elementary symmetric functions in $z_1, \ldots, z_N$ excluding z_l (distinct real non-zero points), we have by Newton's Inequality

$$s_r^2 > s_{r-1} s_{r+1} \tag{2.2.37}$$

Thus,

$$S_r^2 > S_{r-1} S_{r+1} \text{ for } 1 \leq r \leq N-1. \tag{2.2.38}$$

Thus, a contradiction will arise as in the first case. Hence the proof is complete. □

We now state necessary and sufficient conditions on the grid points that ensure (2.0.10) has an order of accuracy that is increased by b. We note that for the case of real grid points, we have already shown $b \leq 1$. We now aim to show that for the case of complex grid points, $b \leq m$.

Theorem 15. *The order of accuracy of the finite difference formula* (2.0.10) *for the m-th derivative is increased by b if and only if $S_{N-m} = S_{N-m+1} = \cdots = S_{N-m+b-1} = 0$. Even with complex grid points, the order of accuracy can never be increased by more than m.*

Proof. A rigorous proof is omitted for the former statement. We merely show the general pattern computationally. Note that the case of $b = 1$ and $b = 2$ have already been established. We illustrate the general procedure for the case $b = 3$. Consider the

$$\det(z_1, \ldots, z_{N+1}; [0, \ldots, N, N+2] - m). \tag{2.2.39}$$

Observe by lemma 12, we have

$$\det(z_1, \ldots, z_{N+1}; [0, \ldots, N, N+2] - m) = \prod_{1 \leq i < j \leq N+1} (z_j - z_i) \times \left(S_1^+ S_{N-m+1}^+ - S_{N-m+2}^+ \right). \tag{2.2.40}$$

Observe

$$\begin{aligned} S_1^+ &= S_1 + z_{N+1} \\ S_{N-m+1}^+ &= S_{N-m+1} + z_{N+1} S_{N-m} \\ S_{N-m+2}^+ &= S_{N-m+2} + z_{N+1} S_{N-m+1}. \end{aligned} \tag{2.2.41}$$

Thus,

$$\begin{aligned} &\det(z_1, \ldots, z_{N+1}; [0, \ldots, N, N+2] - m) = \\ &\qquad \prod_{k=1}^{N} (z_{N+1} - z_k) \prod_{1 \le i < j \le N} (z_j - z_i) \times \\ &\qquad \left(S_1 S_{N-m+1} - S_{N-m+2} + S_1 S_{N-m} z_{N+1} + S_{N-m} z_{N+1}^2 \right). \end{aligned} \tag{2.2.42}$$

As $\prod_{k=1}^{N}(z_{N+1} - z_k)$ can be expanded as

$$\prod_{k=1}^{N} (z_{N+1} - z_k) = z_{N+1}^N - p_1 z_{N+1}^{N-1} + p_2 z_{N+1}^{N-2} \ldots + (-1)^N p_N, \tag{2.2.43}$$

where the p_i's are the elementary symmetric polynomials and in particular, $p_1 = S_1$ and $p_2 = S_2$. Thus, the coefficient of z_{N+1}^N in (2.2.40) is given by

$$\prod_{1 \le i < j \le N} (z_j - z_i) \times \left(S_1 S_{N-m+1} - S_{N-m+2} - S_1^2 S_{N-m} + S_2 S_{N-m} \right). \tag{2.2.44}$$

Moreover, by expanding (2.2.40) by minors of its last column, we observe the coefficient of $z_{N+1}^N$is given by

$$-\det(z_1, \ldots, z_N; [0, \ldots, N-1, N+2] - m). \tag{2.2.45}$$

Hence,

$$\det(z_1, \ldots, z_N; [0, \ldots, N-1, N+2] - m) = \prod_{1 \le i < j \le N} (z_j - z_i) \times \left(S_{N-m+2} + S_1^2 S_{N-m} - S_1 S_{N-m+1} - S_2 S_{N-m} \right). \quad (2.2.46)$$

Thus by the conditions of theorem 8 for the case $b = 3$, the order of accuracy of the finite difference formula (2.0.10) for the m-th derivative is increased by 3 if and only if $S_{N-m} = S_{N-m+1} = S_{N-m+2} = 0$. The case of $b = 4$ and so on are proved in a similar manner.

The proof of the latter statement is by contradiction. That is, suppose the order of accuracy is increased by $m+1$. Then $S_N = 0$. Moreover, as the grid points are distinct, only one of the N grid points is zero. However, this would imply that $S_{N-1} \neq 0$, which is a contradiction. Thus, the order of accuracy can never be increased by more than m. □

CHAPTER III

Barycentric Hermite Weights and Updates

We now consider the Hermite Interpolation problem. Let V represent the space of polynomials whose degree is at most $N-1$ where $N = n_1 + \ldots + n_K$. Let $z_1, \ldots, z_K$ be distinct points. Then given the data $f^{(0)}(z_k), ..., f^{(n_k-1)}(z_k)$, $1 \leq k \leq K$, there exists a unique hermite interpolant, $\pi \in V$, such that $\pi^{(s)}(z_j) = f^{(s)}(z_j)$, $1 \leq j \leq K$ and $0 \leq s < n_j$ [11].

Again, let $f^{(s)}(z_k)$ be denoted by $f_{k,s}$. Moreover, let $\pi^*(z) := \prod_{j=1}^{K}(z - z_j)^{n_j}$. Then the barycentric form of the Hermite interpolant is given by:

$$\pi(z) = \pi^*(z) \sum_{k=1}^{K} \frac{f_{k,n_k-1}}{(n_k-1)!} \left(\frac{w_{k,0}}{(z-z_k)} \right) + \frac{f_{k,n_k-2}}{(n_k-2)!} \left(\frac{w_{k,0}}{(z-z_k)^2} + \frac{w_{k,1}}{(z-z_k)} \right)$$
$$+ \cdots + f_{k,0} \left(\frac{w_{k,0}}{(z-z_k)^{n_k}} + \cdots + \frac{w_{k,n_k-1}}{(z-z_k)} \right). \tag{3.0.47}$$

3.1 Derivation of the Barycentric Form of the Hermite Interpolant

By existence and uniqueness, $\pi(z)$ is the unique polynomial in V whose Taylor series about $z = z_k$ is given by: $f_{k,0} + \ldots + \frac{f_{k,n_k-1}}{(n_{k-1})!}(z - z_k)^{n_k-1}$ for all $1 \leq k \leq K$. Let $\pi^*(z) := \prod_{k=1}^{K}(z - z_k)^{n_k}$, $\pi_k(z) := \pi^*(z)(z - z_k)^{-n_k}$ and

$$W_k(z) := \sum_{r=0}^{n_k-1} w_{k,r}(z - z_k)^r. \tag{3.1.1}$$

Moreover, $w_{k,r}$ is defined so that $W_k(z)$ is merely the Taylor Series of $\pi_k(z)^{-1}$, about $z = z_k$, truncated to the $(n_k - 1)$-th power. Hence, $W_k(z)\pi_k(z) = 1 + O((z - z_k)^{n_k})$ as $z \to z_k$.

Let $\tilde{W}_k(z)$ denote the polynomial $W_k(z)\left(f_{k,0} + \ldots + \frac{f_{k,n_k-1}}{(n_{k-1})!}(z - z_k)^{n_k-1}\right)$ truncated to the $(n_k - 1)$-th power and let $p_k(z) := \pi_k(z)\tilde{W}_k(z)$. Then $p_k(z)$ is a polynomial of degree $N - 1$. Moreover, $p_k(z)$ satisfies the Hermite interpolation conditions at $z = z_k$ (shown below) and is $O((z - z_j)^{n_j})$ for all $j \neq k$. Observe,

$$\begin{aligned}
p_k(z) = \pi_k(z)\tilde{W}_k(z) = \pi_k(z)\Bigg(& f_{k,0}W_k(z) \\
&+ f_{k,1}(z - z_k)(W_k(z) - w_{k,n_k-1}(z - z_k)^{n_k-1}) \\
&+ \frac{f_{k,2}(z - z_k)^2}{2!}\left(W_k(z) - w_{k,n_k-1}(z - z_k)^{n_k-1} - w_{k,n_k-2}(z - z_k)^{n_k-2}\right) \\
&+ \ldots + \frac{f_{k,n_k-2}(z - z_k)^{n_k-2}}{(n_k-2)!}\left(W_k(z) - w_{k,n_k-1}(z - z_k)^{n_k-1} - \ldots - w_{k,2}(z - z_k)^2\right) \\
&+ \frac{f_{k,n_k-1}(z - z_k)^{n_k-1}}{(n_k-1)!}\left(W_k(z) - w_{k,n_k-1}(z - z_k)^{n_k-1} - \ldots - w_{k,1}(z - z_k)\right)\Bigg) \\
&= \sum_{r=0}^{n_k-1}\frac{f_{k,r}}{r!}(z - z_k)^r + O(z - z_k)^{n_k} \text{ as } z \to z_k. \qquad (3.1.2)
\end{aligned}$$

To illustrate further, we would like to explicitly show that the third line in the above expression

$$\pi_k(z)\frac{f_{k,2}(z-z_k)^2}{2!}\left(W_k(z)-w_{k,n_k-1}(z-z_k)^{n_k-1}-w_{k,n_k-2}(z-z_k)^{n_k-2}\right), \tag{3.1.3}$$

reduces to

$$\frac{f_{k,2}(z-z_k)^2}{2!}+O(z-z_k)^{n_k} \text{ as } z\to z_k. \tag{3.1.4}$$

Recall $W_k(z)$ is the Taylor series expansion of $\pi_k(z)^{-1}$, about $z=z_k$, truncated to the (n_k-1)-th power. Hence, $W_k(z)-w_{k,n_k-1}(z-z_k)^{n_k-1}-w_{k,n_k-2}(z-z_k)^{n_k-2}$ is the Taylor series expansion of $\pi_k(z)^{-1}$ truncated to the (n_k-3)-th power. Therefore, $\pi_k(z)(W_k(z)-w_{k,n_k-1}(z-z_k)^{n_k-1}-w_{k,n_k-2}(z-z_k)^{n_k-2})=1+O(z-z_k)^{n_k-2}$ as $z\to z_k$. Multiplication by $\frac{f_{k,2}(z-z_k)^2}{2!}$ confirms that the third line in the above expression reduces to (3.1.4).

Thus, the degree $N-1$ polynomial, $p_k(z)$, satisfies the Hermite interpolation conditions at $z=z_k$ and is $O((z-z_j)^{n_j})$ for all $j\neq k$ by definition of $\pi_k(z)$. That is,

$$p_k^{(r)}(z_j)=f_{k,r}\delta_{j,k} \quad \text{for} \quad 0\le r\le n_j-1 \quad \text{and} \quad 1\le j\le K. \tag{3.1.5}$$

Moreover, as $\sum_{k=1}^K p_k(z)$ is in V, then by uniqueness of the Hermite interpolant:

$$\begin{aligned}\pi(z)=\sum_{k=1}^K p_k(z)=\pi^*(z)\sum_{k=1}^K \frac{f_{k,n_k-1}}{(n_k-1)!}\left(\frac{w_{k,0}}{(z-z_k)}\right)\\ +\frac{f_{k,n_k-2}}{(n_k-2)!}\left(\frac{w_{k,0}}{(z-z_k)^2}+\frac{w_{k,1}}{(z-z_k)}\right)+\cdots+f_{k,0}\left(\frac{w_{k,0}}{(z-z_k)^{n_k}}+\cdots+\frac{w_{k,n_k-1}}{(z-z_k)}\right)\end{aligned} \tag{3.1.6}$$

3.2 Barycentric Weights

To compute the barycentric weights, we observe the following,

$$\pi_k(z)^{-1} = \prod_{j \neq k} (z_k - z_j)^{-n_j} \prod_{j \neq k} \left(1 - \frac{z - z_k}{z_j - z_k}\right)^{-n_j} = C_k T_k(z), \tag{3.2.1}$$

where

$$C_k := \prod_{j \neq k} (z_k - z_j)^{-n_j} \tag{3.2.2}$$

and

$$T_k(z) := \prod_{j \neq k} \left(1 - \frac{z - z_k}{z_j - z_k}\right)^{-n_j}. \tag{3.2.3}$$

A power series expansion of $T_k(z)$ yields

$$T_k(z) = \prod_{j \neq k} \left(1 - \frac{z - z_k}{z_j - z_k}\right)^{-n_j} = 1 + \mathcal{I}_1(z - z_k) + \mathcal{I}_2(z - z_k)^2 + \ldots \tag{3.2.4}$$

where the $\mathcal{I}_i$'s are defined as the Taylor series coefficients in the above expansion.

In our attempt to obtain a recurrence formulae for the $\mathcal{I}_i$'s (and hence the barycentric weights), we differentiate the above expression to obtain

$$\prod_{j \neq k} \left(1 - \frac{z - z_k}{z_j - z_k}\right)^{-n_j} \sum_{l \neq k}^{K} \left(1 - \frac{z - z_k}{z_l - z_k}\right)^{-1} \left(\frac{n_l}{z_l - z_k}\right)$$
$$= \mathcal{I}_1 + 2\mathcal{I}_2(z - z_k) + 3\mathcal{I}_3(z - z_k)^2 + \ldots. \tag{3.2.5}$$

Noting that

$$\left(1-\frac{z-z_k}{z_l-z_k}\right)^{-1}=1+\frac{z-z_k}{z_l-z_k}+\left(\frac{z-z_k}{z_l-z_k}\right)^2+\ldots, \tag{3.2.6}$$

and allowing

$$\mathcal{P}_r:=\sum_{l\neq k} n_l(z_l-z_k)^{-r}, \tag{3.2.7}$$

we plug in (3.2.6) into the LHS of (3.2.5), which yields

$$\begin{aligned}
&\prod_{j\neq k}\left(1-\frac{z-z_k}{z_j-z_k}\right)^{-n_j}\left(\sum_{l\neq k}^{K} n_l\,(z_l-z_k)^{-1}\left[1+\frac{z-z_k}{z_l-z_k}+\left(\frac{z-z_k}{z_l-z_k}\right)^2+\ldots\right]\right)\\
&\qquad=\prod_{j\neq k}\left(1-\frac{z-z_k}{z_j-z_k}\right)^{-n_j}\left(\mathcal{P}_1+\mathcal{P}_2(z-z_k)+\ldots+\mathcal{P}_{m+1}(z-z_k)^m+\ldots\right)\\
&\qquad\qquad=\left(1+\mathcal{I}_1(z-z_k)+\mathcal{I}_2(z-z_k)^2+\ldots\right)\\
&\qquad\qquad\qquad\left(\mathcal{P}_1+\mathcal{P}_2(z-z_k)+\ldots+\mathcal{P}_{m+1}(z-z_k)^m+\ldots\right)
\end{aligned} \tag{3.2.8}$$

Thus,

$$\begin{aligned}
&\left(1+\mathcal{I}_1(z-z_k)+\mathcal{I}_2(z-z_k)^2+\ldots\right)\\
&\qquad\left(\mathcal{P}_1+\mathcal{P}_2(z-z_k)+\ldots+\mathcal{P}_{m+1}(z-z_k)^m+\ldots\right)\\
&\qquad\qquad=\mathcal{I}_1+2\mathcal{I}_2(z-z_k)+3\mathcal{I}_3(z-z_k)^2+\ldots
\end{aligned} \tag{3.2.9}$$

Further, by equating powers of $z - z_k$, we obtain the desired recurrence formulae for the $\mathcal{I}_i$'s.

$$\begin{aligned} \mathcal{I}_1 &= \mathcal{P}_1 \\ 2\mathcal{I}_2 &= \mathcal{P}_2 + \mathcal{I}_1\mathcal{P}_1 \\ 3\mathcal{I}_3 &= \mathcal{P}_3 + \mathcal{I}_1\mathcal{P}_2 + \mathcal{I}_2\mathcal{P}_1 \\ &\cdots \end{aligned} \tag{3.2.10}$$

That is (let $\mathcal{I}_0 := 1$),

$$\mathcal{I}_r = (1/r)\sum_{s=1}^{r} \mathcal{P}_s\mathcal{I}_{r-s} \tag{3.2.11}$$

Hence, the barycentric weights are given by

$$w_{k,r} = C_k\mathcal{I}_r. \tag{3.2.12}$$

3.3 Barycentric Weight Updates

We now show how to update all barycentric weights for the following two update cases in $O(N)$ operations.

1. A new grid point is added and the new data item is the function value at the new grid point.

2. At a pre-existing grid point, the value of the next possible order of the derivative of the function is specified.

Case 1)

In this case, a new grid point is added at $\zeta = z_{K+1}$. Hence, $\pi_k(z)$ must be updated to $\pi_k(z)(z-\zeta)$ for $1 \le k \le K$. Moreover, $W_k(z)$ is updated to $W_k'(z) = \sum_{r=0}^{n_k-1} w'_{k,r}(z-z_k)^r$ for $1 \le k \le K$, where $W_k'(z)$ must satisfy

$$\pi_k(z)(z-\zeta)W_k'(z) = 1 + O((z-z_k)^{n_k}). \tag{3.3.1}$$

As $\pi_k(z)W_k(z) = 1 + O((z-z_k)^{n_k})$, the above condition can be recast as

$$(z-\zeta)W_k'(z) = ((z-z_k) + (z_k-\zeta))\, W_k'(z) = W_k(z) + O((z-z_k)^{n_k}). \tag{3.3.2}$$

Thus,

$$(z_k-\zeta)w'_{k,0} + \sum_{r=1}^{n_k-1} \left((z_k-\zeta)w'_{k,r} + w'_{k,r-1}\right)(z-z_k)^r = \sum_{r=0}^{n_k-1} w_{k,r}(z-z_k)^r. \tag{3.3.3}$$

Equating powers of $z - z_k$ yields

$$\begin{aligned} (z_k-\zeta)w'_{k,0} &= w_{k,0} \\ (z_k-\zeta)w'_{k,r} + w'_{k,r-1} &= w_{k,r} \quad \text{for} \quad 1 \le r < n_k. \end{aligned} \tag{3.3.4}$$

This completes the updates for $w_{k,r}$ for $1 \le k \le K$. We observe that it takes two operations to update each barycentric weight $w_{k,r}$.

The only remaining item to compute is $w_{K+1,0}$. As noted previously (see introductory para-

graph of this section), we require

$$\pi_{K+1}(z)W_{K+1}(z) = 1 + O((z-\zeta)). \tag{3.3.5}$$

Hence, $W_{K+1}(z)$ is the Taylor series of $\pi_{K+1}(z)^{-1}$centered at $z = \zeta$ truncated to the 0-th power. That is, $w_{K+1,0} = \pi_{K+1}(\zeta)^{-1} = \prod_{k=1}^{K}(\zeta - z_k)^{-n_k}$. Thus, the total cost of updating all weights and computing the new weight in this case is $O(N)$.

Case 2)

In this case, the value of the next possible order of the derivative of the function is specified at a pre-existing grid point. That is, f_{κ,n_κ} is introduced at the point $\zeta = z_\kappa$ for some κ, $1 \leq \kappa \leq K$. Hence, $\pi_k(z)$ must be updated to $\pi_k(z)(z-\zeta)$ for $k \neq \kappa$ and therefore the weights, $w_{k,r}$, are updated using (3.3.4).

Moreover, $\pi_\kappa(z) = \prod_{j\neq\kappa}(z - z_j)^{n_j}$ remains unchanged. Thus, $w_{\kappa,r}$ also remains unchanged for $1 \leq r \leq n_\kappa - 1$. Note, $W_\kappa(z)$ is updated by adding an additional term to ensure the condition,

$$\pi_\kappa(z)W'_\kappa(z) = 1 + O((z-z_\kappa)^{n_\kappa+1}) \tag{3.3.6}$$

That is, $W'_\kappa(z) \leftarrow W_\kappa(z) + w_{\kappa,n_\kappa}(z-z_\kappa)^{n_\kappa}$. Therefore, the only term left to compute is w_{κ,n_κ}. However, we also would like to be able to handle a future update which may occur at another point. In that spirit, we introduce the quantity

$$A_k = \left\{ 1/(z_j - z_k) \text{ repeated } n_j \text{ times} \;\middle|\; j \neq k \text{ and } 1 \leq j \leq K \right\} \tag{3.3.7}$$

It should be noted that A_k is a multiset. Moreover, we define $\mathcal{P}_r(A_k)$ as the sum of the r-th powers of the elements of A_k. That is,

$$\mathcal{P}_r(A_k) := \sum_{j \neq k} n_j (z_j - z_k)^{-r} \tag{3.3.8}$$

In addition, let $\mathcal{I}_r(A_k)$ be related to $\mathcal{P}_r(A_k)$ by the triangular identities specified in (3.2.10). Observe that when computing the barycentric weights, $w_{k,0}, \ldots, w_{k,n_k-1}$, as specified in (3.2.12), the following intermediate quantities

$$C_k, \mathcal{P}_1(A_k), \ldots, \mathcal{P}_{n_k-1}(A_k), \mathcal{I}_1(A_k), \ldots, \mathcal{I}_{n_k-1}(A_k) \tag{3.3.9}$$

arise. When $f_{\kappa,n_\kappa}$is added at $z = \zeta$, the intermediate quantities are updated at all grid points.

For the grid points where $z_k \neq \zeta$ (i.e. $k \neq \kappa$), we note $A'_k \leftarrow A_k \cup \{1/(\zeta - z_k)\}$(multiset union). Hence, the intermediate quantities are updated as follows,

$$\begin{aligned} C'_k &\leftarrow C_k/(z_k - \zeta) \\ \mathcal{P}_r(A'_k) &\leftarrow \mathcal{P}_r(A_k) + (\zeta - z_k)^{-r} \quad \text{for} \quad 1 \leq r < n_k \\ \mathcal{I}_r(A'_k) - \frac{\mathcal{I}_{r-1}(A'_k)}{\zeta - z_k} &= \mathcal{I}_r(A_k) \quad \text{for} \quad r = 1, \ldots, n_k - 1 \end{aligned} \tag{3.3.10}$$

Note, the first and second update follow directly from the definition of C'_k and $\mathcal{P}_r(A'_k)$ given in (3.2.2) and (3.3.8) respectively. The proof of the final update is shown below.

Claim 16. $\mathcal{I}_r(A'_k) - \frac{\mathcal{I}_{r-1}(A'_k)}{\zeta - z_k} = \mathcal{I}_r(A_k) \quad \text{for} \quad r = 1, \ldots, n_k - 1$ where $\mathcal{I}_0(A'_k) := 1$.

Proof. The updated $T_k(z)$, $T_k'(z)$, is given by

$$T_k'(z) = T_k(z)\left(1 - \frac{z - z_k}{z_\kappa - z_k}\right)^{-1} \tag{3.3.11}$$

A Taylor Series expansion yields

$$T_k'(z) = T_k(z)\left(1 + \frac{z - z_k}{z_\kappa - z_k} + \left(\frac{z - z_k}{z_\kappa - z_k}\right)^2 + \ldots\right) \tag{3.3.12}$$

Recall the $\mathcal{I}_r(A_k)$'s are simply the Taylor coefficients of $T_k(z)$ about $z = z_k$(and similarly for $\mathcal{I}_r(A_k')$). Thus,

$$\begin{aligned} 1 + \mathcal{I}_1(A_k')(z - z_k) + \mathcal{I}_2(A_k')(z - z_k)^2 + \ldots \\ = \left(1 + \mathcal{I}_1(A_k')(z - z_k) + \mathcal{I}_2(A_k')(z - z_k)^2 + \ldots\right) \\ \left(1 + \frac{z - z_k}{z_\kappa - z_k} + \left(\frac{z - z_k}{z_\kappa - z_k}\right)^2 + \ldots\right) \end{aligned} \tag{3.3.13}$$

Equating powers of $z - z_k$ yields,

$$
\begin{aligned}
\mathcal{I}_1(A'_k) &= \mathcal{I}_1(A_k) + \frac{1}{z_\kappa - z_k} \\
\mathcal{I}_2(A'_k) &= \mathcal{I}_2(A_k) + \frac{\mathcal{I}_1(A_k)}{z_\kappa - z_k} + \frac{1}{(z_\kappa - z_k)^2} = \mathcal{I}_2(A_k) + \frac{\mathcal{I}_1(A'_k)}{z_\kappa - z_k} \\
&\vdots \\
\mathcal{I}_{n_k-1}(A'_k) &= \mathcal{I}_{n_k-1}(A_k) + \frac{\mathcal{I}_{n_k-2}(A_k)}{z_\kappa - z_k} + \frac{\mathcal{I}_{n_k-3}(A_k)}{(z_\kappa - z_k)^2} + \dots \\
&\quad + \frac{\mathcal{I}_1(A_k)}{(z_\kappa - z_k)^{n_k-2}} + \frac{1}{(z_\kappa - z_k)^{n_k-1}} \\
&= \mathcal{I}_{n_k-1}(A_k) + \frac{\mathcal{I}_{n_k-2}(A'_k)}{z_\kappa - z_k}
\end{aligned} \tag{3.3.14}
$$

□

This completes the updates for the intermediate quantities. We observe that the total number of intermediate quantities is $O(N)$. Hence, the total cost of the update procedure for the intermediate quantities where $k \neq \kappa$ is $O(N)$.

For the grid point z_κ, we observe that A_κ is unchanged and furthermore, the intermediate quantities remain unchanged. However, we are left with our original task of computing w_{κ,n_κ}. As specified in (3.2.12), $w_{\kappa,n_\kappa} = C_\kappa \mathcal{I}_{n_\kappa}(A_\kappa)$. Thus, we are simply left with generating $\mathcal{P}_{n_\kappa}(A_\kappa)$ and $\mathcal{I}_{n_\kappa}(A_\kappa)$. Note by (3.3.8) and (3.2.11) it follows that

$$
\begin{aligned}
\mathcal{P}_{n_\kappa}(A_\kappa) &= \sum_{j \neq \kappa} n_j (z_j - z_\kappa)^{-n_\kappa} \\
\mathcal{I}_{n_\kappa}(A_\kappa) &= (1/n_\kappa) \sum_{s=1}^{n_\kappa} P_s(A_\kappa) \mathcal{I}_{n_\kappa - s}(A_\kappa)
\end{aligned} \tag{3.3.15}
$$

respectively. This completes the computation of w_{κ,n_κ}. We note $\mathcal{P}_{n_\kappa}$can be computed using

only $2n_\kappa - 1$ operations [30]. Thus, the total cost of the update procedure is $O(N)$.

CHAPTER IV

Quasi-Uniform Spectral Scheme (QUSS)

In this chapter, we motivate and explain a Quasi-Uniform Spectral Scheme (QUSS) (it is a spectral method that employs a more uniform spatial grid than the Chebyshev grid) and explore three different mappings (KT, Elliptic and Theta) that are capable of producing such a grid (see Section 4.3, Section 4.4 and Section 4.5 for more details). We begin by first reviewing Chebyshev polynomials and the Chebyshev grid.

4.1 Chebyshev Polynomials

Chebyshev polynomials are widely used as a choice of basis functions in pseudospectral methods for non-periodic problems on a bounded domain [4, 5] and have been surveyed in classic numerical analysis and approximation theory textbooks such as [4, 11, 35]. To construct the N-th Chebyshev polynomial, we let $z = e^{i\theta}$ denote a point on the upper half of the unit circle in the complex plane where $Re(z) = x = \cos(\theta)$, $Im(z) = y = \sin(\theta)$ and

$0 \leq \theta \leq \pi$. The N-th Chebyshev polynomial of degree N is then [11, 35]

$$\begin{aligned} T_N(x) &= Re(z^N) \\ &= \cos(N\theta), \end{aligned} \tag{4.1.1}$$

where $\theta = \arccos(x)$. We make use of the fact that on the unit circle $y = \sin(\theta) = \sqrt{(1-x^2)}$ to compute the Chebyshev polynomials. For example,

$$\begin{aligned} T_2(x) &= Re(z^2), \\ &= Re\left(\left(x + i\sqrt{(1-x^2)}\right)^2\right), \\ &= Re\left(x^2 - (1-x^2) + 2x\sqrt{(1-x^2)}\right), \\ &= 2x^2 - 1. \end{aligned} \tag{4.1.2}$$

The first few Chebyshev polynomials are shown below.

$$\begin{aligned} T_0(x) &= Re(z^0) = 1, \\ T_1(x) &= Re(z^1) = x, \\ T_2(x) &= Re(z^2) = 2x^2 - 1, \\ T_3(x) &= Re(z^3) = 4x^3 - 3x. \end{aligned} \tag{4.1.3}$$

The following trigonometric identities are useful for constructing a recurrence relationship

that Chebyshev polynomials satisfy.

$$T_{N+1} = \cos((N+1)\theta) = \cos(N\theta)\cos(\theta) - \sin(N\theta)\sin(\theta), \tag{4.1.4}$$

$$T_{N-1} = \cos((N-1)\theta) = \cos(N\theta)\cos(\theta) + \sin(N\theta)\sin(\theta). \tag{4.1.5}$$

If we add (4.1.4) and (4.1.5) we have the desired recurrence relation [11, 35]

$$\begin{aligned} T_{N+1}(x) &= 2\cos(N\theta)\cos(\theta) - T_{N-1}, \\ &= 2xT_N(x) - T_{N-1}(x), \end{aligned} \tag{4.1.6}$$

where $T_1(x) = \cos(\theta) = x$ and $T_N(x) = \cos(N\theta)$. We note that higher order Chebyshev polynomials can be computed using this recurrence relation.

4.2 The Case for QUSS

The roots of the N-th Chebyshev polynomial play an important role in polynomial interpolation. From (4.1.1), we see that the roots are

$$x_k = \cos\left(\frac{2k-1}{2N}\pi\right), \ k = 1, \ldots, N. \tag{4.2.1}$$

We shall hereby refer to these roots as the points of the Chebyshev grid (though they are often referred to as points of the Chebyshev roots grid). Polynomial interpolation of seemingly simple functions such as $\frac{1}{1+x^2}$ over the interval $-1 \leq x \leq 1$ with equispaced grid points (which we will refer to as the uniform grid) are vulnerable to Runge's phenomenon. However, the problem is remedied when one changes to the non-uniform Chebyshev grid as

we will explain below [4, 35]. We point out that an elegant approach involving potential theory that explains why polynomial interpolation with Chebyshev grid points overcomes Runge's phenomenon can be found in [35].

We now turn to the geometrical construction of the Chebyshev grid points. Consider again the upper half of the unit circle in the complex plane. The points z_k where

$$z_k = e^{i\theta_k},\ k = 1, \ldots, N \tag{4.2.2}$$

$$\theta_k = \frac{2k-1}{2N}\pi,\ k = 1, \ldots, N \tag{4.2.3}$$

lie on the upper half of the unit circle in the complex plane where each successive point is obtained by a rotation of $\frac{\pi}{N}$ radians as seen by the equality $z_{i+1} = z_i e^{i\frac{\pi}{N}}$ for $1 \leq i \leq N-1$. The Chebyshev grid points, x_k, are then simply the projections of the points z_k onto the real axis [35]. Thus,

$$x_k = Re(z_k). \tag{4.2.4}$$

This is graphically illustrated in Figure 4.2.1 on page 55.

We can clearly see from this construction that the Chebyshev grid is much finer near the endpoints, $x = \pm 1$, than the center of the interval, $x = 0$. To quantify this, we let Δ_E and Δ_C represent the grid spacing near the endpoint and center of the Chebyshev grid respectively. From (4.2.1), we have $\Delta_C = |\cos\left(\frac{(N+1)\pi}{2N}\right) - \cos\left(\frac{(N-1)\pi}{2N}\right)|$ and $\Delta_E = |\cos\left(\frac{3\pi}{2N}\right) - \cos\left(\frac{\pi}{2N}\right)|$.

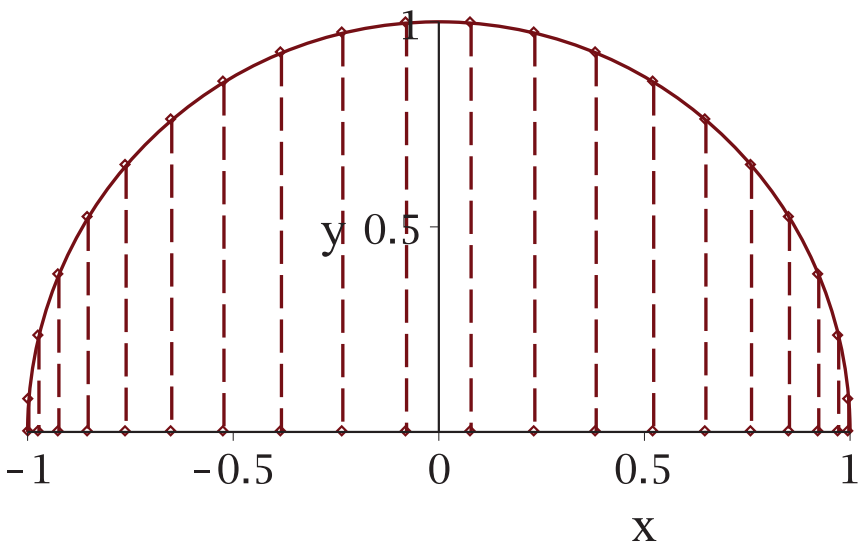

Figure 4.2.1: Graphical Construction of the Chebyshev grid points

The relevant Taylor series are

$$\cos\left(\frac{3\pi}{2N}\right) = 1 - \tfrac{9\pi^2}{8N^2} + \tfrac{27\pi^4}{128N^4} + O\left(\tfrac{1}{N^6}\right) \quad , \tag{4.2.5}$$

$$\cos\left(\frac{\pi}{2N}\right) = 1 - \tfrac{\pi^2}{8N^2} + \tfrac{\pi^4}{384N^4} + O\left(\tfrac{1}{N^6}\right) \quad , \tag{4.2.6}$$

$$\cos\left(\frac{(N+1)\pi}{2N}\right) = -\tfrac{\pi}{2N} + \tfrac{\pi^3}{48N^3} + O\left(\tfrac{1}{N^5}\right) \quad , \tag{4.2.7}$$

$$\cos\left(\frac{(N-1)\pi}{2N}\right) = \tfrac{\pi}{2N} - \tfrac{\pi^3}{48N^3} + O\left(\tfrac{1}{N^5}\right) \quad . \tag{4.2.8}$$

Hence, we have

$$\Delta_E = \frac{\pi^2}{N^2} + O\left(\frac{1}{N^4}\right), \tag{4.2.9}$$

$$\Delta_C = \frac{\pi}{N} + O\left(\frac{1}{N^3}\right). \tag{4.2.10}$$

We conclude from the above formulas that the grid spacing near the endpoints of the Cheby-

shev grid with N points are $O\left(\frac{1}{N^2}\right)$ while the grid spacing near the center is $O\left(\frac{\pi}{2} \times \frac{2}{N}\right)$. However, for a uniform grid with N points on the interval $-1 \leq x \leq 1$, the grid separation Δ_U is given by

$$\Delta_U = \frac{2}{N}. \tag{4.2.11}$$

By comparing Δ_U and Δ_C, we see that the grid spacing near the center of the interval for the Chebyshev grid with N points is larger than the case of the uniform grid with N points by a factor of $\frac{\pi}{2}$. Thus, the Chebyshev grid has a poorer resolution near $x = 0$ than the corresponding uniform grid by a factor of $\frac{\pi}{2}$ [5]. Moreover, by comparing Δ_U and Δ_E we see that near the endpoints $x = \pm 1$, the Chebyshev grid is much finer than the uniform grid. Hence compared to the uniform grid, the Chebyshev grid sacrifices resolution near $x = 0$ to have more resolution near the endpoints $x = \pm 1$. This sacrifice is worth it for polynomial interpolation. As reviewed in [4], the largest errors in polynomial interpolation do not occur near the center of the interval, but rather at the endpoints of the interval. Thus by increasing the resolution near the endpoints, the Chebyshev grid is able to overcome Runge's phenomenon.

We note that this increase in resolution near the endpoints is not mandated by the physics of any underlying problem, but rather by the wild oscillations of high degree polynomials near the endpoints [4], which is strictly a mathematical obstruction. Hence we would expect that the Chebyshev grid to come at a cost! The first obvious cost is that we have poorer resolution near the center of the interval as noted previously. Furthermore, by increasing the resolution near the endpoints to $O\left(\frac{1}{N^2}\right)$, use of the Chebyshev grid for spatial discretization of a time dependent PDE with an explicit scheme for time marching results in a CFL condition that requires a tiny time step of $O\left(\frac{1}{N^2}\right)$ [5, 34]. This is true even for cases where no large

gradients are present near the boundary [34]. In contrast, use of the uniform grid for spatial discretization results in a CFL condition that requires a time step of just $O\left(\frac{1}{N}\right)$.

These downsides to the Chebyshev grid serve as a motivation to develop a spectral method which uses a more uniform spatial grid than the Chebyshev grid. Such a method is dubbed as a "Quasi-Uniform Spectral Scheme" (QUSS) [5]. In this thesis we explore QUSSs in the context of three different mappings that are capable of producing a grid more uniform than the Chebyshev grid coupled with a mapped cosine basis. The three mappings are the KT, Elliptic and Theta mappings. In all of the mappings, we map from the computational grid (τ) to the physical grid (x) via $x = \mathcal{X}(\tau;\beta)$ where β represents the map parameter as detailed in the discussion of the mappings below. Moreover, we map from the physical grid (x) to the computational grid (τ) via $\tau = \mathcal{T}(x;\beta)$. The mappings $\mathcal{T}(x;\beta)$ and $\mathcal{X}(\tau;\beta)$ are inverses in the sense that for a fixed value of β, they satisfy

$$\begin{aligned} \mathcal{X}(\mathcal{T}(x;\beta);\beta) &= x \\ &\text{and} \\ \mathcal{T}(\mathcal{X}(\tau;\beta);\beta) &= \tau. \end{aligned} \tag{4.2.12}$$

We note the important fact that for all of the mappings $\mathcal{X}(\tau;\beta)$ we consider, $\mathcal{X}(\tau;\beta)$ maps the interval $\tau \in [0,\pi]$ to the interval $x \in [-1,1]$ and similarly $\mathcal{T}(x;\beta)$ maps the interval $x \in [-1,1]$ to the interval $\tau \in [0,\pi]$. We now turn to a discussion of the mappings and the resulting grids.

4.3 Elliptic Mapping and Grid

In the construction of the Chebyshev grid, the upper half of the unit circle is divided and the resulting projections onto the x-axis constitute the points in the Chebyshev grid as explained previously. In an attempt to obtain a more *uniform* grid, a natural generalization is to use an ellipse with a *semi-major* axis of 1 that lies along the x axis. By dividing the upper half of the ellipse and taking projections onto the x-axis as shown in Figure 4.3.1 on page 59, the resulting grid points are given by the so-called Elliptic mapping. The Elliptic mapping is given by

$$x = \mathcal{X}(\tau; m) \quad = \quad \bar{E}^{-1}\left(\bar{E}(1;m) - \frac{2\bar{E}(1;m)}{\pi}\tau, m\right) \tag{4.3.1}$$

and the inverse mapping is given by

$$\tau = \mathcal{T}(x; m) = \frac{\pi}{2\bar{E}(1;m)}\left(\bar{E}(1;m) - \bar{E}(x;m)\right) \tag{4.3.2}$$

where

$$\bar{E}(x;m) = \int_0^{\arcsin(x)} \sqrt{1 - m\sin^2(\phi)}d\phi = \int_0^x \frac{\sqrt{1-m\zeta^2}}{\sqrt{1-\zeta^2}}d\zeta. \tag{4.3.3}$$

Moreover, the x derivative of the inverse mapping is given by

$$\frac{d\mathcal{T}}{dx} = \frac{-\pi}{2\bar{E}(1;m)}\frac{\sqrt{1-mx^2}}{\sqrt{1-x^2}}. \tag{4.3.4}$$

A careful derivation of the Elliptic mapping and the resulting grid is shown below.

4.3.1 Construction of the Elliptic Mapping from the Definition of Arclength

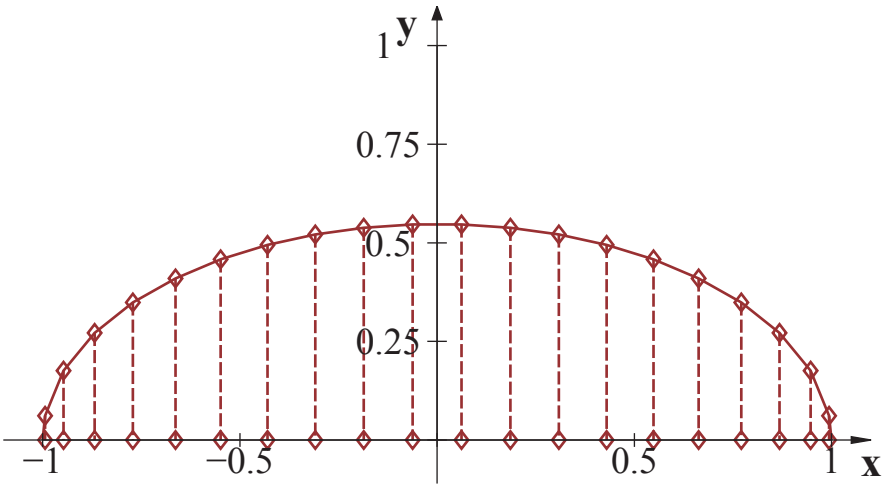

Figure 4.3.1: Graphical Construction of the Elliptic mapping grid points with $m = .7$

We consider an ellipse with a semimajor axis of 1 and a semiminor axis of b that is parametrized by $x = \cos(\varphi)$ and $y = b\sin(\varphi)$ where $0 \leq \varphi < 2\pi$. Then the arclength of this ellipse from 0 to φ' (measured counterclockwise from the x-axis in the first quadrant) is given by

$$\begin{aligned} s(\varphi'; m) &= \int_0^{\varphi'} \sqrt{\left(\frac{\partial x}{\partial \varphi}\right)^2 + \left(\frac{\partial y}{\partial \varphi}\right)^2} d\varphi, \\ &= \int_0^{\varphi'} \sqrt{1 - m\cos^2(\varphi)} d\varphi, \end{aligned} \tag{4.3.5}$$

where

$$m := 1 - b^2. \tag{4.3.6}$$

To express the arclength in terms of the elliptic integral of the second kind, we let $\phi := \frac{\pi}{2} - \varphi$

(i.e. the angle measured clockwise where $\phi = 0$ corresponds to the point $x = 0$ and $y = b$). Then $x = \sin(\phi)$, $y = b\cos(\phi)$ and

$$\begin{aligned} s(\varphi'; m) &= \int_{\frac{\pi}{2}-\varphi'}^{\frac{\pi}{2}} \sqrt{1 - m\sin^2(\phi)}d\phi, \\ &= \int_0^{\frac{\pi}{2}} \sqrt{1 - m\sin^2(\phi)}d\phi - \int_0^{\frac{\pi}{2}-\varphi'} \sqrt{1 - m\sin^2(\phi)}d\phi, \\ &= E\left(\frac{\pi}{2}; m\right) - E\left(\frac{\pi}{2} - \varphi'; m\right), \end{aligned} \tag{4.3.7}$$

where $E(\phi; m)$ is the elliptic integral of the second kind given by

$$E(\phi; m) = \int_0^{\phi} \sqrt{1 - m\sin^2(\phi)}d\phi.$$

It is useful to introduce $\bar{E}(x; m) := E(\arcsin(x); m)$. Using this notation we have

$$s(\varphi'; m) = \bar{E}(1; m) - \bar{E}(\cos(\varphi'); m), \tag{4.3.8}$$

where we use the fact that $\sin(\frac{\pi}{2} - \varphi') = \cos(\varphi')$. Dropping the prime, where $x' = \cos(\varphi')$, we have our formula for the arclength

$$s(x; m) = \bar{E}(1; m) - \bar{E}(x; m). \tag{4.3.9}$$

In all of our mappings, we map from the uniform computational grid (τ) to the physical grid (x). To construct the Elliptic grid, we first construct a set of uniformly spaced arclength points from the uniform grid, $\tau \in [0, \pi]$. To do this, we note that by the definition of the complete elliptic integral of the second kind, the arclength of the upper half of the ellipse is

$2\bar{E}(1;m)$. Hence,

$$s(\tau;m) = \frac{2\bar{E}(1;m)}{\pi}\tau. \tag{4.3.10}$$

Then from (4.3.9) and (4.3.10),

$$\begin{aligned} s(\tau;m) &= s(x(\tau)) = \bar{E}(1;m) - \bar{E}(x(\tau);m), \\ \frac{2\bar{E}(1;m)}{\pi}\tau &= \bar{E}(1;m) - \bar{E}(x;m). \end{aligned} \tag{4.3.11}$$

Inverting the last equation and solving for x yields (4.3.1). The resulting Elliptic grid points x_i, as seen in (4.3.1), are given by

$$\begin{aligned} x_i &= \mathcal{X}(\tau_i;m),\ i = 0,\ldots,N-1, \\ &= \bar{E}^{-1}\left(\bar{E}(1;m) - \frac{2\bar{E}(1;m)}{\pi}\tau_i, m\right),\ i = 0,\ldots,N-1, \\ \tau_i &= \frac{2i+1}{2N}\pi,\ i = 0,\ldots,N-1. \end{aligned} \tag{4.3.12}$$

4.4 Kosloff Tal-Ezer Mapping and Grid

We now introduce the Kosloff Tal-Ezer (KT) mapping [10]. The KT map has a wide audience as noted in Table 4.1 on page 62. Table 4.1 on page 62 is an expanded version of Table 16.4 in [4]. The KT Mapping [10] with map parameter β is given by

$$\mathcal{X}(\tau;\beta) = \frac{\arcsin(\alpha\cos(\tau))}{\arcsin(\alpha)}. \tag{4.4.1}$$

Papers	Notes
Kosloff and Tal-Ezer (1993) [10]	Introduction to the KT map with numerical experiments
Carcione (1994) [6]	Compares Chebyshev and KT grid (see pg. 325)
Carcione (1994) [7]	Wave Propagation
Renaut and Frohlich (1996) [28]	2-D acoustic wave equation
Caricione (1996) [8]	Elastic wave equation
Godon (1997) [20]	Polytropic Accretion Disks
Don and Solmonoff (1997) [13]	Improvement in accuracy of computation of k-th order derivative using KT
Don and Gottlieb (1998) [12]	Shock waves
Raymundo and Archilla (2000) [27]	Error bounds for various choices of the map parameter
Baltensperger and Berrut (2001) [2]	General Hyperbolic Problems
Mead and Renaut (2002) [26]	KT satisfactory resolution with fewer than π points per wavelength
Carcione, Poletto and Gei (2004) [9]	3-D wave simulation
Javidi (2011) [23]	Burger's-Huxley equation

Table 4.1: Brief Literature Overview of the Kosloff/Tal-Ezer Mapping and its Applications

and the inverse mapping is given by

$$\mathcal{T}(x;\beta) = \arccos\left\{\frac{\sin(px)}{\alpha}\right\} = \arccos\left\{\frac{\cos(px-\frac{\pi}{2})}{\alpha}\right\}, \tag{4.4.2}$$

where

$$\alpha := 1-\beta, \tag{4.4.3}$$

$$p := \arcsin(\alpha). \tag{4.4.4}$$

The resulting KT grid is given by

$$\begin{aligned} x_i &= \mathcal{X}(\tau_i;\beta),\ i=0,\ldots,N-1, \\ \tau_i &= \frac{2i+1}{2N}\pi,\ i=0,\ldots,N-1, \end{aligned} \tag{4.4.5}$$

where $\mathcal{X}(\tau;\beta)$ is given by (4.4.1).

4.5 Theta Mapping and Grid

As we will discuss later in this thesis, the Elliptic and KT maps both possess singularities in the complex τ-plane. In an attempt to construct a map which has no singularities, we define the Theta mapping using a Jacobi theta function. We use Jacobi theta functions as they are used in the theory of diffusion and are known to be free of singularities. The particular Jacobi theta function we employ is usually referred to as θ_2 and is defined by either of the

two series

$$\begin{aligned}\theta_2\left(\tau; q = \exp\left(-1/\sigma^2\right)\right) &= 2\sum_{n=0}^{\infty} \exp\left(-\frac{(n+\frac{1}{2})^2}{\sigma^2}\right)\cos\left[(2n+1)\tau\right], \\ &= \sigma\sqrt{\pi}\sum_{m=-\infty}^{\infty}(-1)^m \exp(-\sigma^2(\tau - m\pi)^2). \qquad (4.5.1)\end{aligned}$$

We integrate the Jacobi theta function twice with respect to τ for use in the Theta mapping (see $\Xi(\tau;\sigma)$ below). The Theta Mapping with map parameter σ is given by

$$\mathcal{X}(\tau;\sigma) = \frac{\Xi(\tau;\sigma)}{\Xi(0;\sigma)}, \qquad (4.5.2)$$

where $\Xi(\tau;\sigma)$ is given by

$$\begin{aligned}\Xi(\tau;\sigma) &= 2\sum_{n=0}^{\infty}\frac{-1}{(2n+1)^2}\exp\left(-\frac{(n+\frac{1}{2})^2}{\sigma^2}\right)\cos\left[(2n+1)\tau\right] \qquad (4.5.3)\\ &= \sum_{m=-\infty}^{\infty}(-1)^m V(\tau - \pi m;\sigma). \qquad (4.5.4)\end{aligned}$$

and where

$$V(\tau;\sigma) = \frac{1}{2}\left\{\left[\frac{\pi}{2}\tau\,\mathrm{Erf}(\sigma\tau) - \frac{\sqrt{\pi}}{2\sigma}\exp(-\sigma^2\tau^2)\right] - \left[\frac{\pi}{2}(\tau-\pi)\,\mathrm{Erf}(\sigma[\tau-\pi]) - \frac{\sqrt{\pi}}{2\sigma}\exp(-\sigma^2[\tau-\pi]^2)\right]\right\}. \qquad (4.5.5)$$

The resulting Theta grid is given by

$$\begin{aligned}x_i &= \mathcal{X}(\tau_i;\sigma),\ i = 0,\ldots,N-1, \\ \tau_i &= \frac{2i+1}{2N}\pi,\ i = 0,\ldots,N-1, \qquad (4.5.6)\end{aligned}$$

where $\mathcal{X}(\tau;\beta)$ is given by (4.5.2).

4.6 The Uniform and Chebyshev Limits of the KT, Elliptic and Theta Mapping

In our discussion of the mappings, we map from the interval $\tau \in [0,\pi]$ to the interval $x \in [-1,1]$ via $\mathcal{X}(\tau;\beta)$. We will show in our discussion below that all of the mappings go from the uniform mapping

$$x = \mathcal{X}(\tau) = 1 - \frac{2}{\pi}\tau, \tag{4.6.1}$$

to the Chebyshev mapping

$$x = \mathcal{X}(\tau) = \cos(\tau) \tag{4.6.2}$$

as the map parameter is varied. As the grid points x_i are given by $\mathcal{X}(\tau_i;\beta)$ where τ_i is the uniform grid, the range of grids produced varies from its uniform limit of

$$x_i = -1 + \frac{2}{\pi}\tau_i,\ i = 0,\ldots,N-1, \tag{4.6.3}$$

to its Chebyshev limit of

$$x_i = \cos(\tau_i),\ i = 0,\ldots,N-1. \tag{4.6.4}$$

To illustrate the range of mappings produced as the map parameter is varied, we plot the the uniform mapping, KT mapping with map parameter $\beta = .1$ and Chebyshev mapping below.

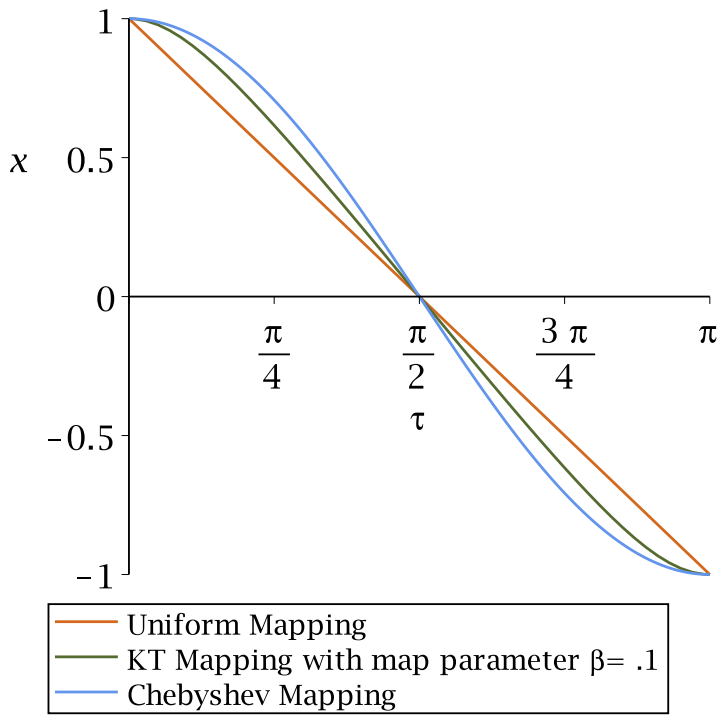

Figure 4.6.1: A plot of the range of mappings

4.6.1 Elliptic Mapping

The Elliptic mapping reduces to the uniform mapping when the map parameter $m = 1$. As m tends to 1, the semi-minor axis of the ellipse seen in Figure 4.3.1 on page 59 goes to zero (see (4.3.6)) and the ellipse collapses to a line. It follows from (4.3.11) that the mapping reduces to the uniform mapping $\mathcal{X}(\tau; 1) = 1 - \frac{2}{\pi}\tau$.

When the map parameter $m = 0$, the Elliptic mapping reduces to the Chebyshev mapping. When $m = 0$, by (4.3.11) we have that since $\bar{E}(1; 0) = \frac{\pi}{2}$,

$$\tau = \bar{E}(1; 0) - \bar{E}(x; 0). \tag{4.6.5}$$

As $\bar{E}(x;0) = \int_0^{arcsin(x)} 1 d\phi = \arcsin(x)$, we have from (4.6.5) that $x = \mathcal{X}(\tau;0) = \sin(\frac{\pi}{2} - \tau) = \cos(\tau)$.

Thus, when $m = 0$, the Elliptic mapping reduces to the Chebyshev mapping.

4.6.2 KT Mapping

The KT mapping reduces to the Chebyshev mapping when the map parameter β approaches 1 (or equivalently as $\alpha = 1 - \beta$ approaches 0). Observe that in the limit as $\alpha \to 0$,

$$\mathcal{X}(\tau;1) = \lim_{\alpha \to 0} \frac{\arcsin(\alpha \cos(\tau))}{\arcsin(\alpha)} = \cos(\tau) \lim_{\alpha \to 0} \frac{\frac{1}{\sqrt{1-(\alpha\cos(\tau))^2}}}{\frac{1}{\sqrt{1-(\alpha)^2}}} = \cos(\tau). \tag{4.6.6}$$

Or equivalently

$$\mathcal{T}(x;1) = \arccos(x). \tag{4.6.7}$$

Thus, the KT mapping reduces to the Chebyshev mapping when $\beta = 1$.

Another important limit of the KT mapping is when the map parameter β approaches 0. In this case

$$\begin{aligned} \mathcal{X}(\tau;0) &= \lim_{\alpha \to 1} \frac{\arcsin(\alpha \cos(\tau))}{\arcsin(\alpha)}, \\ &= \frac{2}{\pi} \arcsin(\cos(\tau)), \qquad (4.6.8) \\ &= \frac{2}{\pi} \arcsin(\sin(\frac{\pi}{2} - \tau)), \\ &= 1 - \frac{2}{\pi}\tau. \qquad (4.6.9) \end{aligned}$$

Equivalently in this limit,

$$\mathcal{T}(x;0) = \frac{\pi}{2}(1-x). \tag{4.6.10}$$

4.6.3 Theta Mapping

The Theta mapping reduces to the Chebyshev mapping when $\sigma = 0$. Observe from (4.5.2) that $\mathcal{X}(\tau;0) = \frac{\Xi(\tau;0)}{\Xi(0;0)} = \cos(\tau)$. Hence, when $\sigma = 0$, the Theta Mapping reduces to the Chebyshev mapping.

In the limit as $\sigma \to \infty$, the Theta mapping reduces to the uniform mapping. From (4.5.2), we have

$$\lim_{\sigma\to\infty} \mathcal{X}(\tau;\sigma) = \frac{\sum_{n=0}^{\infty} \frac{2}{(2n+1)^2} \cos\left[(2n+1)\tau\right]}{\sum_{n=0}^{\infty} \frac{2}{(2n+1)^2}}. \tag{4.6.11}$$

If we compute the Fourier cosine series (i.e. even extension) of the function $1 - \frac{2}{\pi}\tau$, we see that

$$\begin{aligned} 1 - \frac{2}{\pi}\tau &= {\sum_{m=0}^{\infty}}' a_m \cos(m\tau),\ 0 \le \tau \le \pi \\ a_m &= \frac{2}{\pi}\int_0^{\pi} \left(1 - \frac{2}{\pi}\tau\right)\cos(m\tau)d\tau, \\ &= \begin{cases} 0 & \text{if } m \text{ is even,} \\ \left(\frac{2}{\pi}\right)^2 \frac{2}{m^2} & \text{if } m \text{ is odd} \end{cases}, \end{aligned} \tag{4.6.12}$$

where the prime symbol after the summation symbol in the first line of the above equations

indicates that the first term in the series is multiplied by $\frac{1}{2}$. Hence,

$$\begin{aligned} 1-\frac{2}{\pi}\tau &= \left(\frac{2}{\pi}\right)^2 \sum_{n=0}^{\infty} \frac{2}{(2n+1)^2}\cos\left[(2n+1)\tau\right],\ 0\le\tau\le\pi \\ &= \frac{\sum_{n=0}^{\infty}\frac{2}{(2n+1)^2}\cos\left[(2n+1)\tau\right]}{\sum_{n=0}^{\infty}\frac{2}{(2n+1)^2}}, \end{aligned} \tag{4.6.13}$$

where the last line follows from plugging in $\tau = 0$ to the Fourier cosine series of $1-\frac{2}{\pi}\tau$ which after division gives $\left(\frac{2}{\pi}\right)^2 = \frac{1}{\sum_{n=0}^{\infty}\frac{2}{(2n+1)^2}}$. Comparing (4.6.13) and (4.6.11) we observe that in the limit as $\sigma\to\infty$, the Theta mapping reduces to the Fourier series of the even extension of $1-\frac{2}{\pi}\tau$. Hence, for $\tau\in[0,\pi]$,

$$\lim_{\sigma\to\infty}\mathcal{X}(\tau;\sigma) = 1-\frac{2}{\pi}\tau. \tag{4.6.14}$$

Therefore, in the limit as $\sigma\to\infty$, the Theta mapping reduces to the uniform mapping.

4.7 Grid Transformation and Polynomial Interpolation

So far in our treatment of QUSS, we have discussed mapping the grid points using one of the three mappings: KT, Elliptic or Theta. Furthermore, we have seen that the mapping has two limits in the grid it produces. At the two extremes of the choices of the map parameter, a Chebyshev grid or a uniform grid is produced. In other words, the mappings are capable of producing a more uniform grid than the Chebyshev grid where the mapping parameter decides how "uniform" the grid will be. However, in our use of QUSS, we modify the spectral method by not only mapping the grid points, but by also mapping the basis function. We will leave the discussion of the mapped basis functions for the next section. However, the

purpose of this section is to illustrate why it is a bad choice to simply produce a more uniform grid than the Chebyshev grid from one of the mappings and then keep a polynomial basis. In essence, one will be exposed to Runge's phenomenon if this is done. To demonstrate this, we will construct the polynomial cardinal function associated with the center grid point of the interval $[-1, 1]$ for the uniform, Chebyshev and KT grid for various choices of the mapping parameter (we are free to use the Elliptic or Theta grid instead of the KT grid to arrive at a similar conclusion). Moreover, we will call the cardinal function associated with the center grid point C_c and the value of the function at the center grid point f_c. The polynomial interpolant is given by the sum of the products of the cardinal function and the function value at the grid points as noted in (1.3.8) and (1.3.9) (note we use the letter C instead of P in this chapter to denote the cardinal functions).

We aim to show that huge rapid oscillations near the endpoints of the interval $[-1, 1]$ develop in the cardinal function C_c as we move to a more uniform grid away from the Chebyshev grid when the number of grid points are sufficiently high (from numerical experimentation, this number is as small as 9 grid points). Hence, small numerical errors in the value of f_c will be magnified near the endpoints due to the term $f_c C_c$ in the polynomial interpolant (1.3.9) and thus, cause huge catastrophic errors at the ends of the interval in the polynomial interpolant (1.3.9). Thus, we press for the case that we can not only map the grid points, but also the basis functions (we will map the basis function in the next section).

For the purpose of illustration, we pick the total number of grid points, N, to be 21 and denote the grid points by x_i where $0 \leq i \leq N-1$. The center grid point is denoted by x_k where we pick $k = 10$ for the remainder of this section. Moreover, the cardinal function C_c is defined by the formula $C_c(x_i) = \delta_{ik}$ for $0 \leq i \leq N-1$ where δ_{ik} is the Kronecker delta

which is one when $i = k$ and zero otherwise. Hence,

$$C_c := \prod_{i \neq k} \left(\frac{x - x_i}{x_k - x_i} \right). \tag{4.7.1}$$

We now turn to the case of the least uniform grid used in this thesis, the Chebyshev grid.

The Chebyshev grid points are given by

$$x_i = \cos(\tau_i),\ i = 0, \ldots, N-1, \tag{4.7.2}$$

$$\tau_i = \frac{2i+1}{2N}\pi,\ i = 0, \ldots, N-1, \tag{4.7.3}$$

as noted in (4.2.1). Plugging these grid points into (4.7.1) reveals C_c for the case of the Chebyshev grid. We plot the cardinal function C_c in Figure 4.7.1 on page 72 where we observe that the oscillations decrease rapidly from the center to the endpoints of the interval $[-1, 1]$.

How about the cardinal function C_c for a uniform grid on the interval $[-1, 1]$? Well, the uniform grid points on $[-1, 1]$ are given by $x_i = -1 + \frac{2i+1}{N}$ where $i = 0, \ldots, N-1$ (these are the grid points that the mapping produces in its uniform limit as noted earlier). Plugging these grid points into (4.7.1) reveals C_c for the case of the uniform grid. We plot C_c in Figure 4.7.2 on page 72 where we can clearly see the ever increasing oscillations towards the ends of the interval $[-1, 1]$. The values of C_c at the ends of the interval are more than 20 times the value of C_c at the center of the interval! These wild oscillations help explain Runge's phenomenon. Moreover, small numerical errors in the value of f_c will be amplified near the endpoints due to the term $f_c C_c$ in the polynomial interpolant (1.3.9) as was noted earlier.

To illustrate the effects of going from the non-uniform Chebyshev grid to a more uniform

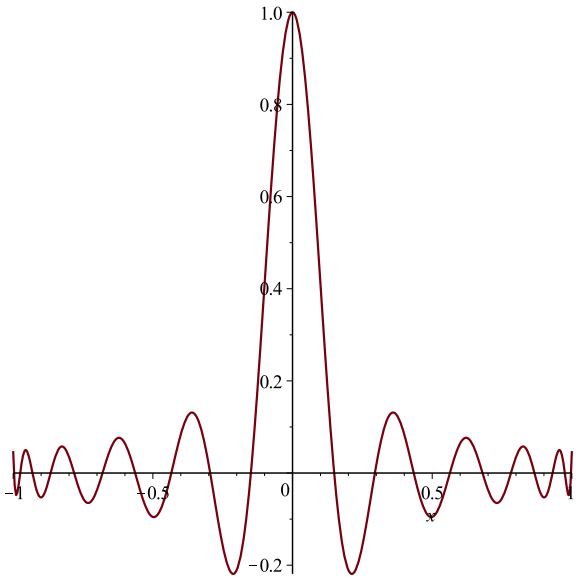

Figure 4.7.1: The Polynomial Cardinal Function C_c with a Chebyshev Grid.

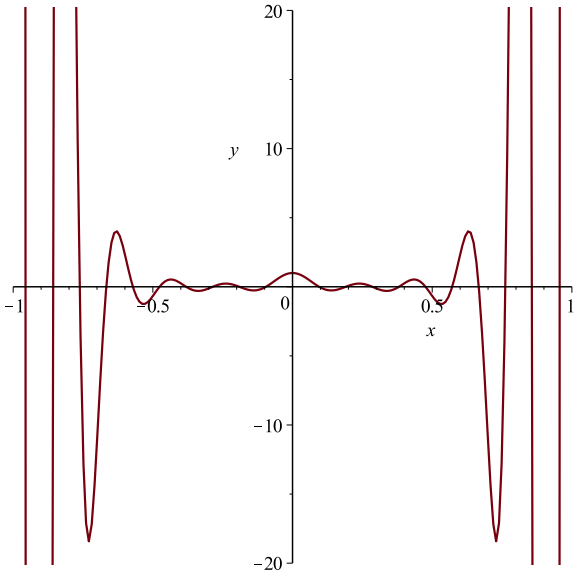

Figure 4.7.2: The Polynomial Cardinal Function C_c with a Uniform Grid.

grid with a polynomial basis, we use the KT mapping with map parameter β and observe the cardinal function C_c as the grid becomes more uniform. As explained in the previous section,

as β goes from 1 to 0, the grid produced goes from the Chebyshev grid to the uniform grid. The i-th grid point produced from the KT mapping is given by

$$x_i \quad = \quad \mathcal{X}(\tau_i;\beta),\, i = 0,\ldots,N-1, \tag{4.7.4}$$

where τ_i are the uniform grid points given by (4.7.3) and where $x(\tau;\beta)$ is given in (4.4.1). The cardinal function C_c(which now also depends on the map parameter β) is given by

$$C_c(x;\beta) \quad = \quad \prod_{i\neq k}\left(\frac{x-\mathcal{X}(\tau_i;\beta)}{\mathcal{X}(\tau_k;\beta)-\mathcal{X}(\tau_i;\beta)}\right). \tag{4.7.5}$$

Plots of the cardinal function C_c for various values of the map parameter β are shown in Figure 4.7.3 on page 73, Figure 4.7.4 on page 73 and Figure 4.7.5 on page 74.

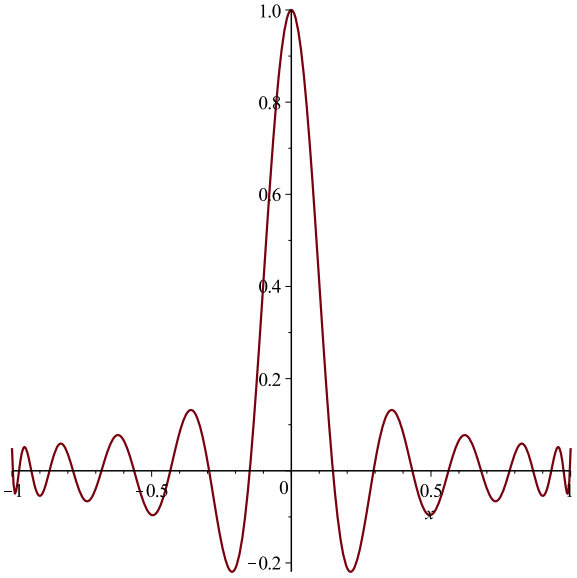

Figure 4.7.3: The Polynomial Cardinal Function C_c with a KT Grid where the mapping parameter β=0.9

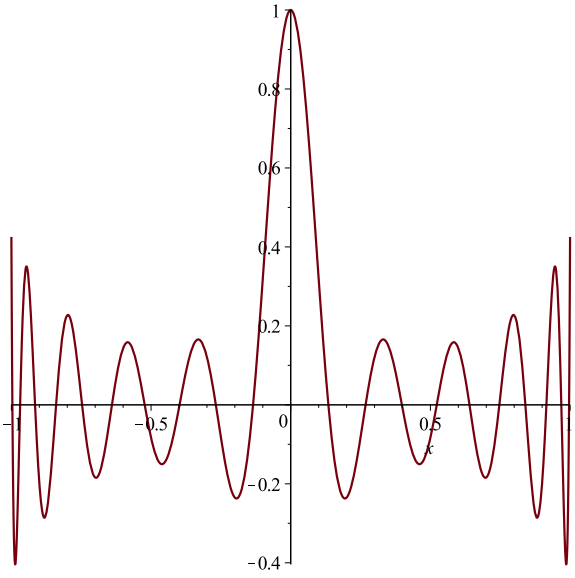

Figure 4.7.4: The Polynomial Cardinal Function C_c with a KT Grid where the mapping parameter β=0.3

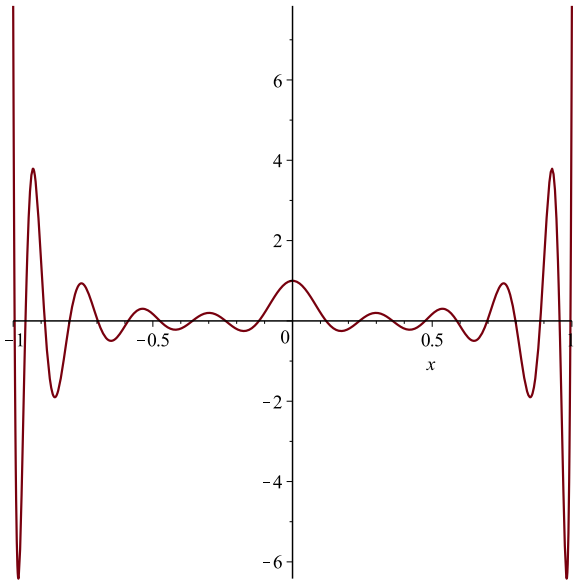

Figure 4.7.5: The Polynomial Cardinal Function C_c with a KT Grid where the mapping parameter β=0.1

We observe from these figures that when $\beta = 0.9$, which is very close to the Chebyshev limit of the KT map, the oscillations produced decrease rapidly from the center of the interval $[-1, 1]$. However as β goes toward 0, the uniform limit of the KT map, we see that the cardinal function C_c tends towards its uniform counterpart. When $\beta = 0.3$, we observe that the oscillations initially decrease from the center of the interval but then increase rapidly towards the endpoints. And when $\beta = 0.1$, we see this effect exaggerated and observe ever increasing oscillations towards the ends of the interval $[-1, 1]$ where values of C_c are more than 6 times the value of C_c at the center of the interval! Thus, we can safely conclude that mapping only the grid points without changing the basis function from the polynomial basis is a poor decision. In the next section, we promote the use of mapped cosine basis.

4.8 The Case for a Mapped Cosine Basis

In this section we would like to illustrate what happens to the cardinal function C_c described in the previous section when we also map the basis function from the basis of polynomials. First, we review the important fact that polynomial interpolation in Chebyshev grid points is equivalent to trigonometric (cosine) interpolation with equispaced grid points.

4.8.1 Polynomial and Trigonometric Interpolation

Let $f(x)$ be the function we wish to approximate by an interpolant $p_{N-1}(x)$ and let x_i be the Chebyshev grid points (4.7.2). Then, as reviewed in Chapter I of this thesis, there exists a unique polynomial interpolant of degree at most $N-1$, $p_{N-1}(x)$, that interpolates the N distinct data points $(x_i, f(x_i))$ where $i = 0, \ldots, N-1$. The polynomial interpolant, $p_{N-1}(x)$, is given by

$$p_{N-1}(x) = \sum_{i=0}^{N-1} f(x_i) C_i(x), \tag{4.8.1}$$

$$C_i(x) = \prod_{j \neq i} \frac{x - x_j}{x_i - x_j}. \tag{4.8.2}$$

As p_{N-1} is in the space of polynomials of degree at most $N-1$ and as $\{T_0(x), \ldots, T_{N-1}(x)\}$ forms a basis for this space [1], we may express (4.8.1) as

$$p_{N-1}(x) = {\sum_{n=0}^{N-1}}' c_n T_n(x), \tag{4.8.3}$$

where the prime symbol after the summation symbol indicates that the first term in the series is multiplied by $\frac{1}{2}$ as before. The Chebyshev grid is obtained by mapping the uniform

computational grid points τ_i over the interval $[0, \pi]$ (4.7.2) to the non-uniform physical grid points x_i on $[-1, 1]$ via the the mapping $x_i = \mathcal{X}(\tau_i)$ where $x = \mathcal{X}(\tau) = \cos(\tau)$. If we also map the basis function using the mapping $x = \mathcal{X}(\tau) = \cos(\tau)$, then (4.8.1),(4.8.2) and (4.8.3) become respectively

$$P_{N-1}(\tau) = \sum_{i=0}^{N-1} F(\tau_i)\tilde{C}_i(\tau), \tag{4.8.4}$$

$$\tilde{C}_i(\tau) = \prod_{j \neq i} \frac{\cos(\tau) - \cos(\tau_j)}{\cos(\tau_i) - \cos(\tau_j)}, \tag{4.8.5}$$

$$P_{N-1}(\tau) = {\sum_{n=0}^{N-1}}' c_n \cos(n\tau), \tag{4.8.6}$$

where $P_{N-1}(\tau) = p_{N-1}(x(\tau))$, $F(\tau) = f(x(\tau))$ and as reviewed in the beginning of this chapter, $T_n(\cos(\tau)) = \cos(n\tau)$. Moreover, we call $\tilde{C}_i(\tau)$ the cosine cardinal functions. The coefficients c_n in (4.8.6) and (4.8.3) can be obtained by a discrete cosine transform (DCT-II) [1, 31] of the vector $P_{N-1}(\tau_i) = F(\tau_i)$, $i = 0, \ldots, N-1$ which makes use of the fact [14] that

$$\sum_{i=0}^{N-1} \cos(j\tau_i)\cos(k\tau_i) = \frac{N}{2}\delta_{j,k},\ 0 \leq j, k \leq N-1. \tag{4.8.7}$$

Alternatively to obtain the coefficients c_n, we may employ an N point trapezoidal rule with the grid points τ_i to the Fourier cosine series coefficient formula

$$c_n = \frac{2}{\pi}\int_0^{\pi} P_{N-1}(\tau)\cos(n\tau)d\tau,\ n = 0, \ldots, N-1. \tag{4.8.8}$$

Nevertheless, the coefficients c_n are given by

$$c_n = \frac{2}{N}{\sum_{i=0}^{N-1}}' F(\tau_i)\cos(n\tau_i). \tag{4.8.9}$$

From (4.8.4) and (4.8.6), we see that $P_{N-1}(\tau)$ is a trigonometric function that interpolates the N distinct data points $(\tau_i, F(\tau_i))$ where $i = 0, \ldots, N-1$. Hence, we conclude that polynomial interpolation on a Chebyshev grid can be transformed to trigonometric interpolation with equispaced grid points under the mapping $x = \mathcal{X}(\tau) = \cos(\tau)$. Of course, the argument can be reversed. That is, we can start with the trigonometric interpolant on the uniform grid and then transform it to the polynomial interpolant on the Chebyshev grid by using the mapping $\tau = \mathcal{T}(x) = \arccos(x)$ and follow the preceding argument backwards. We follow this line of reasoning and inquire about other choices of maps $\mathcal{T}(x)$. In particular, for the KT, Theta and Elliptic maps.

4.8.2 Trigonometric and Mapped Cosine Interpolation

To ensure the notation of this subsection is not confused, we clearly state that we let $f(x)$ be the function we wish to approximate in the physical coordinate x and $F(\tau; \beta)$ be the mapped function in the computational coordinate τ given by

$$F(\tau; \beta) = f(\mathcal{X}(\tau; \beta)), \tag{4.8.10}$$

where $x = \mathcal{X}(\tau; \beta)$ represents either the KT, Theta or Elliptic mapping with a fixed map parameter β (we will later address the extraordinarily important question of how to choose the map parameter β). Moreover, we let $\mathcal{T}(x; \beta)$ represent the inverse of the mapping $\mathcal{X}(\tau; \beta)$ in the sense of 4.2.12. Hence, it follows that for a fixed value of β

$$f(x) = F(\mathcal{T}(x; \beta); \beta). \tag{4.8.11}$$

We let $p_{N-1}(x;\beta)$ denote the interpolant (in general this will not be a polynomial) that approximates $f(x)$ on the physical coordinate x and we let $P_{N-1}(\tau;\beta)$ represent the interpolant on the computational coordinate τ. From 4.2.12, it follows that for a fixed value of β

$$p_{N-1}(x;\beta) = P_{N-1}(\mathcal{T}(x;\beta);\beta). \tag{4.8.12}$$

From equations (4.8.4), (4.8.5), (4.8.6), (4.8.9) we have that the trigonometric interpolant $P_{N-1}(\tau;\beta)$ that interpolates the data $(\tau_i, F(\tau_i;\beta))_{i=0}^{N-1}$ where τ_i is the uniform computational grid (4.7.3) is given by

$$\begin{aligned}
P_{N-1}(\tau;\beta) &= \sum_{i=0}^{N-1} F(\tau_i;\beta)\tilde{C}_i(\tau;\beta), && (4.8.13)\\
\tilde{C}_i(\tau;\beta) &= \prod_{j\neq i} \frac{\cos(\tau)-\cos(\tau_j)}{\cos(\tau_i)-\cos(\tau_j)}, && (4.8.14)\\
P_{N-1}(\tau;\beta) &= {\sum_{n=0}^{N-1}}' c_n \cos(n\tau), && (4.8.15)\\
c_n &= \frac{2}{N}\sum_{i=0}^{N-1} F(\tau_i;\beta)\cos(n\tau_i). && (4.8.16)
\end{aligned}$$

The interpolant on the physical grid, $p_{N-1}(x;\beta)$, is given by (4.8.12). Hence, $p_{N-1}(x;\beta)$ is

$$p_{N-1}(x;\beta) = \sum_{i=0}^{N-1} f(x_i)C_i(x;\beta), \tag{4.8.17}$$

$$C_i(x;\beta) = \prod_{j\neq i} \frac{\cos(\mathcal{T}(x;\beta)) - \cos(\mathcal{T}(x_j;\beta))}{\cos(\mathcal{T}(x_i;\beta)) - \cos(\mathcal{T}(x_j;\beta))}, \tag{4.8.18}$$

$$p_{N-1}(x;\beta) = {\sum_{n=0}^{N-1}}' c_n \cos(n\mathcal{T}(x;\beta)), \tag{4.8.19}$$

$$c_n = \frac{2}{N}{\sum_{i=0}^{N-1}}' f(x_i)\cos(n\tau_i), \tag{4.8.20}$$

where $x_i = \mathcal{X}(\tau_i;\beta)$ and by 4.2.12, $\tau_i = \mathcal{T}(x_i;\beta)$. We also point out that $f(x_i) = f(\mathcal{X}(\tau_i;\beta)) = F(\tau_i;\beta)$. From the above equations, we can see that $p_{N-1}(x;\beta)$ is the interpolant in the physical coordinate x that interpolates the data $\{(x_i, f(x_i))\}_{i=0}^{N-1}$. We call $\{1, \cos(\mathcal{T}(x;\beta)), \ldots, \cos((N-1)\mathcal{T}(x;\beta))\}$ the mapped cosine basis set (irrelevant of whether it actually forms a basis) and say that $p_{N-1}(x;\beta)$, the approximation to $f(x)$, is a mapped cosine interpolant (we also call it the KT mapped cosine interpolant when the map is KT and similarly when the map used is Theta or Elliptic).

Theorem 17. *Let the range and domain of the mapping $\mathcal{T}(x;\beta)$ for a fixed value of β be given by $[0,\pi]$ and $[-1,1]$ respectively. If $\mathcal{T}(x;\beta)$ is invertible with inverse $\mathcal{X}(\tau;\beta)$, then the set of functions $\{1, \cos(\mathcal{T}(x;\beta)), \ldots, \cos((N-1)\mathcal{T}(x;\beta))\}$ is linearly independent over the interval $[-1,1]$ where N is a fixed integer.*

Proof. By contradiction. Suppose that the set of functions $\{1, \cos(\mathcal{T}(x;\beta)), \ldots, \cos((N-1)\mathcal{T}(x;\beta))\}$ are linearly dependent. That is there exists some choice of b_n, all of which are

not zero, such that

$$\sum_{n=0}^{N-1} b_n \cos(n\mathcal{T}(x;\beta)) = 0 \tag{4.8.21}$$

for all $x \in [-1,1]$. We note that every point $x \in [-1,1]$ can be mapped uniquely from a point in $\tau \in [0,\pi]$ using the invertible mapping $x = \mathcal{X}(\tau;\beta)$. Hence by using the mapping $x = \mathcal{X}(\tau;\beta)$ in (4.8.21) and using the definition of the inverse (4.2.12), we have

$$\sum_{n=0}^{N-1} b_n \cos(n\tau) = 0 \tag{4.8.22}$$

for all $\tau \in [0,\pi]$. However as is well known, the set of functions $\{1, \cos(\tau), \ldots, \cos((N-1)\tau)\}$ over the interval $\tau \in [0,\pi]$ is linearly independent. Therefore, the only choice of coefficients b_n that would satisfy (4.8.22) is $b_n = 0$ for all $n = 0, \ldots, N-1$. Hence, we have a contradiction. Therefore the set of functions $\{1, \cos(\mathcal{T}(x;\beta)), \ldots, \cos((N-1)\mathcal{T}(x;\beta))\}$ is linearly independent over the interval $[-1,1]$. □

A plot of the first few KT mapped cosine basis functions are shown in Figure 4.8.1 on page 81, Figure 4.8.2 on page 81 and Figure 4.8.3 on page 81 as the map parameter goes from its uniform limit $\mathcal{T}(x;0) = \frac{\pi}{2}(1-x)$ to its Chebyshev limit $\mathcal{T}(x;1) = \arccos(x)$. The mapped cosine basis set clearly varies from its uniform limit of

$$\{1, \cos(\frac{\pi}{2}(1-x)), \ldots, \cos(\frac{(N-1)\pi}{2}(1-x))\}, \tag{4.8.23}$$

to its Chebyshev limit of

$$\{1, T_1(x), \ldots, T_{N-1}(x)\}, \tag{4.8.24}$$

where $T_i(x)$ is the i-th Chebyshev polynomial as suggested in (4.8.1), (4.8.2) and (4.8.3).

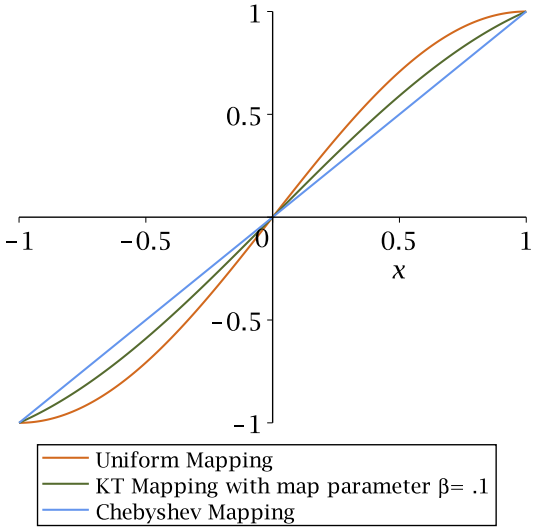

Figure 4.8.1: $\cos(\mathcal{T}(x;\beta))$ as β is varied from its uniform to Chebyshev limit

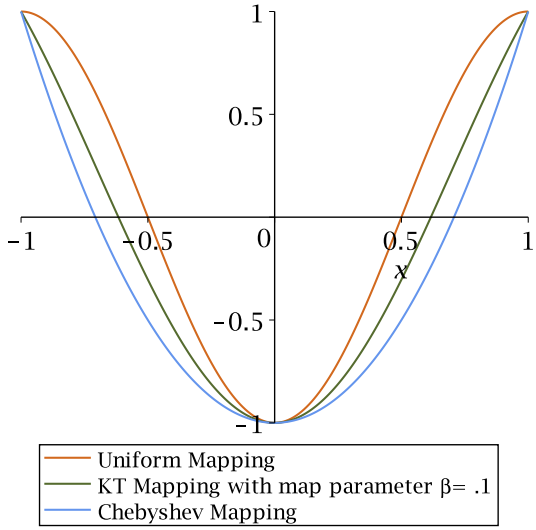

Figure 4.8.2: $\cos(2\mathcal{T}(x;\beta))$ as β is varied from its uniform to Chebyshev limit

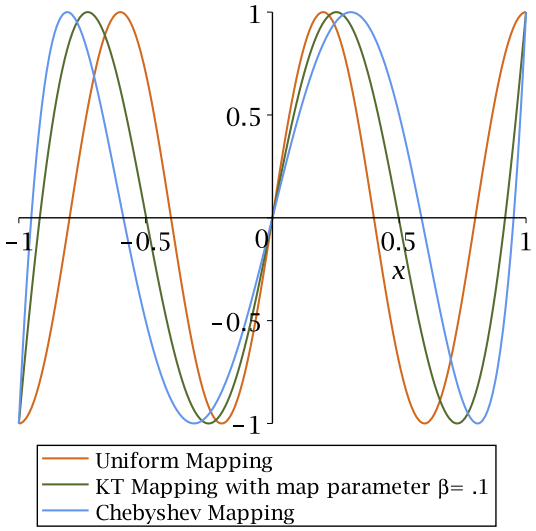

Figure 4.8.3: $\cos(5\mathcal{T}(x;\beta))$ as β is varied from its uniform to Chebyshev limit

We now point out that the mapped cosine cardinal functions, $C_i(x;\beta)$ (4.8.18), under any choice of mapping $\mathcal{T}(x;\beta)$ (KT, Elliptic, Theta or other) will have peaks the same height. In

particular, if we choose the mapping $\mathcal{T}(x;\beta) = \arccos(x)$, then the mapped cosine cardinal functions in the uniform grid points τ_i (4.8.18) can be transformed to the polynomial cardinal function with Chebyshev grid points (4.8.2) as explained in the previous subsection. Hence, the mapped cosine cardinal functions $C_i(x;\beta)$ with any choice of mapping $\mathcal{T}(x;\beta)$ will have peaks the same height as the polynomial cardinal function in Chebyshev grid points. Figure 4.7.1 on page 72 is an illustration of a polynomial cardinal function in Chebyshev grid points.

For an illustration of a mapped cosine cardinal function where $\mathcal{T}(x;\beta)$ depends on β, we plot the cardinal function associated with the center grid point $C_c(x;\beta)$ (4.8.18) with the KT mapping given in (4.4.2) for two choices of β, $\beta = 0.01$ and $\beta = 0.99$ in (4.8.4) and (4.8.5) respectively. We pick the total number of grid points, N, to be 21 and the center grid point to be given by $x_k = \mathcal{X}(\tau_k;\beta)$ where $k = 10$ as in the previous section.

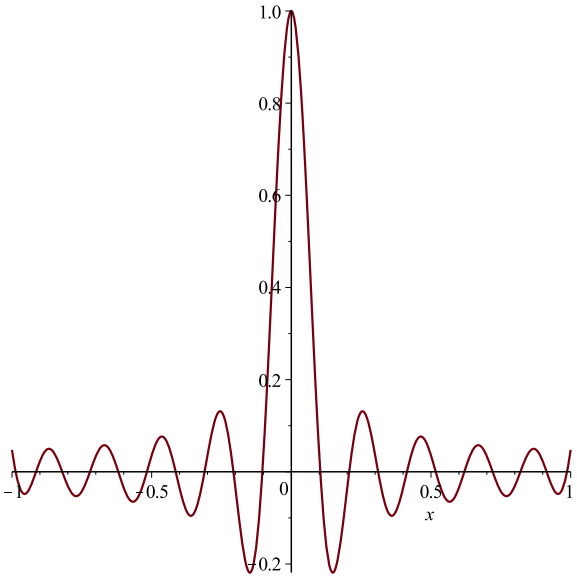

Figure 4.8.4: The KT Mapped Cosine Cardinal Function C_c where the mapping parameter β=.01

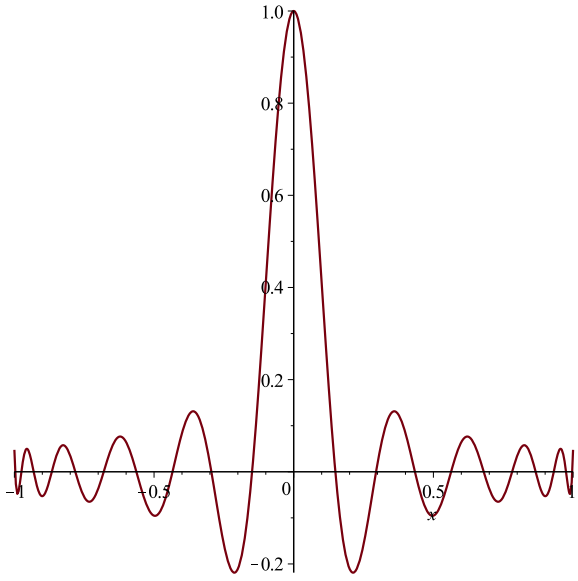

Figure 4.8.5: The KT Mapped Cosine Cardinal Function C_c where the mapping parameter β=.99

We observe the expected, that the oscillations die out toward the ends of the interval $[-1,1]$ or equivalently that the heights of the plots of C_c are no different than in Figure 4.7.1 on page 72. Hence, Runge's phenomenon can be avoided in the mapped trigonometric interpolant $p_{N-1}(x;\beta)$. Moreover, we observe that as the mapping parameter tends from its uniform limit ($\beta = 0$) toward its Chebyshev limit ($\beta = 1$) for the KT mappings, the oscillations become more and more non-uniform towards the ends of the interval $[-1,1]$. The Chebyshev limit represents the case where we have the most non-uniform oscillations.

4.8.3 Example of a Mapped Cosine Interpolant: Runge's Function

For an illustration of mapped cosine interpolants, we approximate Runge's function

$$f(x) = \frac{1}{1+25x^2} \tag{4.8.25}$$

over the interval $[-1,1]$ by a mapped cosine interpolant. The mapped function $F(\tau;\beta)$ (4.8.10) is given by

$$F(\tau;\beta) = \frac{1}{1+25\mathcal{X}(\tau;\beta)^2}, \tag{4.8.26}$$

$$= \frac{\arcsin^2(\alpha)}{\arcsin^2(\alpha)+25\arcsin^2(\alpha\cos(\tau))}, \tag{4.8.27}$$

where we first consider $\mathcal{X}(\tau;\beta)$ to be given by the KT mapping (4.4.1). The KT mapped interpolant $p_{N-1}(x;\beta)$ (4.8.19) in the physical coordinate x_i is given by

$$\begin{aligned} p_{N-1}(x_i;\beta) &= {\sum_{n=0}^{N-1}}' c_n \cos(n\tau_i), \\ c_n &= \frac{2}{N}\sum_{i=0}^{N-1} f(x_i)\cos(n\tau_i), \end{aligned} \tag{4.8.28}$$

where $x_i = \mathcal{X}(\tau_i;\beta)$, $f(x_i) = F(\tau_i;\beta)$ and τ_i are the uniform grid points given in (4.7.3). Evidently, $p_{N-1}(x;\beta)$ interpolates $f(x)$ at the grid points $\{x_i\}_{i=0}^{N-1}$. Plots of the KT mapped interpolant $p_{N-1}(x;\beta)$ are shown in Figure 4.8.6 on page 84, Figure 4.8.7 on page 84 and Figure 4.8.8 on page 85 for various values of the map parameter β where $N = 15$.

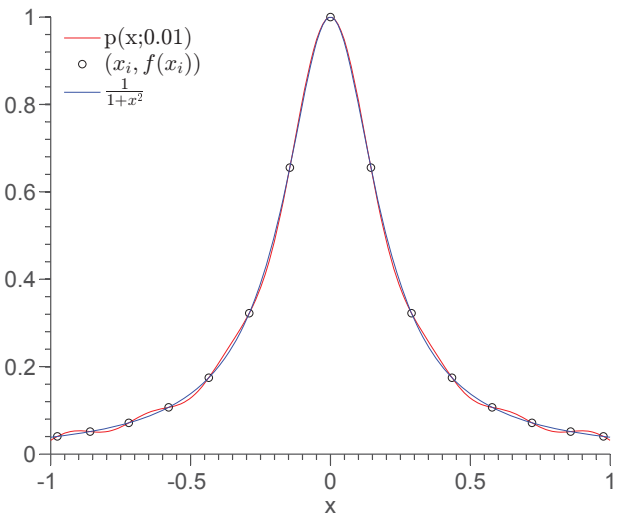

Figure 4.8.6: Runge's function and its KT mapped cosine interpolant with $\beta = 0.01$ and $N = 15$. The 15 interpolated grid points are circled.

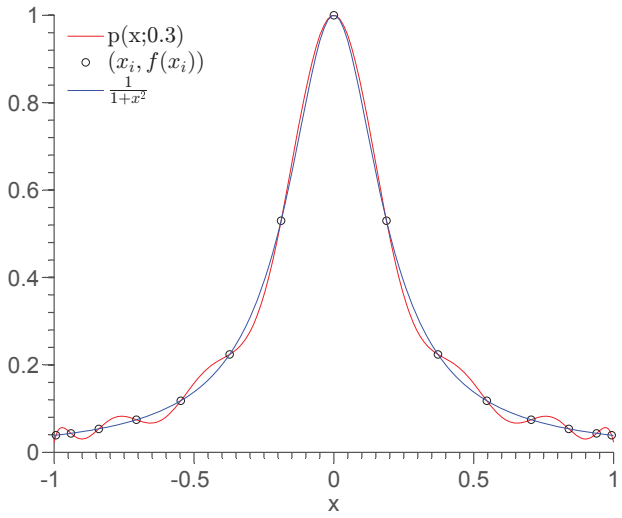

Figure 4.8.7: Runge's function and its KT mapped cosine interpolant with $\beta = 0.3$ and $N = 15$. The 15 interpolated grid points are circled.

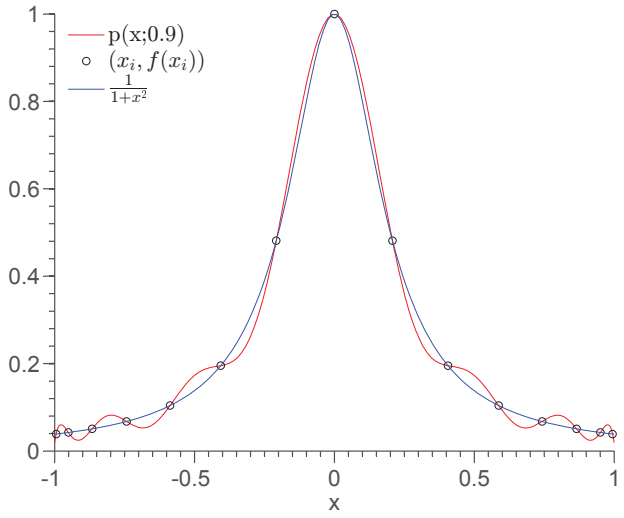

Figure 4.8.8: Runge's function and its KT mapped cosine interpolant with $\beta = 0.9$ and $N = 15$. The 15 interpolated grid points are circled.

We can visually see (N was picked to be small for this purpose) from the above plots that the choice of $\beta = .01$, where the grid points are very close to uniform, is better than $\beta = 0.3$ or $\beta = 0.9$. A plot of the different grid points for the three examples above is shown in Figure 4.8.9 on page 85.

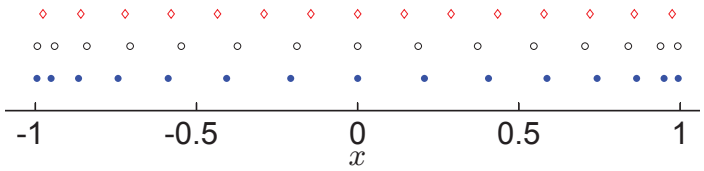

Figure 4.8.9: KT Mapped Grid Points for $\beta = 0.01$(red diamond), $\beta = 0.3$ (black circle) and $\beta = 0.9$ (blue dots) where $N = 15$.

We are now left with the question of how to pick the optimal map parameter? In a sense, this boils down to a question of how we wish to approximate $f(x)$. That is, which set of functions $\{1, \cos(\mathcal{T}(x;\beta)), \ldots, \cos((N-1)\mathcal{T}(x;\beta))\}$ along with the interpolation points $x_i = \mathcal{X}(\tau_i;\beta)$

should we use to approximate $f(x)$? Recall that $\{1, \cos(\mathcal{T}(x;\beta)), \ldots, \cos((N-1)\mathcal{T}(x;\beta))\}$ and $x_i = \mathcal{X}(\tau_i;\beta)$ vary from their uniform limits of (4.8.23) and (4.6.3) respectively to their Chebyshev limits of (4.8.24) and (4.6.4) respectively as the map parameter is varied. In an attempt to find the optimal map parameter we let

$$\mathcal{E}(N-1,\beta) := \max_{x\in[-1,1]} |f(x) - p_{N-1}(x;\beta)|, \tag{4.8.29}$$

where $p_{N-1}(x;\beta)$ interpolates $f(x)$ at the N grid points $(x_i, f(x_i))_{i=0}^{N-1}$ where $x_i = \mathcal{X}(\tau_i;\beta)$ and τ_i are the uniform grid points (4.7.3). The optimal map parameter, β^*_{N-1}, is then defined as

$$\beta^*_{N-1} = \arg\min_{\beta} \mathcal{E}(N-1;\beta). \tag{4.8.30}$$

To have a feel for how $\mathcal{E}(N-1,\beta)$ looks like, we plot $\mathcal{E}(N-1,\beta)$ for the KT mapped cosine interpolant with $N = 50$ in Figure 4.8.10 on page 87. This figure reveals that the optimal map parameter for $N = 50$ for the KT map is roughly $\beta^* \approx .01$. However, we observe a V shaped curve for the approximation error where the magnitude of the slope on the left side of the curve is larger than its right. This has practical significance since if one picks β naively smaller than β^* by an order of magnitude (roughly 10^{-3}) they are penalized *more* than for a choice of β larger than β^* by an order of magnitude (roughly 10^{-1}). This difference in error is roughly an order of magnitude. Hence, we seek the cause of this V shaped curve to give valuable advice of how to pick the map parameter for the practitioner who uses mapped cosine interpolants.

It turns out that the V shaped curve is the result of two different singularities of the function $F(\tau;\beta)$ in the complex τ-plane where $\tau = \tau_r + i\tau_{im}$. One singularity,$\tau_1^{KT}$, is from Runge's function (4.8.25) which has a simple pole located at $x = \frac{i}{5}$. This singularity can be found

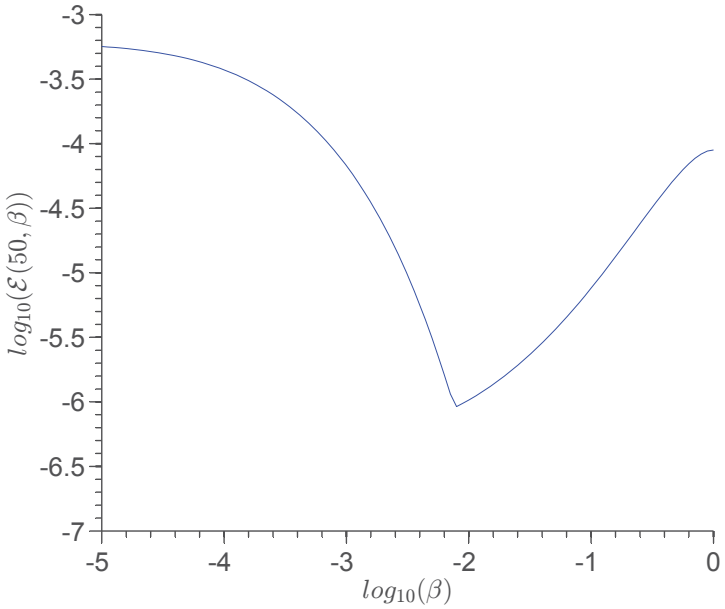

Figure 4.8.10: The KT mapped cosine approximation error (4.8.29) of Runge's function as β is varied and where $N = 50$

by setting $\mathcal{X}(\tau;\beta) = i/5$ and solving for τ which yields

$$\begin{aligned} \tau_1^{KT} &= \mathcal{T}\left(\frac{i}{5},\beta\right), \\ &= \frac{\pi}{2} - i\sinh^{-1}\left(\frac{\sinh\left(\frac{(\sin^{-1}(1-\beta))}{5}\right)}{1-\beta}\right), \end{aligned} \tag{4.8.31}$$

where the last line follows from (4.4.2) and the fact that for real valued y, $\cos^{-1}(iy) = \frac{\pi}{2} - \sinh^{-1}(y)$, $\sin(iy) = i\sinh(y)$ and $\sin^{-1}(iy) = i\sinh^{-1}(y)$.

The other singularity is from a branch point singularity of the KT map. From (4.4.1), we see that the map is singular when

$$(1-\beta)\cos(\tau) = 1. \tag{4.8.32}$$

From the identity $\cos(\tau_r + i\tau_{im}) = \cos(\tau_r)\cosh(\tau_{im}) + i\sin(\tau_r)\sinh(\tau_{im})$ and the fact that $0 < \beta < 1$, we see that the KT map is singular when

$$\tau_2^{KT} = r\pi + i\cosh^{-1}\left(\frac{1}{1-\beta}\right), \tag{4.8.33}$$

where r is an integer. We show in our discussion of error in the next section that the effects of the singularities τ_1^{KT} and τ_2^{KT} on the approximation error $\mathcal{E}(N-1,\beta)$ are

$$[\,]\exp(-(N-1)\mu_1^{KT}) \tag{4.8.34}$$

and

$$[\,]\exp(-(N-1)\mu_2^{KT}) \tag{4.8.35}$$

respectively where $[\,]$ denotes an algebraic function of N and $\mu_i^{KT} = |Im(\tau_i^{KT})|$ for $i = 1, 2$. Hence, the dominant term in the interpolation error will be from the singularity closest to the real axis (modulo the effect of the algebraic function of N in front of the exponential $\exp(-(N-1)\mu_i^{KT})$ for $i = 1, 2$ of course). We plot μ_1^{KT} and μ_2^{KT} as β varies for reference below. We observe from these plots that when β is close to its Chebyshev limit of one, $\mathcal{E}(N-1,\beta)$ is dominated by the singularity from Runge's function τ_1^{KT} and when β is close to its uniform limit of zero, $\mathcal{E}(N-1,\beta)$ is dominated by the singularity from the KT map τ_2^{KT}.

We see from Figure 4.8.10 on page 87 that when β decreases from its Chebyshev limit of one, the error initially drops which corresponds to the fact that the singularity associated with Runge's function is pushed higher into the complex τ plane (see Figure 4.8.11 on page 89). However, as β comes closer to its uniform limit of zero, unfortunately, the KT

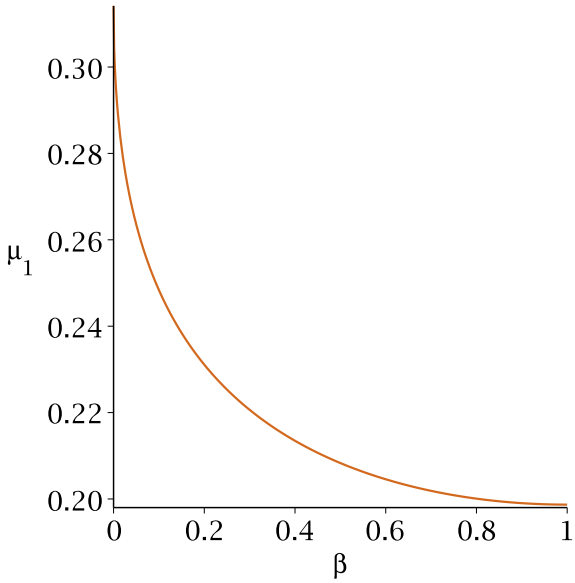

Figure 4.8.11: Plot of $\mu_1 = |Im(\tau_1)|$ as β is varied from 0 to 1.
We observe that as β goes towards its uniform limit of zero, the singularity in the τ-plane that results from the pole of Runge's function, moves away from the real axis.

mapping singularity is pushed closer to the real axis (see Figure 4.8.12 on page 90) and abruptly becomes the dominant singularity. The optimum value of β is then when the two error terms $[\,]\exp(-(N-1)\mu_1^{KT})$ and $[\,]\exp(-(N-1)\mu_2^{KT})$ are equal. As N is fixed in Figure 4.8.10 on page 87, the terms in brackets are constants (though these constants may depend on the map parameter). To discover these constants, we fit the interpolation error curve in Figure 4.8.10 on page 87 with the dominant term in the approximation error $c_1 \exp(-(N-1)\mu_1^{KT})$ when β is close to one and with the dominant error term in the approximation error $c_2 \exp(-(N-1)\mu_2^{KT})$ when β is close to zero. The results of the fit indicate that for β close to zero, the dominant error term is given by

$$7.276 \times 10^{-4} \exp\left(-(N-1)\mu_2^{KT}\right) \tag{4.8.36}$$

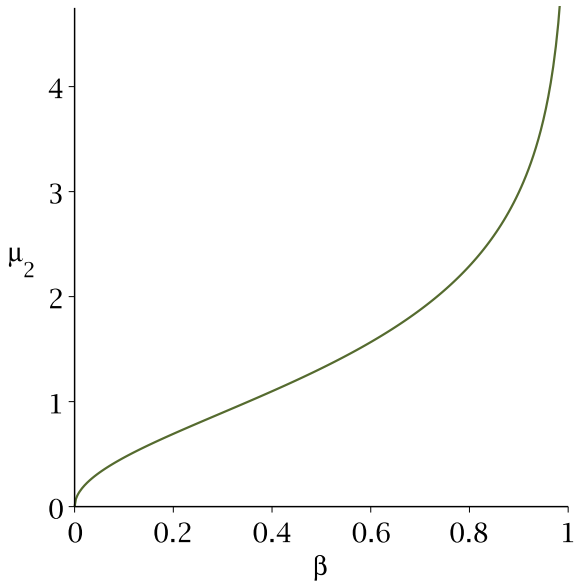

Figure 4.8.12: Plot of $\mu_2 = |Im(\tau_2)|$ as β is varied from 0 to 1.
We observe that as β decreases to 0, the singularity in the τ-plane that results from the branch point singularity of the KT map, moves towards the real axis.

and for β close to one, the dominant error term is given by

$$1.506 \exp\left(-(N-1)\mu_1^{KT}\right). \tag{4.8.37}$$

The plots of the fitted curves and the interpolation error are shown in Figure 4.8.13 on page 91.

Curiosity begs the question of how the approximation error of Runge's function using a mapped cosine interpolant would look like if we employed either of the Elliptic or Theta maps. For the Elliptic mapping we have

$$F(\tau; m) = \frac{1}{1 + 25\left(\bar{E}^{-1}\left(\bar{E}(1;m) - \frac{2\bar{E}(1;m)}{\pi}\tau, m\right)\right)^2} \tag{4.8.38}$$

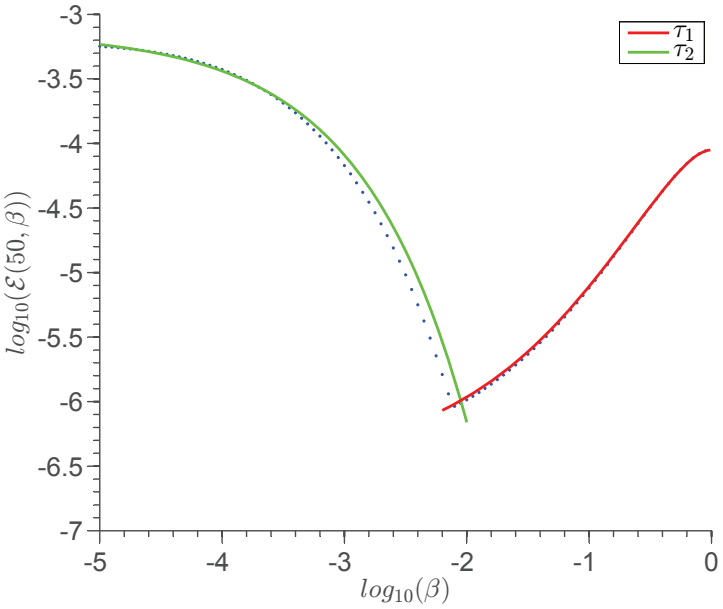

Figure 4.8.13: The KT mapped cosine approximation error of Runge's function (4.8.29) (blue dots) and fits (4.8.36) (green line) and (4.8.37) (red line) as β is varied and where $N = 50$

which follows directly from equations (4.8.26) and (4.3.1). The singularity of Runge's function mapped to the complex τ-plane is given by

$$\begin{aligned} \tau_1^E(m) &= \mathcal{T}\left(\frac{i}{5};m\right), \\ &= \frac{\pi}{2\bar{E}(1;m)}\left(\bar{E}(1;m) - \bar{E}\left(\frac{i}{5};m\right)\right), \end{aligned} \tag{4.8.39}$$

where $\mathcal{T}(x;m)$is given in equation (4.3.2). Hence, $\mu_1 = |Im(\tau_1^E)|$ is given by

$$\mu_1^E(m) = \frac{\pi}{2\bar{E}(1;m)}\left|Im\left(\bar{E}\left(\frac{i}{5};m\right)\right)\right| \tag{4.8.40}$$

A plot of μ_1^E as m is varied is shown in Figure 4.8.14 on page 92. We observe from this plot that when m is close to its Chebyshev limit of zero, $\mathcal{E}(N-1,\beta)$ is dominated by the

singularity from Runge's function τ_1^E.

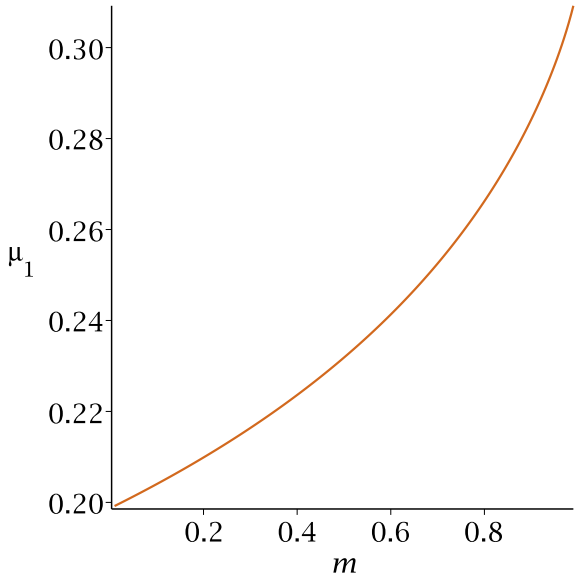

Figure 4.8.14: Plot of $\mu_1 = |Im(\tau_1)|$ as m is varied from 0 to 1.
We observe that as m goes towards its uniform limit of one, the singularity in the τ-plane that results from the pole of Runge's function, moves away from the real axis.

The mapping singularity of $\mathcal{X}(\tau; m)$ can be found from the zeroes of $\frac{d\mathcal{T}}{dx}$ as $\frac{d\mathcal{X}}{d\tau}\big|_{\tau=\mathcal{T}(x;m)} = \frac{1}{\frac{d\mathcal{T}}{dx}\big|_x}$. Hence, from (4.3.4), the zeros of $\frac{d\mathcal{T}}{dx}$ occur when $x_s = \pm 1/\sqrt{m}$. The mapping singularity of $\mathcal{X}(\tau; m)$ is then

$$\begin{aligned} \tau_2^E(m) &= \mathcal{T}(x_s; m), \\ &= \frac{\pi}{2\bar{E}(1;m)} \left(\bar{E}(1;m) - \bar{E}\left(\frac{1}{\sqrt{m}}; m \right) \right), \\ &= \frac{\pi}{2} \left(1 - \frac{\bar{E}\left(\frac{1}{\sqrt{m}}; m \right)}{\bar{E}(1;m)} \right). \end{aligned} \tag{4.8.41}$$

The absolute value of the imaginary part of the singularity $\mu_2^E = |Im(\tau_2)|$ is given by

$$\mu_2^E = \frac{\pi}{2\bar{E}(1;m)} \left| Im\left(\bar{E}\left(\frac{1}{\sqrt{m}}; m \right) \right) \right|. \tag{4.8.42}$$

Using Maple to take a series expansion of 4.8.41 about $m = 1$ suggests that $\mu_2^E \approx \frac{\pi^2}{8}(1 - m)$ for m close to 1. Hence, when m is close to its uniform limit of one, $\mathcal{E}(N-1, \beta)$ is dominated by the singularity from the Elliptic mapping τ_2. We plot the approximation error $\mathcal{E}(N-1, m)$ for the Elliptic mapped cosine interpolant with $N = 100$ in the figure below and fit the approximation error when m is close to its Chebyshev limit ($m = 0$) to the suspected dominant approximation error term $d_1 \exp\left(-(N-1)\mu_1^E\right)$ and when m is close to its uniform limit ($m = 1$) to the suspected dominant approximation error term $d_2 \exp\left(-(N-1)\frac{\pi^2}{8}(1-m)\right)$. The results of the fit indicate that for m close to its Chebyshev limit ($m = 0$), the dominant error term is given by

$$1.154 \exp\left(-(N-1)\mu_1^E\right) \tag{4.8.43}$$

and for m close to its uniform limit ($m = 1$), the dominant error term is given by

$$1.165 \times 10^{-4} \exp\left(-(N-1)\frac{\pi^2}{8}(1-m)\right). \tag{4.8.44}$$

We now turn to a discussion of the approximation error of Runge's function using a mapped cosine interpolant where the Theta map is employed.

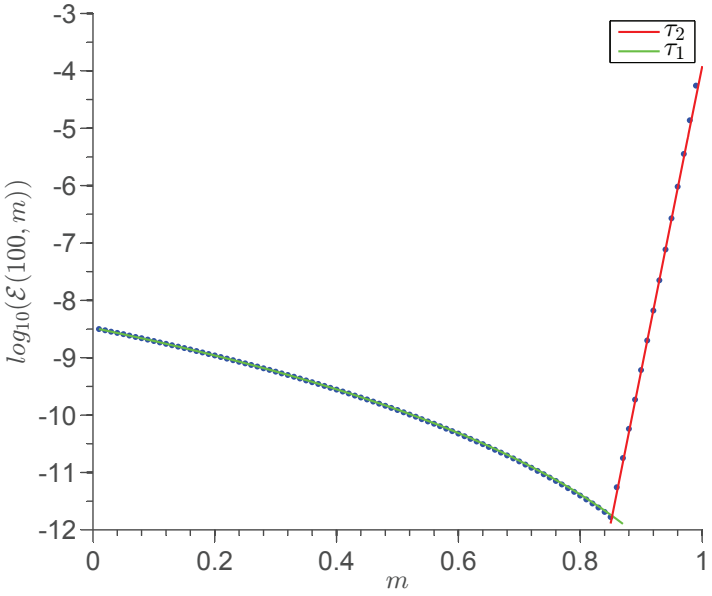

Figure 4.8.15: The Elliptic mapped cosine approximation error of Runge's function (blue dots) and fits (4.8.44) (green line) and (4.8.43)(red line) as m is varied and where N=100

For the Theta mapping, Runge's function mapped to the τ plane is given by

$$F(\tau;m) = \frac{1}{1+25\left(\frac{\Xi(\tau;\sigma)}{\Xi(0;\sigma)}\right)^2} \tag{4.8.45}$$

where $\Xi(\tau;\sigma)$ is given in equation (4.5.4). The Theta mapping possesses no singularities. The only singularity is that of Runge's function mapped to the complex τ-plane, τ_1^{Θ}, which can be obtained by solving

$$\Xi(\tau_1^{\Theta};\sigma) \;=\; \frac{i}{5}\Xi(0;\sigma). \tag{4.8.46}$$

Inverting (4.8.46) is relatively challenging; hence, we will only show numerical results for the approximation error (4.8.29). The approximation error of Runge's function using a Theta

mapped cosine interpolant is shown in 4.8.16 for $N = 100$. In this figure we observe a decrease in error by roughly 4 orders of magnitude when σ initially moves away from its Chebyshev limit ($\sigma = 0$). We suspect this decrease in error is due to the singularity τ_1^{Θ} being pushed further from the real axis for small values of σ. While the Theta mapping possesses no singularities, it does however, as σ tends toward its uniform limit ($\sigma \to \infty$), reduce to the Fourier series of the even extension of $1 - \frac{2}{\pi}\tau$ as noted earlier in this thesis and hence, develops sharp peaks at $\tau = 0$ and $\tau = \pi$. We suspect these sharp peaks may be behind the increase in error seen as σ tends to its uniform limit.

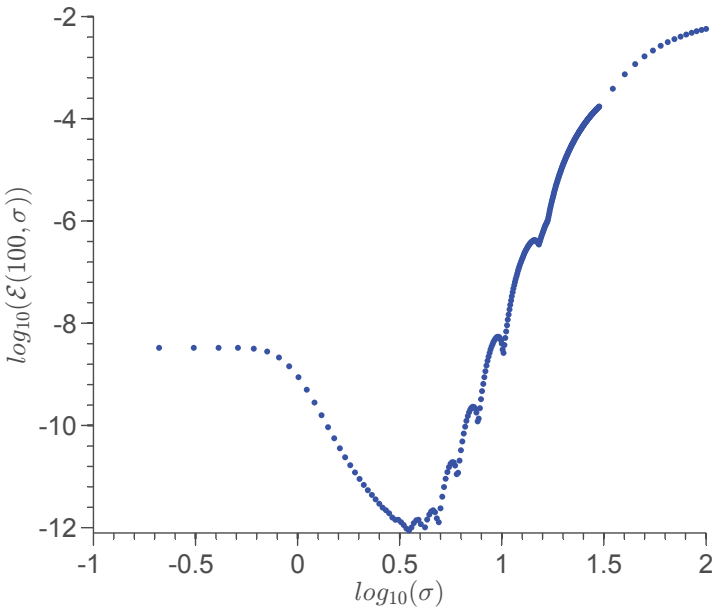

Figure 4.8.16: The Theta mapped cosine approximation error of Runge's function (blue dots) as σ is varied and where N=100

To compare all of the mappings in the context of the example of Runge's function, we show $\mathcal{E}(N-1,\beta)$ for all three of the mappings with $N = 100$ next to one another in one plot. We observe that the mapped cosine interpolants outperform Chebyshev interpolants with an appropriate choice of the map parameter for all of the mappings!

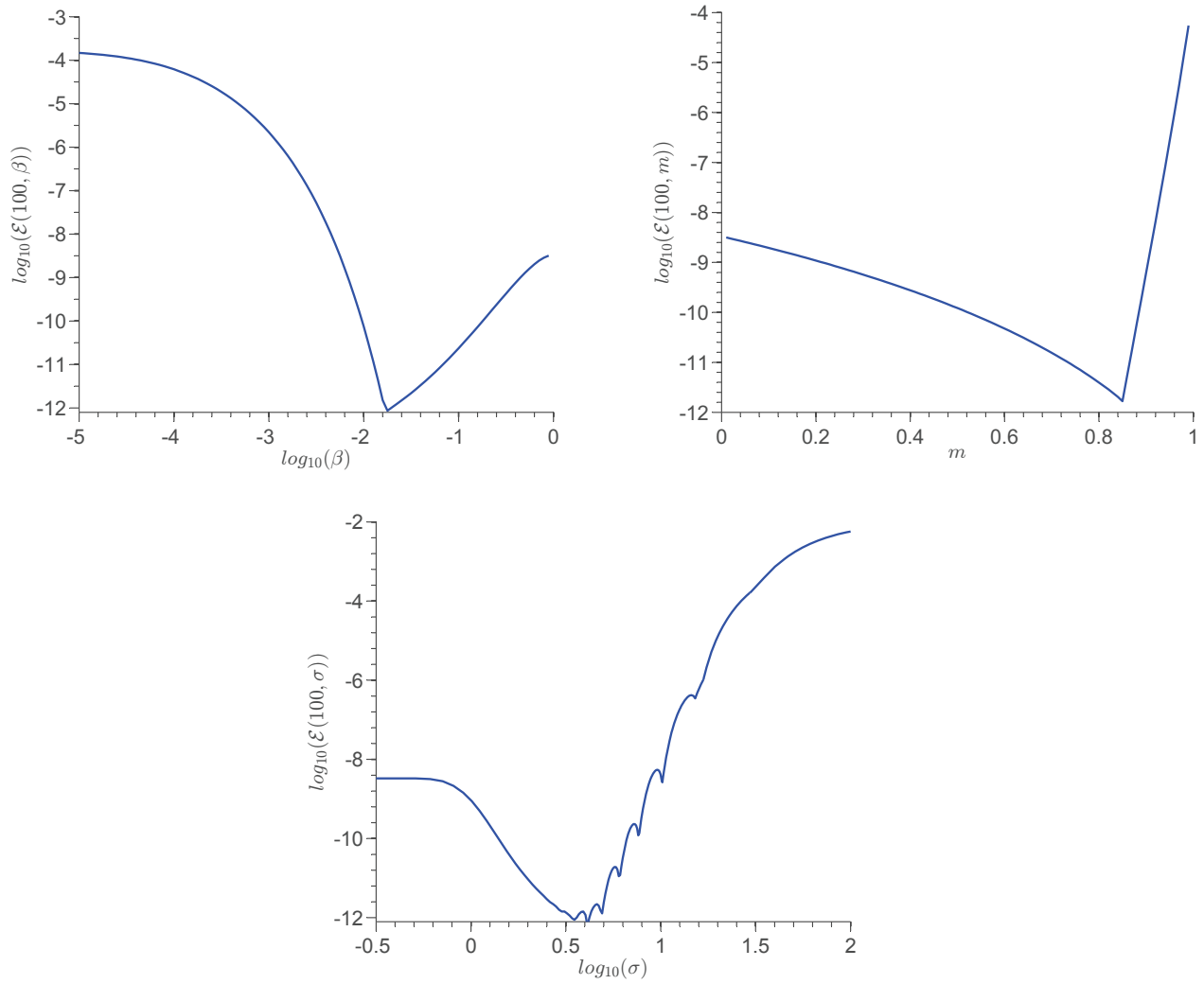

Figure 4.8.17: The KT mapped cosine approximation error as β is varied (top left), the Elliptic mapped cosine approximation error as m is varied (top right) and the Theta mapped cosine approximation error as σ is varied (center bottom) of Runge's function where N=100 Observe that as the map moves away from its Chebyshev limit ($\beta = 1$ for KT, $m = 0$ for Elliptic and $\sigma = 0$ for Theta) to its uniform limit ($\beta = 0$ for KT, $m = 1$ for Elliptic and $\sigma = \infty$ for Theta) an increase in accuracy is initially seen for all of the mappings. Thus for Runge's function, mapped cosine interpolants outperform Chebyshev interpolants with an appropriate choice of the map parameter!

4.9 Error from a Theoretical Viewpoint

As usual, we let $f(x)$ denote the function we wish to approximate and let $x = \mathcal{X}(\tau;\beta)$ be one of the three mappings KT, Elliptic or Theta that maps the interval $\tau \in [0,\pi]$ to the interval $x \in [-1,1]$ with inverse $\tau = \mathcal{T}(\tau;\beta)$. So far, we have motivated the use of mapped cosine interpolants to approximate $f(x)$ where we first approximate the mapped function $F(\tau;\beta)$ by interpolation at the uniform grid points τ_i (4.7.3) with a cosine interpolant, $P_{N-1}(\tau;\beta)$ (see equations (4.8.17)-(4.8.16)). The approximation to $f(x)$ is then $P_{N-1}(\tau;\beta)$ mapped back to the physical domain, $p_{N-1}(x;\beta)$, as illustrated in equations (4.8.12). Moreover, $p_{N-1}(x;\beta)$ interpolates $f(x)$ at the grid points $x_i = \mathcal{X}(\tau_i;\beta)$ (see equations (4.8.17)-(4.8.20)).

The error in the approximation of $f(x)$ by $p_{N-1}(x;\beta)$ over the interval $x \in [-1,1]$ is the same as the error in approximating $F(\tau;\beta)$ with $P_{N-1}(\tau;\beta)$ over the interval $\tau \in [0,\pi]$. This is because

$$|f(x) - p_{N-1}(x;\beta)| = |f(\mathcal{X}(\tau;\beta)) - p_{N-1}(\mathcal{X}(\tau;\beta);\beta)| = |F(\tau;\beta) - P_{N-1}(\tau;\beta)| \qquad (4.9.1)$$

and since the point $(x, f(x) - p_{N-1}(x;\beta))$ is mapped uniquely to the point $(\tau; F(\tau;\beta) - P_{N-1}(\tau;\beta))$ for $x \in [-1,1]$ and $\tau \in [0,\pi]$. Thus, for a fixed choice of map parameter β and number of interpolation points N,

$$\max_{x\in[-1,1]} |f(x) - p_{N-1}(x;\beta)| = \max_{\tau\in[0,\pi]} |F(\tau;\beta) - P_{N-1}(\tau;\beta)|. \qquad (4.9.2)$$

We now consider an even extension (2π periodic) of the function $F(\tau;\beta)$ defined on the interval $\tau \in [0,\pi]$ to the interval $\tau \in [-\pi,\pi]$. The Fourier series of the even extension is

given by

$$F(\tau;\beta) = \sum_{n=0}^{\infty} a_n \cos(n\tau). \tag{4.9.3}$$

Truncating the above series at term $N-1$ yields an approximation to $F(\tau;\beta)$ given by

$$F_{N-1}(\tau;\beta) = \sum_{n=0}^{N-1} a_n \cos(n\tau). \tag{4.9.4}$$

To understand the error in interpolating $f(x)$ with $p_{N-1}(x;\beta)$ for a fixed value of β, we point out the fact that the error in approximating $F(\tau;\beta)$ with a trigonometric interpolant $P_{N-1}(\tau;\beta)$ is at worst a factor of two times the error in approximating $F(\tau;\beta)$ with a truncated cosine series expansion $F_{N-1}(\tau;\beta)$ [4,36]. In other words, the approximation error from interpolation

$$\mathcal{E}_I(N-1) := |F(\tau;\beta) - P_{N-1}(\tau;\beta)| \tag{4.9.5}$$

and from truncation

$$\mathcal{E}_T(N-1) := |F(\tau;\beta) - F_{N-1}(\tau;\beta)| \tag{4.9.6}$$

are related by

$$\mathcal{E}_I \leq 2\mathcal{E}_T. \tag{4.9.7}$$

A classic result [3,4] from Fourier convergence theory illustrates that the rate of convergence of the coefficients of the Fourier series expansion of a function $g(\tau) = \frac{A_0}{2} + \sum_{n=1}^{\infty} A_n \cos(n\tau) + B_n \sin(n\tau)$, where $\tau \in [-\pi, \pi]$, are related to the singularities of the function $g(\tau)$. In particular, if $g(\tau)$ possesses singularities that are branch points/poles whose imaginary parts are given by $\mu_i > 0$ for $1 \leq i \leq M$, the coefficients of its Fourier series expansion (A_n and B_n) for large n have geometric convergence in the sense that $A_n, B_n \sim \sum_{i=1}^{M} \gamma_i p_i^n$ where

$p_i := exp(-\mu_i)$ and γ_i is an algebraic function of n that depends on the order of the pole/type of branch point as reviewed in [4]. Applying this result to the coefficients of the even extension of $F(\tau;\beta)$, a_n, we expect that for large n,

$$a_n \sim \sum_{i=1}^{M} \gamma_i p_i^n \tag{4.9.8}$$

where μ_i, $1 \leq i \leq M$ is now the imaginary parts of the branch points/poles of the function $F(\tau;\beta)$. Moreover, the dominant term in the sum (4.9.8) will be $[\,]p^n$ where $[\,]$ denotes an algebraic function of N and where $p := exp(-\mu)$ and $\mu := \min_i |\mu_i|$, is the imaginary part of the closest singularity to the real axis. Hence for large n,

$$a_n \sim [\,]exp(-n\mu). \tag{4.9.9}$$

In addition, for series whose coefficients fall geometrically, the truncation error, where we truncate at term $N-1$ in the series, asymptotically behaves like $O(|a_{N-1}|)$ [4]. Thus, the truncation error in approximating $F(\tau;\beta)$ with $F_{N-1}(\tau;\beta)$ is

$$\mathcal{E}_T(N-1) \sim O\left([\,]\exp(-(N-1)\mu)\right). \tag{4.9.10}$$

From equation (4.9.7), the interpolation error in approximating $F(\tau;\beta)$ with $P_{N-1}(\tau;\beta)$ is also

$$\mathcal{E}_I(N-1) \sim O\left([\,]\exp(-(N-1)\mu)\right). \tag{4.9.11}$$

It follows from 4.9.2 that the error in the approximation of $f(x)$ by $p_{N-1}(x;\beta)$ over the interval $x \in [-1,1]$ behaves for large N like (4.9.11).

In the previous section we worked through the example of Runge's function and we observed the effects on the approximation error 4.8.29 that the mapping singularity and the inherent singularity of Runge's function had as the map parameter was varied. We learned from both of the KT and Elliptic maps that initially, as the map moved away from its Chebyshev limit toward its uniform limit, the mapped singularity of Runge's function in the τ-plane moved away from the real axis which resulted in an increase of accuracy. However, as the map moved further toward the uniform limit, the inherent singularity of the map, which is moving closer to the real axis as the map tends to its uniform limit, abruptly becomes the dominant singularity in the complex τ-plane and accuracy is lost. In the next section, we set out to answer the question of whether there is an ideal map in terms of accuracy.

4.10 Ideal Map?

In an attempt to numerically answer the question of whether there is an ideal map in terms of accuracy for use in the construction of the cosine mapped interpolants, we interpolate the function

$$f(x;s,\gamma) = \frac{\gamma^2}{\gamma^2 + (x-s)^2} \tag{4.10.1}$$

with a mapped cosine interpolant (see equations (4.8.17)-(4.8.20)) for various values of s and γ. The mapped cosine interpolant with map parameter β that interpolates (4.10.1) for a given choice of s and γ using N interpolation points is denoted by $p_{N-1}(x;\beta,s,\gamma)$. The singularities of (4.10.1) are evidently at $x_s = s \pm i\gamma$. We let

$$\mathcal{E}(N-1,\beta,\gamma) : \quad = \quad \max_{s\in[0,1]} ||f(x;s,\gamma) - p_{N-1}(x;\beta,s,\gamma)||_\infty, \tag{4.10.2}$$

where $||f(x;s,\gamma) - p_{N-1}(x;\beta,s,\gamma)||_\infty := \max_{x\in[-1,1]} |f(x;s,\gamma) - p_{N-1}(x;\beta,s,\gamma)|$. We point out that $\mathcal{E}(N-1,\beta,\gamma)$ denotes the maximum interpolation error of $f(x;s,\gamma)$ as the real part of the singularity in the complex x-plane, s, varies between zero and one over the whole interval $-1 \le x \le 1$ when the imaginary part of the singularity of $f(x;s,\gamma)$ in the complex x-plane is fixed as γ. To gauge the accuracy of the maps, we let $\beta^*(N,\gamma)$ denote the optimum map parameter in the sense that it produces the minimum interpolation error in $\mathcal{E}(N-1,\beta,\gamma)$ and we let $\mathcal{E}^{\mathcal{B}}(N,\gamma)$ denote this minimum possible error. That is,

$$\beta^*(N,\gamma) := \arg\min_{\beta} \mathcal{E}(N-1,\beta,\gamma), \tag{4.10.3}$$

$$\mathcal{E}^{\mathcal{B}}(N,\gamma) := \mathcal{E}(N-1,\beta^*(N,\gamma),\gamma). \tag{4.10.4}$$

We point out that $\mathcal{E}^{\mathcal{B}}(N,\gamma)$ represents the best (as defined above) possible approximation error using N interpolation points with the choice of mapping $\mathcal{X}(\tau;\beta)$ to construct the mapped cosine interpolant of $f(x;s,\gamma)$ whose singularity in the complex x-plane is γ units above/below the real axis. By plotting $\mathcal{E}^{\mathcal{B}}(N,\gamma)$ in the N,γ plane, we hope to answer the question of which (if any) of the mappings KT, Elliptic or Theta is the ideal map for a function whose singularity is γ units above/below the real axis. For the KT map, we denote $\mathcal{E}^{\mathcal{B}}(N,\gamma)$ as $\mathcal{E}^{\mathcal{B}}_{KT}(N,\gamma)$ and with subscripts of E and Θ (instead of KT) for the Elliptic and Theta maps respectively. Plots of $\mathcal{E}^{\mathcal{B}}_{KT}(N,\gamma)$, $\mathcal{E}^{\mathcal{B}}_{E}(N,\gamma)$ and $\mathcal{E}^{\mathcal{B}}_{\Theta}(N,\gamma)$ are shown in Figure 4.10.1 on page 102, Figure 4.10.3 on page 103 and Figure 4.10.5 on page 103 respectively. Plots of the mapping parameter (4.10.3) are also shown below for the Elliptic and KT mappings in Figure 4.10.4 on page 103 and Figure 4.10.2 on page 102 respectively. The plot of (4.10.3) for the Theta mapping is omitted due to the lack of smoothness in the plot (a smoother plot is computationally expensive). In the plots below, we denote the mapping

parameter (4.10.3) as $m^*(N,\gamma)$ and $\beta^*(N,\gamma)$ for the Elliptic and KT mapping respectively. We learn from these plots that the mapping parameter (4.10.3) is really a function of how far the singularity is from the real axis and not so much on the number of interpolation points N (particularly for the KT mapping).

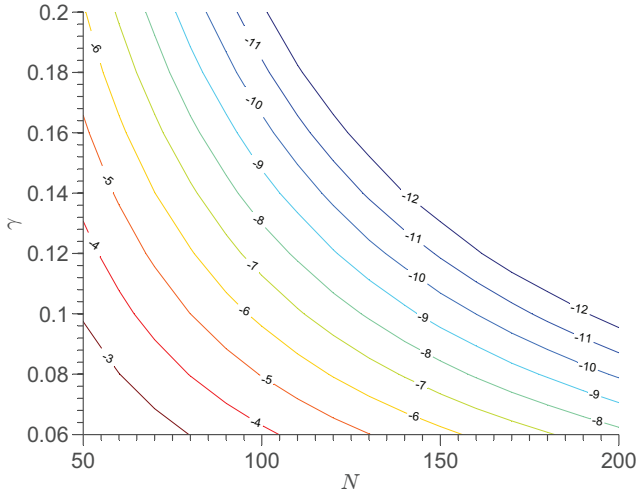

Figure 4.10.1: Contour plot of $\log_{10}\left(\mathcal{E}^{\mathcal{B}}_{KT}(N,\gamma)\right)$

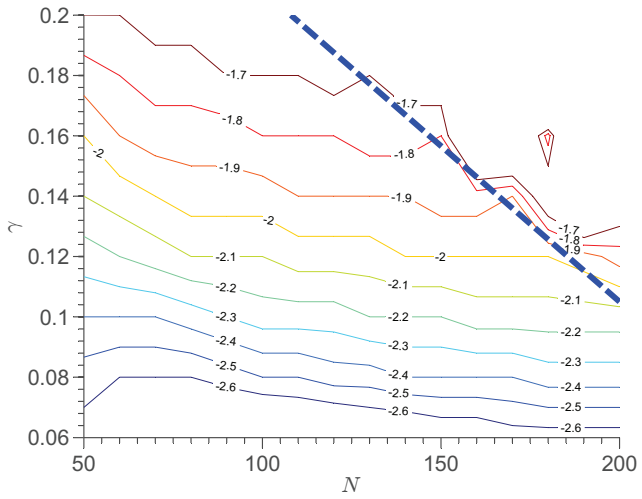

Figure 4.10.2: Contour plot of $\log_{10}\left(\beta^*(N,\gamma)\right)$
The portion of the graph right of the dashed line is ignored as the error has saturated to 10^{-12} in this region of the N,γ plane (see Figure 4.10.1 on page 102).

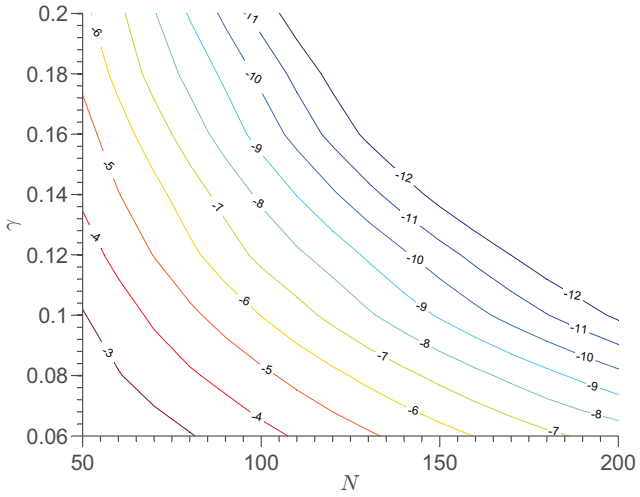

Figure 4.10.3: Contour plot of $\log_{10}\left(\mathcal{E}_E^{\mathcal{B}}(N,\gamma)\right)$

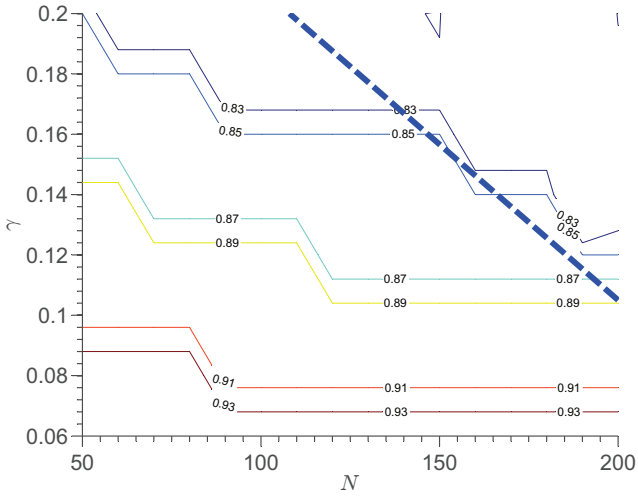

Figure 4.10.4: Contour plot of $m^*(N,\gamma)$ The portion of the graph right of the dashed line is ignored as the error has saturated to 10^{-12} in this region of the N,γ plane (see Figure 4.10.3 on page 103).

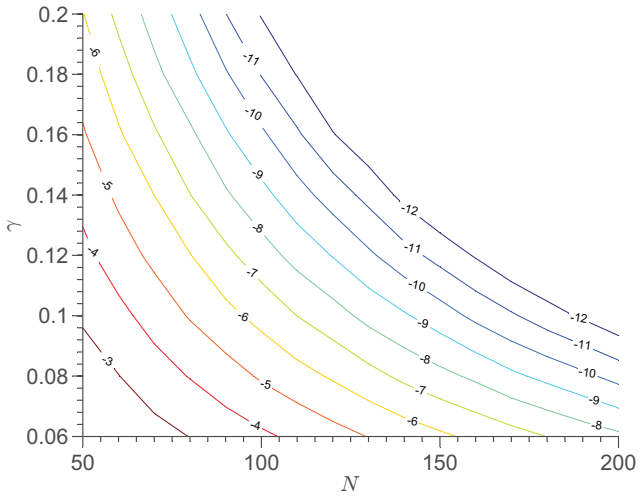

Figure 4.10.5: Contour plot of $\log_{10}\left(\mathcal{E}_\Theta^{\mathcal{B}}(N,\gamma)\right)$

To determine which map performs better in a region of the N,γ plane, we plot the ratios

of $\frac{\mathcal{E}^{\mathcal{B}}_{E}(N,\gamma)}{\mathcal{E}^{\mathcal{B}}_{KT}(N,\gamma)}$, $\frac{\mathcal{E}^{\mathcal{B}}_{E}(N,\gamma)}{\mathcal{E}^{\mathcal{B}}_{\Theta}(N,\gamma)}$ and $\frac{\mathcal{E}^{\mathcal{B}}_{KT}(N,\gamma)}{\mathcal{E}^{\mathcal{B}}_{\Theta}(N,\gamma)}$ in the figures below. The white regions in the plots of the ratios of $\frac{\mathcal{E}^{\mathcal{B}}_{E}(N,\gamma)}{\mathcal{E}^{\mathcal{B}}_{KT}(N,\gamma)}$, $\frac{\mathcal{E}^{\mathcal{B}}_{E}(N,\gamma)}{\mathcal{E}^{\mathcal{B}}_{\Theta}(N,\gamma)}$ and $\frac{\mathcal{E}^{\mathcal{B}}_{KT}(N,\gamma)}{\mathcal{E}^{\mathcal{B}}_{\Theta}(N,\gamma)}$ are regions where the errors of the two maps (i.e. numerator and denominator) are roughly the same. The figures below indicate that for the most part, $\mathcal{E}^{\mathcal{B}}(N,\gamma)$ has the same order of magnitude for all of the mappings. We do see a point in the N,γ plane (roughly when $N = 60$ and $\gamma = .36$) where $\mathcal{E}^{\mathcal{B}}(N,\gamma)$ differs by at most an order of magnitude. However, the values of $\mathcal{E}^{\mathcal{B}}_{E}(N,\gamma)$, $\mathcal{E}^{\mathcal{B}}_{KT}(N,\gamma)$ and $\mathcal{E}^{\mathcal{B}}_{\Theta}(N,\gamma)$ at this point are respectively 1.3×10^{-11}, 1.5×10^{-12} and 10^{-12}. So while the Theta map and the KT map have errors at this point that are roughly an order of magnitude smaller than the Elliptic map, the errors are already quite small.

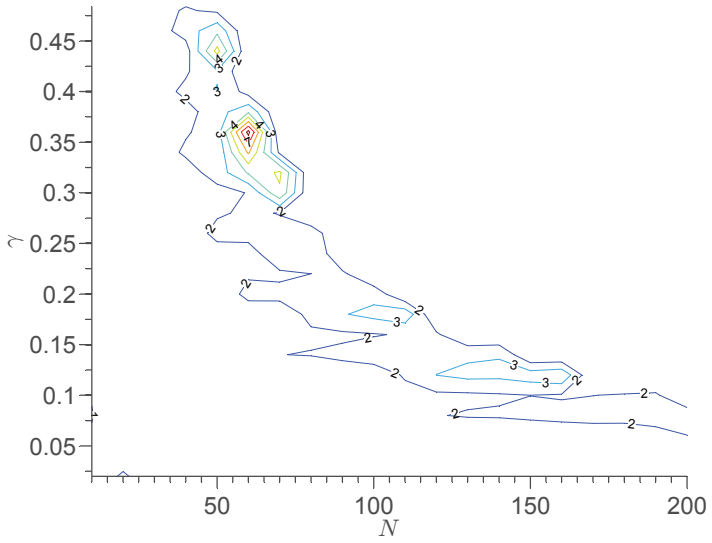

Figure 4.10.6: Plot of $\frac{\mathcal{E}^{\mathcal{B}}_{E}(N,\gamma)}{\mathcal{E}^{\mathcal{B}}_{KT}(N,\gamma)}$
Observe at the point $N = 60$ and $\gamma = .36$, the value of $\mathcal{E}^{\mathcal{B}}_{KT}(N,\gamma)$ is smaller than $\mathcal{E}^{\mathcal{B}}_{E}(N,\gamma)$ by more than a factor of 7. The values of $\mathcal{E}^{\mathcal{B}}_{E}(N,\gamma)$ and $\mathcal{E}^{\mathcal{B}}_{KT}(N,\gamma)$ at this point are given by $\mathcal{E}^{\mathcal{B}}_{E}(N,\gamma) = 1.3 \times 10^{-11}$ and $\mathcal{E}^{\mathcal{B}}_{KT}(N,\gamma) = 1.5 \times 10^{-12}$.

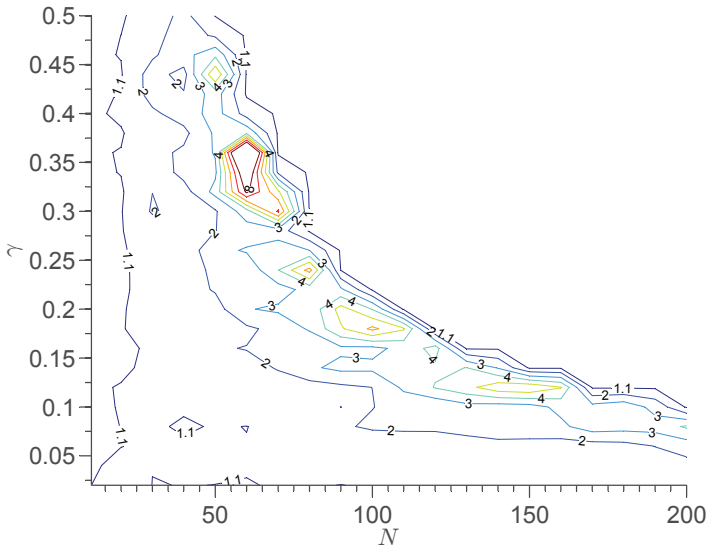

Figure 4.10.7: Plot of $\frac{\mathcal{E}_E^{\mathcal{B}}(N,\gamma)}{\mathcal{E}_\Theta^{\mathcal{B}}(N,\gamma)}$

Observe at the point $N = 60$ and $\gamma = .36$, the value of $\mathcal{E}_\Theta^{\mathcal{B}}(N,\gamma)$ is smaller than $\mathcal{E}_E^{\mathcal{B}}(N,\gamma)$ by more than a factor of 8. The values of $\mathcal{E}_E^{\mathcal{B}}(N,\gamma)$ and $\mathcal{E}_\Theta^{\mathcal{B}}(N,\gamma)$ at this point are given by $\mathcal{E}_E^{\mathcal{B}}(N,\gamma) = 1.3 \times 10^{-11}$ and $\mathcal{E}_\Theta^{\mathcal{B}}(N,\gamma) = 10^{-12}$.

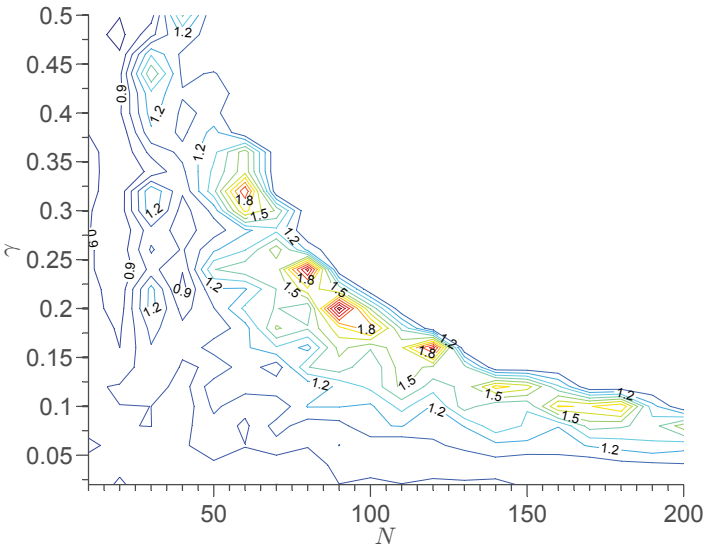

Figure 4.10.8: Plot of $\frac{\mathcal{E}_{KT}^{\mathcal{B}}(N,\gamma)}{\mathcal{E}_\Theta^{\mathcal{B}}(N,\gamma)}$

Observe that $\mathcal{E}_{KT}^{\mathcal{B}}(N,\gamma)$ and $\mathcal{E}_\Theta^{\mathcal{B}}(N,\gamma)$ are roughly the same over the N,γ plane.

4.11 Conclusions

In this chapter, we have motivated the use of Quasi-Uniform Spectral Schemes (QUSSs) and explored three different mappings (KT, Elliptic and Theta) that are capable of producing a grid more uniform than the Chebyshev grid. We showed that it is a poor idea to simply use the mappings to generate a more uniform grid while still using a polynomial basis. We have motivated the use of a mapped cosine basis $\{1, \cos(\mathcal{T}(x;\beta)), \ldots, \cos((N-1)\mathcal{T}(x;\beta))\}$ along with the associated grid points given by $x_i = \mathcal{X}(\tau_i;\beta)$ where τ_i are the uniform grid points (4.7.3), $0 \leq i \leq N-1$ (see Section 4.8) and $\mathcal{X}(\tau;\beta)$ is one of three mappings: KT, Elliptic or Theta. We observed that for these three mappings, as the map parameter was varied, the set of functions $\{1, \cos(\mathcal{T}(x;\beta)), \ldots, \cos((N-1)\mathcal{T}(x;\beta))\}$ and its associated grid points $x_i = \mathcal{X}(\tau_i;\beta)$, vary from their uniform limits of $\{1, \cos(\frac{\pi}{2}(1-x)), \ldots, \cos(\frac{(N-1)\pi}{2}(1-x))\}$ and $x_i = -1 + \frac{2}{\pi}\tau_i,\ i = 0, \ldots, N-1$ respectively to their Chebyshev limits of $\{1, T_1(x), \ldots, T_{N-1}(x)\}$ and $x_i = \cos(\tau_i),\ i = 0, \ldots, N-1$ respectively. We noted that a discussion of which map parameter β to pick in the context of interpolating a function $f(x)$ is really a discussion of which mapped cosine interpolant (which is a linear combination of the functions $\{1, \cos(\mathcal{T}(x;\beta)), \ldots, \cos((N-1)\mathcal{T}(x;\beta))\}$) to use along with the interpolation points $x_i = \mathcal{X}(\tau_i;\beta)$.

In addition, we interpolated Runge's function at the grid points $x_i = \mathcal{X}(\tau_i;\beta)$ with a mapped cosine interpolant. We observed that this mapped cosine interpolant, with an appropriate choice of the map parameter, has better accuracy than a polynomial interpolant in Chebyshev grid points. Moreover, we observed the effects of the singularity of both Runge's function and the mapping singularity on the accuracy of the mapped cosine interpolant for the cases of the KT and Elliptic maps. Indeed, we learned from both of the KT and Elliptic maps

that initially, as the map moved away from its Chebyshev limit toward its uniform limit, the mapped singularity of Runge's function in the complex τ-plane moved away from the real axis which resulted in an increase of accuracy. However, as the map moved further toward the uniform limit, the inherent singularity of the map, which is moving closer to the real axis as the map tends to its uniform limit, abruptly becomes the dominant singularity in the complex τ-plane and accuracy is lost resulting in a V-shaped curve which is seen for the approximation error (see 4.8.3). Our practical advice to the practitioner who uses the KT, Elliptic or Theta map, is that he should be wary of being too greedy and picking a choice of map parameter very close to the uniform limit due to the effects of the map singularity for the KT and Elliptic maps, and the loss of smoothness in the Theta map. Indeed, we observed for the KT map, that if one picks β naively smaller than β^* by an order of magnitude (roughly 10^{-3}) they are penalized *more* than for a choice of β larger than β^* by an order of magnitude (roughly 10^{-1}) and that the penalty was roughly an order of magnitude (see 4.8.3).

Finally, we numerically investigated whether there is an ideal map among the three mappings: KT, Elliptic and Theta in terms of accuracy of the mapped cosine interpolant of the function

$$f(x; s, \gamma) = \frac{\gamma^2}{\gamma^2 + (x - s)^2}. \tag{4.11.1}$$

We learned that for all three mappings $\mathcal{E}^{\mathcal{B}}(N, \gamma)$, which is the best (as defined in (4.10.3) and (4.10.2)) possible approximation error using N interpolation points with the given choice of mapping to construct the mapped cosine interpolant of $f(x; s, \gamma)$ whose singularity in the complex x-plane is γ units above/below the real axis, was roughly similar in the N, γ plane. We also learned that the optimum mapping parameter (4.10.3) for the KT and Elliptic maps is not so much a function of the number of interpolation points, but rather is heavily

dependent on how far the singularity is from the real axis.

Bibliography

[1] N. M. Temme A. Gil, J. Segura. *Numerical Methods for Special Functions*. SIAM, 2007.

[2] R. Baltensperger and J. Berrut. The linear rational collocation method. *Journal of Computational and Applied Mathematics*, 134:243–258, 2001.

[3] J. P. Boyd. The Rate of Convergence of Fourier Coefficients for Entire Function of Infinite Order with Application to the Weideman-Cloot Sinh-Mapping for Pseudospectral Computations on an Infinite Interval. *Journal of Computational Physics*, 110:360–372, 1994.

[4] J. P. Boyd. *Chebyshev and Fourier spectral methods*. Dover publications, 2001.

[5] J. P. Boyd. Prolate spheroidal wavefunctions as an alternative to Chebyshev and Legendre polynomials for spectral element and pseudospectral algorithms. *Journal of Computational Physics*, pages 688–716, 2004.

[6] J. Carcione. Boundary conditions for wave propagation problems. *Finite Elements in Analysis and Design*, 16:317–327, 1994.

[7] J. Carcione. The wave equation in generalized coordinates. *GEOPHYSICS*, 59:1911–1919, 1994.

[8] J. Carcione. A 2d chebyshev differential operator for the elastic wave equation. *Computer Methods in Applied Mechanics and Engineering*, 130:33–45, 1996.

[9] J. Carcione D. Gei and F. Poletto. 3-d wave simulation in anelastic media using the kelvin-voigt constitutive equation. *Journal of Computational Physics*, 196:282–297, 2004.

[10] H. Tal-Ezer D. Kosloff. A Modified Chebyshev Pseudospectral Method with an $O(N^{-1})$ Time Step Restriction. *Journal of Computational Physics*, 104:457–469, 1993.

[11] P. Davis. *Interpolation & Approximation*. Dover Publications, Inc., New York, USA, 1975.

[12] W. Don and D. Gottlieb. Spectral simulation of supersonic reactive flows. *SIAM Journal on Numerical Analysis*, 35:2370–2384, 1998.

[13] W. Don and A. Solomonoff. Accuracy Enhancement for Higher Derivatives using Chebyshev Collocation and a Mapping Technique. *SIAM Journal on Scientific Computing*, 18:1040–1055, 1997.

[14] D. Elliott. Truncation Errors in Two Chebyshev Series Approximations. *Mathematics of Computation*, 19:234–248, 1965.

[15] B. Fischer and L. Reichel. Newton Interpolation in Fejer and Chebyshev points. *Mathematics of Computation*, 53(187):265–278, 1989.

[16] B. Fornberg. Generation of finite difference formulas on arbitrarily spaced grids. *Mathematics of Computation*, 51(184):699–706, 1988.

[17] B. Fornberg. *A Practical Guide to Pseudospectral Methods*. Cambridge Univ Pr, 1998.

[18] B. Fornberg. Calculation of weights in finite difference formulas. *SIAM Review*, 40(3):685–691, 1998.

[19] J.E. Littlewood G.H. Hardy and G. Polya. *Inequalities*. Cambridge Univ Pr, 1988.

[20] P. Godon. Numerical modeling of tidal effects in polytropic accretion disks. *The Astrophysical Journal*, 480, 1997.

[21] K. Hoffman and R. Kunze. *Linear Algebra*. Prentice Hall, New Jersey, USA, 1971.

[22] N. Jacobson. *Basic Algebra, volume I*. Freeman, 1985.

[23] M. Javidi. A modified chebyshev pseudospectral dd algorithm for the gbh equation. *Computers & Mathematics with Applications*, 62:3366–3377, 2011.

[24] L. Gonzalez-Vega J.C. Butcher, R.M. Corless and A. Shakoori. Polynomial algebra for Birkhoff interpolants. *Numerical Algorithms*, 56:1–29, 2011.

[25] R. J. LeVeque. *Finite Difference Methods for Ordinary and Partial Differential Equations*. SIAM, 2007.

[26] J. Mead and R. Renaut. Accuracy, resolution, and stability properties of a modified chebyshev method. *SIAM Journal on Scientific Computing*, 24:143–160, 2002.

[27] M. Raymundo and B. Archilla. Approximation properties of a mapped chebyshev method. *Applied Numerical Mathematics*, 32:119–136, 2000.

[28] R. Renaut and J. Frohlich. A pseudospectral chebychev method for the 2d wave equation with domain stretching and absorbing boundary conditions. *Journal of Computational Physics*, 124(2):324 – 336, 1996.

[29] B. Sadiq and D. Viswanath. Finite difference weights, spectral differentiation and superconvergence. *Accepted in Mathematics of Computation.*

[30] B. Sadiq and D. Viswanath. Barycentric hermite interpolation. *SIAM Journal on Scientific Computing (SISC)*, 35, 2013.

[31] G. Strang. The discrete cosine transform. *SIAM Review*, 41:135–147, 1999.

[32] W. A. Strauss. *Partial Differential Equations.* John Wiley & Sons, Inc., 1992.

[33] J. Szabados. On the order of magnitude of fundamental polynomials of Hermite interpolation. *Acta Mathematica Hungarica*, 61(3):357–368, 1993.

[34] H. Tal-Ezer. High degree polynomial interpolation in Newton form. *SIAM Journal on Scientific and Statistical Computing*, 12:649–667, 1991.

[35] L. N. Trefethen. *Spectral Methods in MATLAB.* SIAM, 2000.

[36] L. N. Trefethen. *Approximation Theory and Approximation Practice.* SIAM, 2013.